Numerical Studies of the Non-Linear Vlasov Equation*

by

Thomas P. Armstrong**

A dissertation submitted in partial fulfillment of the requirements for the degree of Doctor of Philosophy in the Department of Physics and Astronomy in the Graduate College of the University of Iowa

August 1966

Chairman: Associate Professor David Montgomery

*Research supported in part by the National Aeronautics and Space Administration under Contract NsG-233-62.

**National Aeronautics and Space Administration Graduate Research Fellow.

ACKNOWLEDGEMENTS

The author is indebted to Dr. D. Montgomery who suggested the problem which is the subject of this dissertation and whose advice and encouragement made possible the carrying out of the problem. We are also indebted to Dr. P. Kellogg and Dr. B. Hubbard for helpful discussions. The author also expresses his appreciation to Mr. Chin Ming Tsai who assisted in preparing the manuscript, Mr. Cary Wong and Miss Ruth Rogers who plotted the graphs, and Mrs. Evelyn Robison who typed the manuscript. Financial support for this research is due in part to the National Aeronautics and Space Administration through the author's predoctoral fellowship and through grant NsG-233-62.

ABSTRACT

The subject of this dissertation is the numerical integration of the initial-value problem for the non-linear Vlasov equation. The Vlasov equation is used to describe the dynamics of a "collisionless", one-dimensional, classical electron gas confined between two perfectly reflecting boundaries. Only the long-range Coulomb interactions of the electrons are considered; effects associated with the discrete structure are neglected.

The numerical results obtained for non-linear Landau damping compare well with similar results obtained by Knorr. A general statement of the results on stable initial conditions is: As the degree of non-linearity of the initial conditions is increased, the deviation from linear Landau damping appears sooner and is more severe. In some cases damping was observed to cease. Curves showing the time dependence of the damping decrement are derived and compared with predictions of non-linear theories.

New results obtained in this study include the observation that for strongly non-linear cases, the damping of the electric

field causes an initially Maxwellian f_o (v, 0) to develop a peak in the neighborhood of the phase velocity; strong growth of the second harmonic is seen after f_o (v, t) develops such a peak.

Also new in this study is the interpretation of the development of a certain class of strongly unstable initial conditions as approaching an inhomogeneous equilibrium.

TABLE OF TABLES

TABLE OF CONTENTS

Chapter Page

I. INTRODUCTION

1.1 General Remarks

It is the purpose of this dissertation to study the dynamics of a plasma in the "collisionless" limit. The physical requirement is that the number of particles in a Debye sphere be very large. Collective effects will be included in a self-consistent manner, but close encounters between particles will be ignored. Also we will consider only processes which occur on a time scale of the order of the electron plasma frequency, so that ion inertial effects can be ignored.

The substance of the material to be discussed consists of an investigation of non-linear effects in the initial value problem for Vlasov's equation for both stable and unstable equilibria using numerical methods. We solve for the electric field and for the electron distribution function as a function of time.

The present numerical work on the non-linear Vlasov equation is comparable with work done by Knorr [1963a, b] and, to a lesser extent, Kellogg [1965], but is quite different in approach. The points of agreement and disagreement of the present work with that of Knorr will be discussed. It should be emphasized that the

problem considered in this work does not include any effects connected with the discrete structure of the plasma, and should be regarded as distinct from prior numerical calculations on "charged sheet" plasma models which necessarily include collisions [Dawson, 1962; Smith and Dawson, 1963; Buneman, 1959; Buneman, 1963; Burger, 1965].

1.2 Vlasov Equation: Specialization to One Dimension

A "collisionless" plasma is described in the electrostatic, or $c \to \infty$ limit, by the Vlasov equation, also known as the correlationless kinetic equation, which is

$$\frac{\partial f}{\partial t}(\vec{x}, \vec{v}, t) + \vec{v} \cdot \frac{\partial f}{\partial \vec{x}} - \frac{e \vec{E}(\vec{x}, t)}{m} \cdot \frac{\partial f}{\partial \vec{v}} = 0 . \qquad (1.1)$$

$\vec{E}(\vec{x}, t)$ is the self consistent field in the plasma, given by

$$\frac{\partial \cdot \vec{E}(\vec{x}, t)}{\partial \vec{x}} = 4\pi N_o e \left(1 - \int f(\vec{x}, \vec{v}, t)\, d\vec{v}\right) . \qquad (1.2)$$

The plasma is assumed to be macroscopically neutral with a uniform, "smeared out", immobile ion background of density N_o. The $f(\vec{x}, \vec{v}, t)$ is the electron distribution function, -e the electronic

charge, and m the electron mass. We limit the problem to solving (1.1) and (1.2) in the infinite domain when f $(\vec{x}, \vec{v}, 0)$ is specified. The class of f $(\vec{x}, \vec{v}, 0)$'s to be considered is restricted to small perturbations which vary spatially in only one direction (say, x) about a spatially-uniform initial distribution. We now define a reduced or one-dimensional distribution function f (x, v, t) which is related to f $(\vec{x}, \vec{v}, t)$ by

$$f(x, v, t) = \iint dv_y \, dv_z \, f(x, \vec{v}, t) \tag{1.3}$$

and which satisfies

$$\frac{\partial f(x, v, t)}{\partial t} + v \frac{\partial f(x, v, t)}{\partial x} - \frac{eE(x, t)}{m} \frac{\partial f(x, v, t)}{\partial v} = 0 \tag{1.4}$$

and

$$\frac{\partial E(x, t)}{\partial x} = 4\pi N_o e \left(1 - \int_{-\infty}^{\infty} f(x, v, t) \, dv\right) . \tag{1.5}$$

The problem is to find f (x, v, t) and E (x, t), given f (x, v, 0).

In the next section we describe Landau's perturbation-theoretic solution to (1.4) and (1.5).

1.3 Linearization: The Landau Solution

The linearization of the Vlasov equation consists of expanding the distribution function, $f(x, v, t)$, about a spatially uniform equilibrium as

$$f(x, v, t) = f^{(0)}(v) + \varepsilon f^{(1)}(x, v, t) + \varepsilon^2 f^{(2)}(x, v, t) + \ldots \tag{1.6}$$

where $\varepsilon \ll 1$, and $\int dv\, f^{(0)}(v) = 1$. No externally produced electric fields are allowed, and $E(x, t)$ has a similar expansion

$$E(x, t) = \varepsilon E^{(1)}(x, t) + \varepsilon^2 E^{(2)}(x, t) + \ldots \tag{1.7}$$

The expansions (1.6) and (1.7) are then substituted into (1.4) and (1.5), and terms of $0(\varepsilon^2)$ or higher are neglected, which results in

$$\frac{\partial f^{(1)}(x, v, t)}{\partial t} + v \frac{\partial f^{(1)}}{\partial x} - \frac{e E^{(1)}(x, t)}{m} \frac{\partial f^{(0)}(v)}{\partial v} = 0 \tag{1.8}$$

and

$$\frac{\partial E^{(1)}(x, t)}{\partial x} = -4\pi N_o e \int f^{(1)}(x, v, t)\, dv . \qquad (1.9)$$

We require that

$$\int f^{(0)}(v)\, dv = 1, \quad \text{and} \quad \int f^{(1)}\, d x\, dv = 0 . \qquad (1.10)$$

It is important to note that, in (1.8), terms of the form $E^{(1)}(x, t) \frac{\partial f^{(1)}(x, v, t)}{\partial v}$ have been neglected. In order for the solutions of (1.8) and (1.9) to be an accurate representation of $f(x, v, t)$, the terms neglected must be small compared to the terms retained; hence we require

$$\left| E^{(1)} \frac{\partial f^{(0)}}{\partial v} \right| \gg \left| E^{(1)} \frac{\partial f^{(1)}}{\partial v} \right|$$

or that

$$R = \left| \frac{\partial f^{(1)}/\partial v}{\partial f^{(0)}/\partial v} \right| \ll 1 . \qquad (1.11)$$

The conditions under which (1.11) is not satisfied will be discussed

further in section 1.4; we only observe now that it represents one potential shortcoming of the linearized equations (1.8) and (1.9).

Another possible difficulty with the linear solution to the Vlasov equation comes from the assumption that $f^{(0)}(v)$ is independent of time, which neglects the effect of the initial spatial perturbation in causing changes in the spatially-uniform part of f. It is shown numerically in Chapter IV that even for very small ($\frac{f^{(1)}}{f^{(0)}} = 0.04$) perturbations, the spatially uniform part of f does change appreciably, especially around the "resonant" velocity.

We now follow Montgomery and Tidman [1964] in describing the Landau solution. Landau's [1946] procedure for solving (1.8) and (1.9) consists of first applying the Fourier transforms.

$$f^{(1)}(x, v, t) = \int_{-\infty}^{\infty} e^{ikx} f_k^{(1)}(v, t)\, dk$$
$$E^{(1)}(x, t) = \int_{-\infty}^{\infty} e^{ikx} E_k^{(1)}(t)\, dk \qquad (1.12)$$

obtaining

$$\frac{\partial f_k^{(1)}}{\partial t} + ikv\, f_k^{(1)} - \frac{eE_k^{(1)}}{m} \frac{\partial f^{(0)}}{\partial v} = 0 , \tag{1.13}$$

and

$$ikE_k^{(1)}(t) = -4\pi N_o e \int f_k^{(1)} (v, t)\, dv . \tag{1.14}$$

Landau next applied a Laplace transform to $f_k^{(1)}$ and $E_k^{(1)}$ as

$$f_k^{(1)} (v, p) = \int_o^\infty e^{-pt} f_k^{(1)} (v, t)\, dt \tag{1.15}$$

and

$$E_k^{(1)} (p) = \int_o^\infty e^{-pt} E_k^{(1)} (t)\, dt \tag{1.16}$$

where it can be shown under weak restrictions, that the integrals converge for Re $p \geq$ some positive constant [Backus, 1960]. Using (1.15) and (1.16), we obtain from (1.13) and (1.14) the expressions

$$f_k^{(1)} (v, p) = \frac{1}{p + ikv} \left[f_k^{(1)} (v, t = 0) + \frac{e}{m} E_k^{(1)} (p) \frac{\partial f^{(0)}}{\partial v} \right] \tag{1.17}$$

and

$$E_k^{(1)}(p) = \frac{4\pi N_o e i}{k D(k, p)} \int_{-\infty}^{\infty} \frac{dv\, f_k^{(1)}(v, t = 0)}{p + ikv} \qquad (1.18)$$

where $D(k, p) = 1 - \frac{4\pi N_o e^2 i}{mk} \int_{-\infty}^{\infty} \frac{dv\, \partial f^{(0)}/\partial v}{p + ikv}$. (1.19)

The solution of (1.18) for the quantity of interest $E_k^{(1)}(t)$ consists of using the inversion theorem for Laplace transforms, namely

$$E_k^{(1)}(t) = \frac{1}{2\pi i} \int_{\sigma-i\infty}^{\sigma+i\infty} e^{pt}\, E_k^{(1)}(p)\, dp \qquad (1.20)$$

where the contour is taken to the right of all the singularities of the integrand. The integrals in (1.17-1.20) are far too complicated to do for the Maxwellian $f^{(0)}(v)$, for example. Landau observed, however, that some information about $E_k^{(1)}(t)$ in the limit $t \to \infty$ could be extracted from (1.20) by deforming the integration contour under certain restrictions on the analytic properties of the initial conditions.*

---

*We observe that the distributions we shall deal with in the later numerical calculations are all entire functions of velocity and thus satisfy the analytic requirements of Landau for the continuation of the transforms.

Landau was able to show in the $t \to \infty$ limit that the

$$E_k^{(1)}(t) \xrightarrow[t \to \infty]{} \sum_i R_i \, e^{-i\omega_i(k)t} \, e^{-\gamma_i(k)t} \tag{1.21}$$

where

$$-i\,\omega_i(k) - \gamma_i(k) = p_i(k)$$

$$(\omega_i,\ \gamma_i \ \text{real}) \tag{1.22}$$

and $p_i(k)$ are the zero of the analytically-continued Landau denominator or "plasma dielectric function",

$$D(k, p_i(k)) = 0 \,. \tag{1.23}$$

R_i is the residue:

$$R_i = \lim_{p \to p_i(k)} (p - p_i(k))\, E^{(1)}(k, p) \,. \tag{1.24}$$

We restrict ourselves to the case of simple zeros of $D(k, p)$. For a further exposition and criticism of Landau's analytic continuation procedure, the reader is referred to the following

references: Landau [1946], Backus [1960], Hayes [1961], Weitzner [1963], Saenz [1965], Taylor [1965].

Now if γ_i (k) > 0, we notice that in the long-time limit, the $E_k^{(1)}$ (t) is exponentially damped. This phenomenon is called "Landau damping". If γ_i (k) < 0, the equation (1.21) predicts growing electric fields and is an electrostatic instability.

Figure 40 shows the solutions, γ (k) and ω (k), of (1.23) for a Maxwellian $f^{(0)}$ (v) and for k = 0.25 to 1.0. (Numerical data for Figure 40 is from Table 1 of Gary [1966].)

The solutions of (1.23) for arbitrary $f^{(0)}$ (v), small k, are

$$\omega^2 = \omega_p^2 \left(1 + \frac{3k^2 v_{th}^2}{\omega_p^2} + \dots\right), \quad \frac{\omega}{k} \gg v_{th}, \tag{1.25}$$

and

$$\gamma(k) = \frac{\pi}{2} \omega \left(\frac{\omega_p}{k}\right)^2 \left.\frac{\partial f^{(0)}}{\partial v}\right|_{v=\omega/k} \left(1 - \frac{k}{\omega} \frac{d\omega}{dk}\right),$$

$$\frac{\gamma}{\omega} \ll 1 . \tag{1.26}$$

Specializing (1.26) to the case of a Maxwellian $f^{(0)}$ (v) yields

$$\gamma(k) = \omega_p \sqrt{\frac{\pi}{8}} \left(\frac{k_D}{k}\right)^3 \exp\left(-\frac{1}{2}\left(\frac{k}{k_D}\right)^2 - \frac{3}{2}\right) . \tag{1.27}$$

Now ω/k is just the phase velocity of the plane wave solution for the k^{th} Fourier component of the electric field, hence one may conclude that the k^{th} wave will damp if

$\frac{\partial f^{(0)}(\omega(k)/k)}{\partial v}$ is negative or will grow if

$\frac{\partial f^{(0)}(\omega(k)/k)}{\partial v}$ is positive. The qualitative physical interpretation which is given to damping or growth in terms of $\frac{\partial}{\partial v} f^{(0)}(\omega(k)/k)$ is that the particles with velocities slightly greater than $\omega(k)/k$ give up energy to the wave and those with velocities slightly less than $\omega(k)/k$ gain energy from the wave. If $\frac{\partial f^{(0)}(\omega(k)/k)}{\partial v}$ is negative, there are more particles gaining energy from the wave then losing energy and the wave damps; if $\frac{\partial f^{(0)}(\omega(k)/k)}{\partial v}$ is positive, then the former situation is reversed and the wave grows. It will be evident in the numerical data to be

presented in Chapter IV that this intuitive picture is only in an approximate sense correct. It applies best to the situation when the phase velocity of the wave, $\omega(k)/k$, is $\gg$ the thermal velocities of the particles. When $\omega(k)/k$ becomes comparable to a thermal velocity, the situation becomes more complicated. In Dawson's [1961] model for the stable case, this idea is expressed as the plasma oscillation being maintained by the entire plasma and the damping being caused by the "resonant" particles. It is observed in several of the stable cases, as described in Chapter IV, that there are some particles energized for <u>all</u> $v < \omega(k)/k$. The largest effect is observed, however, near $\omega(k)/k$.

The presence of an electrostatic instability requires that there be at least a relative minimum of $f^{(0)}(v)$, i.e., streaming. This theorem is demonstrated by Jackson [1960]. The necessary and sufficient condition for growing waves (i.e., $\gamma(k) < 0$) is Penrose's [1960] criterion:

$$\int_{-\infty}^{\infty} dv \left\{ \frac{f^{(0)}(v) - f^{(0)}(\xi)}{(v - \xi)^2} \right\} > 0 \qquad (1.28)$$

where

$$f'(v) \Big|_{v=\xi} = 0 \quad \text{and} \quad f''(v) \Big|_{v=\xi} > 0 .$$

1.4 Breakdown of Linearization

There are several ways which the linearized solution can break down. The first as suggested in section 1.3 is for the terms neglected in the linearization to become comparable to those retained. Quantitatively we must have

$$R = \frac{|\partial f^{(1)}/\partial v|}{|\partial f^{(0)}/\partial v|} \ll 1 . \tag{1.29}$$

Backus [1960] shows that the value of R must grow proportionately to t; hence, no matter how small the initial perturbation, the perturbation-theoretic solution must eventually break down.

Differing estimates of the time required for breakdown of linearization (because of the growth of the ratio R) in (1.29) are derived by Dawson [1961], Montgomery [1964], and O'Neil [1965]. Dawson and O'Neil compute the time required for R to become O (1) in the region of resonance $v = \omega(k)/k$ as

$$\tau = \frac{1}{\omega_p} \sqrt{2/\varepsilon}, \quad \left(\varepsilon = \frac{f^{(1)}(v, 0)}{f^{(0)}(v, 0)}\right),$$

subject to the restrictions that $\gamma_L \tau \ll 1$ and k not be too small. The requirement $\gamma_L \tau \ll 1$ is essentially that the initial field amplitude not change appreciably from $t = 0$ to $t = \tau$. Montgomery [1964] estimates the time required for breakdown to occur in the non-resonant part of the distribution as $t_M = 1/k \varepsilon v_{th}$. It has not yet been shown how the breakdown (1.29) affects the electric field although O'Neil [1965] has calculated the long time limit of γ in the case that $\gamma_L \tau \ll 1$.

The second way in which the linearization of Vlasov's equation can break down is through the presence of instabilities. If the solution of $D(k, p(k)) = 0$ yields values of $\gamma < 0$, then the electric fields grow, causing the eventual breakdown of the perturbation series. There is at present no theory adequate to treat strongly unstable initial conditions for the Vlasov equation.

What is needed, then is numerical data to illuminate the range of applicability of the linearized solution to the Vlasov equation for stable cases. Also it is desired to investigate numerically some of the strongly unstable cases in order to gain some insight into how an analytic theory for such cases might be formulated. Such numerical calculations have been done previously by Knorr [1963a, 1963b] and Kellogg [1965], and are used as a

basis for this numerical study. The present numerical results are obtained by quite different procedures but are in qualitative agreement with Knorr's published data.

1.5 Summary of Predictions of Non-Linear Theories for Stable Initial Conditions

The first theory we consider is that of O'Neil [1965]. O'Neil observes that if the amplitude of $E^{(1)}$ does not change appreciably in a time given by $\tau = \sqrt{2/\varepsilon}$ and if k is not too small, then τ can be shown to be the time after which (1.27) is not valid in the vicinity of $v = \omega(k)/k$. Quantitatively expressed, the requirement on τ is that $\tau\ \chi_L(\text{linear}) \ll 1$.

If the requirement $\chi_L \tau \ll 1$ is met and k is not too small, then O'Neil is able to show that γ (asymptotic) = 0. This prediction is subject to test and is tested in the present work, the results being discussed in Chapter V. The requirement $\chi_L \tau \ll 1$ is severely restrictive since it does not allow the electric field to deviate significantly from its initial amplitude. Many of the cases for which Knorr, as well as this writer, observed changes in the damping decrement lie quite outside the range of applicability of O'Neil's results, because

the electric field has damped through orders of magnitude before deviations from linearity are observed.

A non-linear theory of somewhat wider applicability is due to Gary, who makes use of the Landau solution to compute the second order correction to the uniform part of the distribution $f_o^{(2)}(v, t_A)$ in an asymptotic limit. The $f_o^{(2)}$ is used to compute a corrected solution to the Landau denominator for the ω and γ. In this paper we will compare a numerically derived $f_o^{(2)}(v, t_A)$ with Gary's analytic prediction (Figure 39) using initial conditions of the form

$$f(x, v, 0) = \frac{e^{-v^2/2}}{\sqrt{2\pi}} (1 + \varepsilon \cos k x) . \qquad (1.30)$$

In addition we will compare a numerical value of the v^2 moment of the $f_o^{(2)}$ with the theoretical prediction as well as the asymptotic values of γ (numerical versus analytic) for several different values of k and ε in initial conditions of the form (1.30).

1.6 Inhomogeneous Equilibria: The Bernstein-Greene-Kruskal Solutions

This section outlines a special class of equilibrium solutions to the Vlasov equation [Bernstein, Greene, and Kruskal, 1957]. It is easily verified by substitution into equation (1.1) that any function, say $g(\mathcal{E})$, where $\mathcal{E} = \frac{1}{2} mv^2 - e\phi(x)$, is an equilibrium solution of the Vlasov equation. Only in the trivial case where $\phi(x) = \text{const}$ would the $\partial g/\partial x = 0$; otherwise $\partial g/\partial x \neq 0$, and there exists a non-uniform charge density in the equilibrium. The potential, $\phi(x)$, is determined from the solution of Poisson's equation,

$$\frac{\partial^2 \phi(x)}{\partial x^2} = -4\pi N_o e \left(1 - \int_{-\infty}^{\infty} dv\, g\left(\frac{1}{2} mv^2 - e\phi(x)\right)\right). \tag{1.31}$$

Equation (1.29) can be rewritten as

$$\frac{\partial^2 \phi(x)}{\partial x^2} = -\frac{\partial V(\phi)}{\partial \phi} \tag{1.32}$$

which is formally equivalent to the equation describing the position, 'ϕ', of a hypothetical particle moving in an effective potential, '$V(\phi)$', as a function of time, 'x'. Equation (1.32) has a first integral

$$\frac{1}{2}\left(\frac{\partial\phi(x)}{\partial x}\right)^2 + V(\phi) = A\,, \tag{1.33}$$

where A is some constant.

For the present work we are interested in the periodic, $\phi(x) = \phi(x+L)$, solutions of (1.32). Such periodic solutions exist if $V(\phi)$ has a relative minimum, or "well", and if the total "energy", A, is less than the height of the "well". If $g(\varepsilon)$ is not a monotonically decreasing function of energy, then periodic solutions of (1.32) can be found.

Considerable analytical effort has been expended in the investigation of inhomogeneous equilibria [Dawson, 1959; Montgomery, 1960; Krall and Rosenbluth, 1961; Low, 1961; Wilhelmsson, 1961; Pearlstein, 1964]. In this paper we will present numerical results which we believe indicate that such inhomogeneous equilibria are approached as the asymptotic limit of a certain

class of strong electrostatic instabilities. These results are presented in section 4.2 and are discussed in section 5.3 of this paper and also in Armstrong and Montgomery [1966].

1.7 Quasi-Linear Theory

The formalism of Vedenov, Velikhov, and Sagdeev [1962] and Drummond and Pines [1962], known as "quasi-linear" theory of plasma oscillations, describes the development in time of weakly unstable initial conditions. Although the numerical results obtained in this study do not correspond to physical situations in which the quasi-linear theory applies, we include a brief outline of the theory for purposes of reference and then discuss the reasons why the present results are not comparable with quasi-linear predictions.

Bodner and Frieman [1963] give a short summary of quasi-linear theory which we will follow closely here. The development begins with the Fourier analyzed Vlasov equation,

$$\frac{\partial f_k}{\partial t} + ikv\, f_k - \frac{e}{m} \sum_{k'} E_{k-k'} \frac{\partial f_{k'}}{\partial v} = 0 . \qquad (1.34)$$

We assume $E_o = 0$ and rewrite (1.34) as

$$\frac{\partial f_k}{\partial t} + ikv\, f_k - \frac{e}{m} E_k \frac{\partial f_o}{\partial v} - \frac{e}{m} \sum_{k'}{}' E_{k-k'} \frac{\partial f_{k'}}{\partial v} = 0 \tag{1.35}$$

where the prime on the sum means that the $k' = 0$ term is omitted. Now for $k \neq 0$ we neglect the third term on the left hand side of (1.35) and obtain

$$\frac{\partial f_k}{\partial t} + ikv\, f_k - \frac{e}{m} E_k \frac{\partial f_o}{\partial v} = 0, \quad k \neq 0 . \tag{1.36}$$

Note that $f_o = f_o(v, t)$.

For $k = 0$ we have

$$\frac{\partial f_o(v, t)}{\partial t} - \frac{e}{m} \sum_{k'} E_{-k} \frac{\partial f_k}{\partial v} = 0 . \tag{1.37}$$

The reader is referred to Drummond and Pines [1962] for a discussion of the range of validity of the neglect of the "mode coupling" term in (1.36). The next step in the procedure is to

solve (1.36) for f_k using a WKB approximation for f_k and E_k. Making use of the f_k in Poisson's equation yields

$$1 = \frac{4\pi e^2}{mk} \int \frac{dv \frac{(\partial f_o(v, t)}{\partial v}}{kv - \omega_k - i\gamma_k}, \tag{1.38}$$

where ω_k and γ_k are the customary oscillation frequency and growth rate, respectively. Equation (1.36) can be solved in the small k approximation to give

$$\omega = \omega_p \tag{1.39}$$

and $$\gamma_k = \frac{\pi}{2} \omega_k \frac{4\pi e^2}{mk^2} \frac{\partial g}{\partial v}\Big|_{\omega/k} . \tag{1.40}$$

The remainder of the procedure, which we will not belabor here, involves substituting the solution for f_k from (1.36) into (1.37), making use of the expression (1.40) for γ_k, observing that for a weak instability $\gamma_k/\omega_k \ll 1$, and going over to the limit of continuous k's. If one does all this, one obtains a diffusion-like equation

$$\frac{\partial f_o(v, t)}{\partial t} = \frac{e^2}{m^2} \frac{\partial}{\partial v} [D \frac{\partial f_o(v, t)}{\partial v}]; \quad D = D(v, t) \tag{1.41}$$

for f_o (v, t) which leads, in the long time limit, to a flattening of f_o (v, t) around $v = \omega_k/k$. The field in the plasma in the long time limit has a spectrum of phase velocities peaked at ω_k/k.

The reasons why the numerical results in this study are not comparable with the predictions of quasi-linear theory are:

1. We do not work in the $k \to 0$ limit numerically.
2. We have at most k, 2k, 3k, discrete k's present in the numerical problem, not a continuous k spectrum.
3. We must of necessity treat unstable initial conditions in the numerical problem having $\gamma \geq 0.1$ in order to reach an "asymptotic" regime in a time during which we can accurately compute the solutions.
4. The phase velocity of the growing waves is $\ll$ thermal velocity, rather than the opposite situation which is specified for the quasi-linear theory.

II. STATEMENT OF THE COMPUTATIONAL PROBLEM

2.1 Reduction of Equations to Dimensionless Form: Perfectly Reflecting Boundaries

It is desired to study the dynamics of an electron plasma, using the non-linear Vlasov equation. We will numerically integrate the initial value problem in order to study non-linear effects on both stable and unstable equilibria. The equations governing a collisionless electron plasma are:

$$\frac{\partial f_e(\vec{x}, \vec{v}, t)}{\partial t} + \vec{v} \cdot \frac{\partial f_e(\vec{x}, \vec{v}, t)}{\partial \vec{x}} - \frac{eE(\vec{x}, t)}{m} \cdot \frac{\partial f_e(\vec{x}, \vec{v}, t)}{\partial \vec{v}} = 0 \qquad (2.1)$$

and

$$\frac{\partial}{\partial \vec{x}} \cdot \vec{E}(\vec{x}, t) = 4\pi e N_o \left(1 - \int_{-\infty}^{\infty} f_e(\vec{x}, \vec{v}, t)\, d\vec{v}\right), \qquad (2.2)$$

where $f_e(\vec{x}, \vec{v}, t)$ specifies the distribution function of electrons

at position $\vec{x}$, with velocity $\vec{v}$, at time t. The plasma is assumed to be macroscopically neutral with a "smeared-out" immobile ion background of density N_o.

Equations (2.1) and (2.2) properly describe the dynamics of a plasma in the limit $g = (N_o L_D^3)^{-1} \to 0$

$$L_D = \left(\frac{K T_e}{4\pi N_o e^2} \right)^{1/2} \equiv \text{Debye Length}$$

$$T_e \equiv \text{Electron Temperature} = \frac{m v_{th}^2}{K}$$

and for time scales on the order of the reciprocal plasma frequency ($\omega_p = (4\pi N_o e^2/m)^{1/2}$). The restriction of the time scale is necessary for the assumption of immobile ions to remain valid.

We apply equations (2.1) and (2.2) to a plasma which is assumed to be disturbed only in one dimension, and go to the one-dimensional distribution ($v_x \to v$):

$$\int dv_y \, dv_z \, f_e (\vec{x}, \vec{v}, t) = f (x, v, t)$$

$$\vec{E} (\vec{x}, t) = \vec{E} (x, t) = \uparrow_x E (x, t) \quad .$$

Then (2.1) and (2.2) become

$$\frac{\partial f\ (x,\ v,\ t)}{\partial t} + v\,\frac{\partial f}{\partial x} - \frac{eE}{m}\,\frac{\partial f}{\partial v} = 0 \qquad (2.3)$$

$$\frac{\partial E}{\partial x} = 4\pi\ e\ N_o\ \left(1 - \int_{-\infty}^{\infty} f\ (x,\ v,\ t)\ dv\right) . \qquad (2.4)$$

It is convenient to introduce a set of dimensionless units and also to use a distribution function f of unit average norm.

$$x = \tilde{x}\ L_D$$

$$v = \tilde{v}\ v_{th}$$

$$t = \tilde{t}/\omega_p$$

$$E = k\ T_e\ \tilde{E}/e\ L_D$$

$$v_{th} = \omega_p\ L_D$$

$$v_{th}\ f\ (x,\ v,\ t) = \tilde{f}\ (\tilde{x},\ \tilde{v},\ \tilde{t})$$

Equations (2.3) and (2.4) become

$$\frac{\partial \tilde{f}}{\partial \tilde{t}} + \tilde{v}\,\frac{\partial \tilde{f}}{\partial \tilde{x}} - \tilde{E}\,\frac{\partial \tilde{f}}{\partial \tilde{v}} = 0 \qquad (2.5)$$

$$\frac{dE}{d\tilde{x}} = 1 - \int_{-\infty}^{\infty} \tilde{f}\,(\tilde{x}, \tilde{v}, t)\, d\tilde{v} \,. \tag{2.6}$$

Henceforth we will drop the ~, and all quantities will be expressed in the appropriate dimensionless units.

It is also desirable to use a finite representation of the unbounded plasma. Montgomery and Gorman [1962] show that for small perturbations about a stable equilibrium, the dynamics of a plasma confined by perfectly reflecting boundaries are the same as for an unbounded plasma, provided the following conditions are satisfied:

$$\begin{aligned} f\,(0, v, t) &= f\,(0, -v, t) \\ f\,(L, v, t) &= f\,(L, -v, t) \\ E\,(0, t) &= E\,(L, t) = 0, \end{aligned} \tag{2.7}$$

where $x = 0$ and $x = L$ are assumed perfectly reflecting boundaries as illustrated in Figure 1. By specifying initially that

$$\begin{aligned} f\,(x, v, 0) &= f\,(-x, -v, 0), \\ & \qquad -L \leq x \leq L, \end{aligned} \tag{2.8}$$

Montgomery and Gorman show that equations (2.7) are satisfied and that no initial perturbations are excluded from such solutions. It may also be shown that (2.7) and (2.8) imply the relations

$$f(x, v, t) = f(-x, -v, t)$$
$$E(x, t) = -E(-x, t). \tag{2.9}$$

Equations (2.9) have also been shown to hold in the non-linear case as well by Gartenhaus [1963].

We now expand $f(x, v, t)$ and $E(x, t)$ in a Fourier series of period 2L as

$$f(x, v, t) = \sum_{n=-\infty}^{\infty} e^{inkx} f_n(v, t) \tag{2.10}$$

$$E(x, t) = \sum_{n=-\infty}^{\infty} e^{inkx} E_n(t) \tag{2.11}$$

where $$f_n(v, t) = \frac{1}{2\pi} \int_{-L}^{L} e^{-inkx} f(x, v, t)\, dx \tag{2.12}$$

$$E_n(t) = \frac{1}{2\pi} \int_{-L}^{L} e^{-inkx} E(x, t)\, dx \tag{2.13}$$

$$k = \frac{2\pi}{2L} \quad . \tag{2.14}$$

Because f (x, v, t) and E (x, t) are real, we must have

$$f_n (v, t) = f^*_{-n} (v, t) \tag{2.15}$$

$$E_n (t) = E^*_{-n} (t) \quad . \tag{2.16}$$

Substituting (2.10) and (2.11) into (2.5) and (2.6), we obtain the following set of equations:

$$\frac{\partial f_n}{\partial t} + ink\, v\, f_n (v, t) - \sum_{q=-\infty}^{\infty} E_{n-q} \frac{\partial f_q}{\partial v} = 0 \tag{2.17}$$

$$ink\, E_n = \delta_{n,o} - \int_{-\infty}^{\infty} f_n (v, t)\, dv \tag{2.18}$$

$$n = 0, \pm 1, \pm 2, \pm 3, \cdots$$

From the symmetry relations (2.9) we have

$$E_n (t) = - E_{-n} (t) \tag{2.19}$$

$$f_n (v, t) = f_{-n} (-v, t) \quad . \tag{2.20}$$

We will also need the expressions for the field potential energy and particle kinetic energy in order to verify energy conservation in the numerical calculations. In dimensionless units

$$W_p \text{ (particle kinetic)}$$

$$= \int_{-L}^{L} \int_{-\infty}^{\infty} \frac{v^2}{2} f(x, v, t)\, dv \qquad (2.21)$$

$$= 2L \int_{-\infty}^{\infty} \frac{v^2}{2} f_0(v, t)\, dv$$

and

$$W_F \text{ (field)} = \int_{-L}^{L} \frac{E^2}{2} dx \,. \qquad (2.22)$$

And, of course,

$$W_{TOT} = W_p + W_F = \text{const.} \qquad (2.23)$$

2.2 Expansion in Hermite Polynomials, the Gram-Charlier Series

Several methods of numerically integrating the system (2.5) and (2.6) in x,v variables were tried and found to be

unsatisfactory due to poor conservation of charge and energy. Also the criterion for numerical stability of the "direct" x,v methods requires that Δt be very small if the velocity grid is taken fine enough to represent the Backus-type velocity space wrinkles. Kellogg [1965] discusses such a "direct" method. What is desired is a representation of f (x, v, t) which could be numerically integrated accurately for a time long enough to see the physical effects of interest and still to retain the effect of the Backus terms.

It was decided that for this purpose an expansion of

$$f_n(v, t) = \sum_{m=0}^{\infty} e^{-v^2/2} h_m(v) Z_{mn}(t) \qquad (2.24)$$

would be useful, where

$$h_m(v) = \frac{(-1)^m}{(m!\ (2\pi)^{1/2})^{1/2}} e^{v^2/2} \frac{d^m (e^{-v^2/2})}{d v^m} \qquad (2.25)$$

is the ortho-normal set of Hermite polynomials [Jackson, 1961]. An expansion similar to (2.24) was used by Engelmann et al. [1963], in a theoretical calculation of non-linear effects. The coefficients $Z_{mn}(t)$ can be complex, but our restrictions on

the symmetry of f (x, v, t) will require that Z_{mn} (t) be either purely real or purely imaginary. The rigorous mathematical question of the convergence of the representation (2.24) will not be discussed here other than to say that f_n (v, t) must go to zero at least as fast as $e^{-v^2/2}$ for large values of v, in order that (2.24) be valid.

Now using equations (2.15) and (2.20) we obtain

$$f_n (v, t) = f_n^* (-v, t) \tag{2.26}$$

which implies that

$$Z_{mn} (t) = (-1)^m Z_{mn}^* (t) \tag{2.27}$$

or

$$\text{Re } Z_{mn} (t) = 0, \quad m = 1, 3, 5, 7, \ldots \tag{2.28}$$

$$\text{Im } Z_{mn} (t) = 0, \quad m = 0, 2, 4, \ldots \ . \tag{2.29}$$

Substituting the expansion (2.24) into (2.18) and (2.17), we obtain

$$E_n(t) = \frac{i(2\pi)^{1/4}}{nk} \operatorname{Re} Z_{0n}(t) \qquad n \neq 0 \tag{2.30}$$

$$E_0(t) = 0$$

and

$$\dot{Z}_{mn}(t) + ink\left(\sqrt{m}\, Z_{m-1\,n} + \sqrt{m+1}\, Z_{m+1\,n}\right)$$

$$+ \frac{i(2\pi)^{1/4}\sqrt{m}}{k} \sum_{\substack{q=-\infty \\ n\neq q}}^{\infty} \frac{Z_{0\,n-q}}{n-q} Z_{m-1\,q} = 0$$

$$m = 1, 2, \ldots; \quad n = 0 \pm 1, \pm 2, \ldots$$

$$Z_{0n}(t) + ink\, Z_{1n} = 0$$

$$n = 0, \pm 1, \pm 2, \ldots \tag{2.31}$$

by making use of the orthogonality properties and recursion relations for Hermite polynomials which are

$$\frac{\partial}{\partial v} h_m(v) = v\, h_m(v) - (m+1)^{1/2} h_{m+1}(v)$$

and

$$v\, h_m(v) = (m+1)^{1/2}\, h_{m+1}(v) + (m)^{1/2}\, h_{m-1}(v).$$

We have now succeeded in reducing the original differentio-integro system (2.17) and (2.18) into a set of first order, non-linear, coupled differential equations which are convenient for numerical integration.

Equations (2.31) do not, unfortunately, form a closed system in either m or n if we choose, as we must, to integrate a finite number of such equations. Suppose one chooses to integrate the equations for m = 0, 1, 2, ..., M; n = 0, 1, 2, ... N. Then the expression for $\dot{Z}_{Mn}$, n = 0, 1, 2 ... N depends on $Z_{M+1\ n}(t)$, n = 0, 1, 2 ... which are unknown. The $Z_{M+1\ n}$ enters equations (2.31) in such a way that it may be neglected only if

$$\left| \frac{Z_{M+1\ n}(t)}{Z_{M-1\ n}(t)} \right| \ll 1 . \qquad (2.32)$$

It will be shown in the next section that inequality (2.32) is valid only for $t < \frac{\sqrt{M}}{n\,k}$ in the free streaming problem, and in

the plasma case the numerical calculations show that the time for (2.32) to be satisfied is also $t < \frac{\sqrt{M}}{n\,k}$. In order to maintain an accurate solution for $t > \frac{\sqrt{M}}{n\,k}$, we must either obtain a good approximation to $Z_{M+1\ n}(t)$ or else find some other way to simulate, as far as the numerical solution for the first few $Z_{mn}(t)$'s is concerned, the infinite set of all $Z_{mn}(t)$'s. Such a method of simulation is described in section 3.2.

2.3 The "Free-Streaming" Problem

The equation

$$\frac{\partial f}{\partial t} + v\,\frac{\partial f}{\partial x} = 0\,, \tag{2.33}$$

which is obtained from (1.1) by setting the electronic charge $e = 0$, corresponds to a freely streaming gas of neutral particles. This equation has a simple analytic solution in terms of the initial values, namely

$$f(x, v, t) = f(x - vt, v, 0). \tag{2.34}$$

Although the solution of (2.33) is much simpler than for the plasma

case (1.1), equation (2.33) exhibits all of the properties which make the Vlasov equation difficult to treat numerically. As can be seen from (2.34), the solutions of (2.33) contain terms whose velocity derivatives grow proportionately to t, producing a rippling of the distribution function in velocity space. This fact has been observed by both Knorr [1963a] and Kellogg [1965]. The rippling in velocity space makes the distribution function very difficult to represent accurately on an x,v grid, hence the "direct" methods of integrating (2.33) are limited to times for which the finite grid spacing is less than the wavelength of the ripples in velocity space.

The Fourier analyzed equation (2.33) is

$$\frac{\partial f_n}{\partial t} + ink\, v\, f_n = 0 \tag{2.35}$$

where all Fourier modes are decoupled. Using the expansion (2.24), we obtain

$$\frac{dZ_{mn}(t)}{dt} + ink\left(\sqrt{m}\, Z_{m-1\ n}(t) + \sqrt{m+1}\, Z_{m+1\ n}(t)\right) = 0 \tag{2.36}$$

for the free streaming problem. If the initial f_n (v, 0) is a Maxwellian,

$$f_{\pm 1}(v, 0) = \frac{\epsilon\, e^{-v^2/2}}{2\sqrt{2\pi}};$$

$$f_n(v, 0) = 0 \qquad n \neq \pm 1, \tag{2.37}$$

then it may easily be verified by substitution that the solution of (2.36) for Z_{mn} (t) is

$$Z_{mn}(t) = \frac{(ink\,t)^m\,\epsilon}{\sqrt{2\pi}\sqrt{m!\,2}}\, e^{-(nkt)^2/2} \qquad \begin{matrix} n = \pm 1 \\ m = 0, 1, 2, \ldots \end{matrix}$$

$$Z_{mn}(t) = 0 \qquad n \neq \pm 1\,. \tag{2.38}$$

The solutions Z_{ml} (t) of the free streaming problem have similar characteristics to the solutions of the plasma problem; hence we will examine the solutions (2.38) in detail. First we notice that the m^{th} coefficient attains its maximum value at a time $t = \frac{\sqrt{m}}{k}$. All coefficients approach zero for large t; however, the largest coefficient in the representation of f_1 (v, t) occurs at larger and larger values of m as time advances. The representation of

f_1 (v, t) in the Gram-Charlier series does remain convergent, although more and more terms are required to represent f_1 (v, t) accurately as t increases.

It is necessary, therefore, in numerically solving the set of M + 1 equations (2.36) to use an estimated value of $Z_{M+1\ 1}(t)$ in computing $\dot{Z}_{M\ 1}(t)$ as $t \to \frac{\sqrt{M}}{k}$. Since it is mainly the m = 0, 1, 2 coefficients of the solutions of (2.36) which are of interest, it is possible to maintain accurate solutions for m = 0, 1, 2 by beginning at $t = \frac{\sqrt{M}}{k}$ to solve for <u>one less coefficient at each time step</u>. Practically speaking, this allows the m = 0, 1, 2 coefficients to be obtained as accurately as if the entire infinite set of equations (2.36) were being solved. Thus, the total time in this representation for which accurate numerical solutions can be maintained is $t = \frac{\sqrt{M}}{k} + (M - 2)\ \Delta t$ where M and Δt can be chosen so that solutions can be obtained for a period sufficiently long to see the physical effects of interest. By "accurate solution" in this context, it is meant that the errors in the solution are composed only of the truncation errors in the algorithm and the round-off errors which accumulate proportionately to the square root of the number of iterations of the solution.

A graphical comparison of the numerical and analytic solutions of the free-streaming problem is shown in Figure 2. The algorithm and the details of the numerical solution will be discussed fully in Chapter III.

2.4 Linear System

All of the formulae which were used in the integration of the Vlasov equation will now be fully tabulated so that it will be completely clear which terms have been included in each version of the solutions presented in Chapter IV. We begin here with the simplest, linear version, which was integrated as a test. The linear system is obtained by keeping the following parts of (2.17) and neglecting all the rest

$$\frac{\partial f_1}{\partial t} + ik\, v\, f_1 - E_1 \frac{\partial f_0}{\partial v} = 0$$

$$ik\, E_1 = -\int_{-\infty}^{\infty} f_1\,(v,\, t)\, dv$$

$$\frac{\partial f_0}{\partial t} = 0 \,. \qquad (2.39)$$

Equations (2.39) lead to the expressions

$$\dot{Z}_{m\,1}(t) + i\,k\,(\sqrt{m}\,Z_{m-1\,1} + \sqrt{m+1}\,Z_{m+1\,1})$$

$$+ \frac{i\,(2\pi)^{1/4}\sqrt{m}}{k}\,Z_{0\,1}\,Z_{m-1\,0} = 0$$

$$m = 0, 1, 2, \ldots M$$

$$\dot{Z}_{m\,0}(t) \equiv 0 \qquad (2.40)$$

for the time derivatives of the $\dot{Z}_{m1}(t)$'s.

If we let

$$Z_{mn} = \xi_{mn} + i\,\eta_{mn}, \qquad (2.41)$$

where ξ_{mn}, η_{mn} are both real, we obtain for the real and imaginary parts

$$\dot{\xi}_{m1}(t) - k\,(\sqrt{m}\,\eta_{m-1\,1} + \sqrt{m+1}\,\eta_{m+1\,1}) = 0 \qquad (2.42)$$

$$\dot{\eta}_{m1}(t) + k\,(\sqrt{m}\,\xi_{m-1\,1} + \sqrt{m+1}\,\xi_{m+1\,1})$$

$$+ \frac{(2\pi)^{1/4}\sqrt{m}}{k}\,\xi_{0\,1}\,\xi_{m-1\,0} = 0\,. \qquad (2.43)$$

In (2.42) and (2.43) we have made use of the fact that $\eta_{m\,0} = 0$. In the numerical integration, equations (2.42) and (2.43) were solved, using Gill's method as discussed in Chapter III.

2.5 Quasi-Quasi Linear System

The next degree of complication from the linear solution to the Vlasov equation is obtained by letting only the uniform part of the distribution function change. This procedure is not exactly the same as that of Drummond and Pines [1962], but is similar.

A numerical integration of the "quasi" linear Vlasov equation was performed in order to further the understanding of the damping process. We now include for reference the relevant equations:

$$\frac{\partial f_1 (v, t)}{\partial t} + i k v f_1 (v, t) - E_1 (t) \frac{\partial f_0 (v, t)}{\partial v} = 0 \tag{2.44}$$

$$\frac{\partial f_0 (v, t)}{\partial t} + E_1 \frac{\partial f_1}{\partial v} - E_1 \frac{\partial f_1^*}{\partial v} = 0 \tag{2.45}$$

$$i k E_1 = - \int_{-\infty}^{\infty} f_1 (v, t)\, dv . \tag{2.46}$$

And in terms of the expansion coefficients $Z_{mn}(t)$, we have the same two equations, (2.42) and (2.43), as in the linear system plus the equations

$$\dot{\eta}_{m\,0}(t) \equiv 0 \tag{2.47}$$

$$\dot{\xi}_{m\,0}(t) = -\frac{(2\pi)^{1/4}}{k}\,(2\xi_{0\,1}\,\eta_{m-1\,1}) \tag{2.48}$$

for the time variation of the uniform part of the distribution function.

2.6 Second Order System

The extension to second order is accomplished by keeping the terms in (2.17) which would be of order ϵ^4 in a perturbation expansion of the distribution function. The second order system is

$$\frac{\partial f_0}{\partial t} + E_1 \frac{\partial}{\partial v}(f_1 - f_1^*) + E_2 \frac{\partial}{\partial v}(f_2 - f_2^*) = 0 \tag{2.49}$$

$$\frac{\partial f_1}{\partial t} + i\,k\,v\,f_1(v,\,t) - E_1 \frac{\partial f_0}{\partial v} + E_1 \frac{\partial f_2}{\partial v} - E_2 \frac{\partial f_1^*}{\partial v} = 0 \tag{2.50}$$

$$\frac{\partial f_2}{\partial t} + 2i\,k\,v\,f_2(v,t) - E_2\frac{\partial f_0}{\partial v} - E_1\frac{\partial f_1}{\partial v} = 0 \qquad (2.51)$$

and the corresponding Poisson equations for E_1 and E_2. The equation for $\partial f_2/\partial t$ contains an $0(\epsilon^4)$ term which has been neglected, namely $E_{-1}\,\partial f_3/\partial v$, which is assumed to have a negligible effect on the solution for E_1, since it can only influence the $\partial f_1/\partial t$ in $0(\epsilon^5)$. Furthermore, it will be shown numerically in section 3.3 that dropping the 4th order term in (2.49) has a negligible effect on the solution for f_1.

In terms of the $Z_{mn}(t)$'s, equations (2.49-2.51) become

$$\dot{Z}_{m\,0}(t) - \frac{i\,(2\pi)^{1/4}}{k}\,\xi_{0\,1}(t)\left\{\sqrt{m}\,(Z_{m-1\,1}(t) - Z^*_{m-1\,1}(t))\right\}$$

$$- \frac{i\,(2\pi)^{1/4}}{k}\,\xi_{0\,2}(t)\left\{\sqrt{m}\,(Z_{m-1\,2}(t) - Z^*_{m-1\,2}(t))\right\} = 0 \qquad (2.52)$$

$$\dot{Z}_{m\,1}(t) + i\,k\,(\sqrt{m}\,Z_{m-1\,1} + \sqrt{m+1}\,Z_{m+1\,1}) + \frac{i\,(2\pi)^{1/4}\sqrt{m}}{k}$$

$$\left\{\xi_{01}\,Z_{m-1\,0} - \xi_{01}\,Z_{m-1\,2} + \frac{1}{2}\,\xi_{02}\,Z^*_{m-1\,1}\right\} = 0 \qquad (2.53)$$

$$\dot{Z}_{m2}(t) + 2\,i\,k\,(\sqrt{m}\,Z_{m-1\,1} + \sqrt{m+1}\,Z_{m+1\,1}) + \frac{i\,(2\pi)^{1/4}\sqrt{m}}{k}$$

$$\cdot\left\{\frac{\xi_{02}}{2}\,Z_{m-1\,0} + \xi_{0\,1}\,Z_{m-1\,1}\right\} = 0\,, \qquad (2.54)$$

where $\xi_{mn} = \mathrm{Re}\,Z_{mn}$.

2.7 Third Order System

The extension to third order of (2.17) consists of retaining terms to order ϵ^5 as follows:

$$\frac{\partial f_0}{\partial t} - \sum_{g=-2}^{2} E_{-g}\,\frac{\partial f_g}{\partial v} = 0 \qquad (2.55)$$

$$\frac{\partial f_1}{\partial t} + i\,k\,v\,f_1 - \sum_{g=-2}^{3} E_{1-g}\,\frac{\partial f_g}{\partial v} = 0 \qquad (2.56)$$

$$\frac{\partial f_2}{\partial t} + 2\,i\,k\,v\,f_2 - \sum_{g=-1}^{3} E_{2-g}\,\frac{\partial f_g}{\partial v} = 0 \qquad (2.57)$$

$$\frac{\partial f_3}{\partial t} + 3\,i\,k\,v\,f_3 - \sum_{g=0}^{3} E_{3-g}\,\frac{\partial f_g}{\partial v} = 0 \qquad (2.58)$$

and the corresponding Poisson equations for E_1, E_2, and E_3. We have neglected of necessity a term $E_{-1}\ \partial f_4/\partial v$ in equation (2.58) which is of the same order as some of the terms retained, but the error made is presumably of $O(\epsilon^5)$. The representation of equations (2.55) to (2.58) in terms of $Z_{mn}(t)$'s is a trivial extension of the formulae (2.52-2.54) and will not be included here.

2.8 Development of Initial Conditions

2.8.1 Stable Cases

For the stable cases the initial conditions were taken to be of the form

$$f(x, v, 0) = \frac{e^{-v^2/2}}{\sqrt{2\pi}} (1 + \epsilon \cos k x) . \qquad (2.59)$$

The values of k and ϵ were chosen so that the damping could be easily seen and the non-linearities could be studied using only 2 or 3 harmonics.

2.8.2 Unstable Cases

It is well-known that certain initial distributions are unstable and small initial electrostatic perturbations grow instead of damp. It was shown by Penrose [1960] that a sufficient condition for the initial distribution $f_o(v)$ to be unstable to growth of waves of some wavenumber k is

$$\int_{-\infty}^{\infty} \frac{[f_o(v) - f_o(\xi)]}{(v - \xi)^2} \, dv > 0, \tag{2.60}$$

where $f_o'(\xi) = 0$;

$f_o''(\xi) > 0$.

There must exist a relative minimum in $f_o(v)$. If (2.60) is satisfied, then there must exist at least one $p_i(k)$ for which

$$D(k, p_i(k)) = 0$$

and

$$\text{Re } p_i(k) > 0 .$$

We now choose an $f_o(v)$, subject to the requirements that

$$f_o(v) \to e^{-v^2/2}, \quad v \to \pm \infty$$

and

$$f_o(v) = f_o(-v)$$

which is also unstable. Such an $f_o(v)$ is

$$f_o(v) = \frac{(v^2 + b)\, e^{-v^2/2}}{\sqrt{2\pi}\,(1+b)} , \qquad (2.61)$$

which is unstable according to (2.60) if $b < 1$. Rather than compute the Landau dispersion relation for this $f_o(v)$, the stability of the distribution for various k's was checked numerically by integrating for a few plasma periods using the initial condition,

$$f(x, v, 0) = \frac{(v^2 + b)}{\sqrt{2\pi}\,(1 + b)} (1 + \epsilon \cos k x), \qquad (2.62)$$

and observing either growth or damping, depending upon the value of k.

The considerations which dictated the choice of the k, b were as follows:

1. The growth rate should be large enough so that the limiting amplitude could be obtained at $t \lesssim 20$.

2. ϵ was chosen small enough to allow for growth.

3. k was chosen so that only k, and not harmonics of it, were unstable wave numbers.

A typical parameter set which satisfies 1, 2, and 3 is $k = 0.5$, $\epsilon = 0.01$, and $b = 0$. The results of the numerical calculations for several unstable cases are discussed in section 4.3.

III. NUMERICAL ALGORITHM

3.1 Gill's Method

A specialization of the Runge-Kutta method due to Gill [1951] was used to solve the set of coupled, first order, non-linear differential equations for the set of $Z_{mn}(t)$ which represent the f (x, v, t). For the time development of the Z_{mn}, we have a set of equations of the general form

$$\frac{d\, Z_{mn}(t)}{dt} = G_{mn}\,(t,\, Z_{00}(t),\, Z_{01}(t) \cdots Z_{0N}(t) \cdots Z_{M0},\, \cdots Z_{MN}) \qquad (3.1)$$

$m = 0, 1, \ldots M$

$n = 0, 1, \ldots N$

(see equation 2.31).

The dependence of G_{mn} on many of the Z_{mn}'s is trivial, but the method to be used is quite independent of the way the Z_{mn}'s enter the G_{mn}. We will write for a shorter notation,

$$\frac{dZ_{mn}}{dt} = G_{mn}(t, \{ Z_{mn} \}), \tag{3.2}$$

where $\{ Z_{mn} \}$ is taken to represent the entire set of Z_{mn}'s. We will now quote the algorithm for Gill's method without going into detail about its derivation.

Let $\mathbf{Z}_{mn}(j)$ represent the value of Z_{mn} at the j^{th} time step. The

$$Z_{mn}(0)$$
$$m = 0, 1, 2, \ldots M$$
$$n = 0, 1, 2, \ldots N$$

are given initially. We compute

$$\begin{aligned} Z^0_{mn} &= \mathbf{Z}_{mn}(0) \\ K^1_{mn} &= \Delta t \; G_{mn}(t, \{ Z_{mn}(0) \}) \\ Z^1_{mn} &= \mathbf{Z}^0_{mn} + 1/2 \; K^1_{mn} \\ K^2_{mn} &= \Delta t \; G_{mn}(t + \frac{\Delta t}{2}, \{ \mathbf{Z}^1_{mn} \}) \end{aligned} \tag{3.3}$$

$$Z^2_{mn} = Z^0_{mn} + (-1/2 + \sqrt{1/2})\, K^1_{mn} + (1 - \sqrt{1/2})\, K^2_{mn}$$

$$K^3_{mn} = \Delta t\, G_{mn}\left(t + \frac{\Delta t}{2}, \left\{ Z^2_{mn} \right\}\right)$$

$$Z^3_{mn} = Z^0_{mn} - \sqrt{1/2}\, K^2_{mn} + (1 + \sqrt{1/2})\, K^3_{mn}$$

$$K^4_{mn} = \Delta t\, G_{mn}\left(t + \Delta t, \left\{ Z^3_{mn} \right\}\right)$$

$$Z^4_{mn} = Z^0_{mn} + 1/6\,(K^1_{mn} + 2\,(1 - \sqrt{1/2})\, K^2_{mn} + 2\,(1 + \sqrt{1/2})\, K^3_{mn} + K^4_{mn}) .$$

Now $Z_{mn}(1) = Z^4_{mn}$ and let

$Z^0_{mn} = Z_{mn}(1)$ and iterate.

The truncation error term for this algorithm is of order $(\Delta t)^5\, \dot{Z}_{mn}(t)$.

3.2 Numerical Integration Procedure

The major difficulty encountered in the numerical integration was with the m = M boundary of the matrix in the m or velocity space direction. As we noted in sections 2.2 and 2.3, the solutions of the free streaming equation have the property in the $Z_{mn}(t)$ representation that although a Maxwellian distribution is represented by only the Z_{On} coefficient, the solution must spread out into the rest of the matrix in the m-direction as time advances. The solution to the Vlasov equation is similar in having the property of spreading out as time increases. At first, various schemes were tried in an attempt to estimate the value of the M + 1 coefficient in a small matrix (typically M = 80). No such procedure was found to be satisfactory.

The spreading out of the solution is a real effect which is due to the presence of terms in f_n (v, t) which have velocity dependence e^{-ikvt}. It was then decided that a very large number of coefficients were really necessary to represent f (x, v, t) for a few tens of plasma periods. The matrix $Z_{mn}(t)$ was then expanded to approximately 1200 coefficients in the m-direction, as large a number of feasible to compute on the hardware available. A series of computer programs was written in

Fortran for use on the I.B.M. 7044 at the University of Iowa computer center. A sample of one of these programs is included in Appendix I.

The solution of the set of equations for the $Z_{mn}(t)$'s was extended to times greater than the time necessary for the coefficients at the boundary, m = M, to attain their maximum value by simply dropping off one coefficient at each time step. This allowed a solution for the first few coefficients which was the same as if the entire infinite set of $Z_{mn}(t)$'s was being computed. This procedure was suggested to us by Dr. Hubbard to whom we are indebted.

It should be emphasized here that the solutions of the non-linear Vlasov equation presented in this paper include the Backus-type e^{ikvt} terms. This is a major difference between the present work and the work of Knorr [1963a, b]. By solving the "free-streaming" problem for the initial conditions (2.37) using Knorr's continuous Fourier transformation in velocity, it can be seen that the maxima of the transformed representation of f (x, v, t) eventually migrate out of the finite range of the velocity transform variable. Knorr asserts that by the time the e^{ikvt} produced terms move out of the range of the transform

variable that their effect on the moments of f (x, v, t) is negligible. The results of the present study seem to agree with Knorr's assertion. Nonetheless it has proved to be possible to compute the solutions to the non-linear Vlasov equation including the effects of these e^{ikvt} terms.

The choice of the number of the Fourier wave numbers to keep is determined by the requirement that if N harmonics are retained, then keeping N + 1 harmonics should not change the n = 0, 1 solutions appreciably. This procedure was followed in the numerical calculations and is described in section 3.3.

3.3 Checks of the Accuracy of the Numerical Results

In order to interpret physically the results of the numerical integration of the Vlasov initial value problem it is necessary to know how accurately the numerical solution traces out the true solution. The true solution to the non-linear Vlasov equation is not analytically obtainable which is, of course, the reason for attempting this numerical solution. It is possible, however, to learn a considerable amount about the accuracy of the numerical solution by numerically integrating problems which are similar to the non-linear Vlasov equation but for which the analytic solutions are known.

One problem similar to the Vlasov problem is that of a freely streaming gas as discussed in section 2.3. The explicit solution is just

$$f(x, v, t) = f(x - vt, v, 0)$$

in terms of the initial distribution function

$$f(x, v, 0) = \frac{e^{-v^2/2}}{\sqrt{2\pi}} (1 + \epsilon \cos k x)$$

$$f(x, v, t) = \frac{e^{-v^2/2}}{\sqrt{2\pi}} (1 + \epsilon \cos k (x - vt)).$$

For this particular initial condition the analytic solution is given by equation (2.38). A graphical comparison of the numerical solution for $\Delta t = 0.01$ and the analytic solution is shown in Figure 2. The most important errors are apparently due to the 8 digit arithmetic of the 7044 and not the truncation error of Gill's algorithm which, in this case, would be of order $10^{-10} \times \dot{Z}_{mn}(t)$ (at worst $10^{-10} \times Z_{mn}(t)$). It is clear from Figure 1 that the solutions agree well for more than 7 orders of magnitude. In Table 1 we have tabulated the results of another

run of the free-streaming case with a $\Delta t = 0.025$ for comparison. Fortunately in the plasma case for intermediate values of k, the solutions $Z_{mn}(t)$ do not fall so rapidly and can be followed accurately for a longer time than the streaming solutions. For values of k larger than 1.0, it would clearly be necessary even in the plasma case to use more digits of accuracy than 8 in order to observe the solutions even for a few tens of plasma periods.

A second initial value problem which was run as a test of the accuracy of the integration scheme was the purely linear system as described in section 2.4. In this system one expects a strictly exponentially damped electric field to appear after the effects of the initial value terms become negligible. As can be seen in Figure 3, the linear system does damp exponentially. This exponential damping persists through the times when the non-linear cases will later be seen to deviate from strict exponential damping, which indicates that the variations in damping rate in the non-linear cases are due to the presence of non-linear terms rather than failure of the numerical solution to represent the true solution.

Another check of the accuracy of the numerical program is accomplished by numerically integrating the same initial conditions using different values of the time increment Δt. The values of the coefficient $Z_{01}(t)$ in the solution of $k = 0.5$, $\epsilon = 0.1$ initial conditions are given in Table 2. At $t = 25$ for example, the effect of changing Δt from 0.0125 to 0.025 was to change the value of Z_{01} by 0.0032%.

Still another estimate of the reliability of the solutions may be extracted from the constancy of the total energy for the plasma slab under numerical integration. Table 3 gives such an estimate. The change of total energy in this case ($\epsilon = 0.1$, $k = 0.5$) was about 0.01% of the initial energy in the electric field.

A further test of the sensitivity of the solutions to the presence of high order terms in the Fourier harmonics was performed by running the second order system with and without the term $E_2 \, \partial/\partial v \, (f_2 - f_2^*)$ in the expression for $\partial f_o/\partial t \, (v, t)$. The results are shown in Table 4 from which it may be seen that, for example, at $t = 35$ the value of Z_{01} was changed less than 1% by the omission of the 4^{th} order term.

After considering the numerical accuracy of the integration of a given second or third order system there is the question of how well the Fourier harmonics retained represent the entire solution to the non-linear Vlasov equation. Since we are particularly interested in the validity of the results for the n = 1 Fourier mode, we will check the effect of neglecting high order harmonics on the value of Z_{01}. Table 5 displays a comparison of the values obtained for Z_{01}, and Z_{02} in a second and third order system.

The deviation at t = 15 for Z_{01} was 0.86%. The Z_{02}'s have different values in the table because the phase of Z_{02} is slightly changed by going to the third order. Nevertheless, the agreement of the Z_{01}'s indicates that the second order system is satisfactory in this case ($\epsilon = 0.25$) and presumably for all smaller values of ϵ. The fact that the second and the third order solutions are in close agreement indicates that the Fourier expansion is rapidly convergent.

IV. SUMMARY OF NUMERICAL RESULTS

This chapter is intended to be an objective summary of the numerical results obtained by integrating the initial value problem for various initial conditions. Comments on the solutions will be made only as they are necessary to the proper understanding of the data presented. Chapter V contains our assessment of the significance of the data. Because we realize that there may be other interpretations given to the data, we attempt to present the numerical data in a form separated from our interpretation of it.

4.1 Summary of Results: Stable Initial Conditions

In all of the cases to be described in this section the form of the initial conditions is the same, namely

$$f(x, v, 0) = \frac{e^{-v^2/2}}{\sqrt{2\pi}} (1 + \epsilon \cos k x) . \qquad (4.1)$$

When expressed in terms of the expansion coefficients Z_{mn}, the initial conditions (4.1) become

$$Z_{00}(0) = \frac{1}{(2\pi)^{1/4}} \tag{4.2}$$

and

$$Z_{0\,1}(0) = \frac{\epsilon}{2} \frac{1}{(2\pi)^{1/4}} \tag{4.3}$$

where all of the remaining

$$Z_{mn}(0) = 0 \qquad \begin{aligned} m &= 0, 1, \ldots M \\ n &= 0, \pm 2, \pm 3, \ldots \pm N. \end{aligned}$$

The numerical solution consists of using a set of dynamical equations for the $\dot{Z}_{mn}(t)$ as described in sections 2.2 to 2.7 to advance the initial conditions (4.2) and (4.3) using Gill's algorithm (section 3.1) as the finite difference scheme. The quantities of primary interest in the numerical solution are the Fourier components of the electric field, which are related to the Z_{mn}'s by

$$E_n(t) = \frac{i\,(2\pi)^{1/4}}{nk} \; Z_{0n}(t) \; . \tag{4.4}$$

In the presentation of the numerical data, the $Z_{0n}(t)$ will be used, since the $Z_{0n}(t)$ is the number actually computed in the solution and $E_n(t)$ is easily derived from it. We will now discuss briefly each case which was computed, as listed in Table 6, beginning with the k = 0.5 cases in order of increasing epsilon, i.e., increasing non-linearity. Following the k = 0.5 cases we discuss several k = 1.0, 0.375, and 0.35 cases which were run in order to verify that the results for k = 0.5 were not peculiar.

An additional reason for the choice of initial conditions of the form given in (4.1) is that it is one of the very few for which numerical integration of Vlasov's equation has been attempted [Knorr, 1963a, b]. Agreement between the results from two very different integration schemes would both increase confidence in Knorr's results and in the new situations to be reported later in this work.

Beginning with Case I ($k = 0.5$, $\epsilon = 0.025$), we observe in Figure 4 that $Z_{01}(t)$ has the form of an exponentially damped plasma oscillation until $t \tilde{=} 30$ when the effective damping decrement begins to decrease. The effective damping decrement for the fundamental wavenumber has been computed from the ratio of adjacent electric field maxima and plotted for Case I in Figure 5.

The damping decrement curve has the characteristic form of following the linear value for some time, in this case until $t \tilde{=} 30$, and then falling below the linear value. There is a slight "leveling-off" of the damping decrement curve at about $t = 50$ to 55. The last several points on this curve are uncertain to perhaps 10%; hence conclusions regarding an asymptotic value of γ for this case are uncertain.

Figure 6 shows the results of numerically integrating Case II ($k = 0.5$, $\epsilon = 0.04$) which is similar to, but not identical with, Knorr's Case III ($k = 0.5$, $\epsilon = 0.05$). The present numerical results agree well with those of Knorr. The behavior of Z_{01} in Case II follows the linear prediction until $t = 26$ when the damping decrement falls below the linear value. At $t \tilde{=} 42$ the damping decrement curve "levels-off" at $\gamma \tilde{=} .08$, as can be seen in Figure 7.

In order to illuminate the cause of the changes in the damping decrement and to show graphically the effect of Landau damping on the spatially uniform part of the distribution function, we reconstructed f_o (v, t) by summing all of the significant terms in the series representation:

$$f_o(v, t) = \sum_{m=0}^{M} e^{-v^2/2} h_m(v) Z_{mo}(t) . \qquad (4.5)$$

This summation was performed for 500 velocity points at several different times for Cases II, III, IV, and V, in order that the effect, on $f_o(v, t)$, increasingly non-linear initial conditions would be evident. Another function, $f_o^{(2)}(v, t)$, defined by

$$f_o^{(2)}(v, t) = f_o(v, t) - f_o(v, 0),$$

was computed in order to show the fine detail of the corrections to the uniform part of the distribution produced by the non-linear terms. As a point of reference in all the $f_o(v, t)$ and $f_o^{(2)}(v, t)$ curves (cf. Figures 8a, b; 9a, b; 12a, b; 13a, b; 14a, b; 17a, b; 18a, b; 19a, b) which are displayed, the linear phase velocity $v = \omega_L/k$ is indicated on the velocity axis. The non-linear corrections to ω_L will, in some cases, significantly change the phase velocity; however, for purposes of reference, the linear phase velocity seems adequate.

Figures 8a and 8b show the $f_o^{(2)}(v, 20)$ and $f_o(v, 20)$, respectively, for Case II. It can be seen that for this case the function $f_o^{(2)}(v, 20)$ has a sharp decrease slightly below

$v = \omega_L/k$ and a sharp increase slightly above $v = \omega_L/k$. In addition $f_o^{(2)}$ (v, 20) has velocity space ripples which are clearly seen for $v < \omega_L/k$. The period of the ripples in velocity is very close to $2\pi/kt$, the value one expects from e^{-ikvt}. The effect of $f_o^{(2)}$ (v, 20) on the entire distribution function f_o (v, 20) is to cause a slight flattening, or decrease of ∂f_o (v, 20)/∂v, in the neighborhood of $v = \omega_L/k$.

Figures 9a and 9b show the $f_o^{(2)}$ (v, 35) and f_o (v, 35) for Case II. Again the e^{-ikvt} wrinkles are present but smaller in amplitude. The negative and positive peaks in the neighborhood of $v = \omega_L/k$ are larger and sharper at t = 35 than at t = 20. The entire distribution function is flattened even more around $v = \omega_L/k$ for t = 35 than for t = 20.

Figure 10 shows the next situation which was integrated, Case II ($k = 0.5$, $\epsilon = 0.1$). This case has exactly the same initial conditions as Knorr's Case IV, shown in his Figure 3d [Knorr, 1963b]. The results of Knorr's Case IV and our Case III agree to the precision with which they may be compared, using numbers extracted from Knorr's published graph. There is one exception, however, in that we do <u>not</u> see the regrowth and subsequent peaking of the second harmonic around t = 45 which

Knorr does. The plot of γ versus time (Figure 11) shows that the damping decrement deviates from the linear rate beyond t = 7.5. After t = 7.5 the damping rate is larger than the linear rate until t = 17.5 when the decrement decreases and then reaches a "plateau" of $\gamma = 0.048$ at $t \geq 26$. Figures 12a and 12b show the $f_o^{(2)}$ (v, 10) and f_o (v, 10) for Case III. The velocity wrinkles are comparatively large and the "notch" around ω_L/k is not yet well developed. Some flattening of f_o (v, 10) is evident in Figure 12b. At t = 20, as shown in Figure 13b, f_o (v, 20) appears more flattened around ω_L/k. Figure 13a shows that the ripples in $f_o^{(2)}$ (v, 20) of period $2\pi/kt$ are smaller in amplitude for t = 20 than for t = 10. Finally, at t = 30 (Figures 14a and 14b) the derivative of f_o (v, 30) has gone almost to zero around ω_L/k and the amplitude of the "notch" in $f_o^{(2)}$ (v, 30) around ω_L/k is still increasing. The e^{-ikvt} terms are still present at t = 30 but have smaller amplitude than at t = 20. Another point to observe about f_o (v, t) is that the region slightly above $v = \omega_L/k$ has been enhanced, not only from the region slightly below $v = \omega_L/k$ but also for all $v < \omega_L/k$.

The next case we consider is Case IV ($k = 0.5$, $\epsilon = 0.25$), as shown in Figure 15. Many of the characteristics of this case

are similar to Case III and are evident in the figures, and only the peculiar features will be discussed. The most obvious way in which the $\epsilon = 0.25$ case is different from the $\epsilon = 0.1$ case is that for $\epsilon = 0.25$ the second harmonic starts growing when the damping in the first harmonic has ceased at about $t = 15$. The γ versus t plot (Figure 16) for this case shows that the γ never attains the linear value and even fluctuates negative and positive beyond $t = 25$. A very interesting effect in Case IV is seen in f_o (v, t) shown in Figures 17a, b; 18a, b; and 19a, b. At $t = 5$, f_o (v, 5) is merely enhanced at large velocities, but by $t = 10$, f_o (v, 10) has become very flattened in the neighborhood of ω/k. At $t = 15$, however, the f_o (v, 15) has developed a peak at $v \tilde{=} 3$ and is no longer monotonically decreasing, which allows the possibility of unstable roots to the Landau denominator for this distribution. The growth of E_2 after $t = 15$ may be due to such an unstable root.

In order to check the validity of the second order solution for $k = 0.5$, $\epsilon = 0.25$, these same initial conditions were run in a third order system (Case V) shown in Figure 20. The behavior of the first two harmonics is almost the same in the third order system as in the second order system. The value of Z_{01}, for example, was changed about 2% at $t = 17$ (a maximum).

In Figures 21 and 22 we show the results obtained for a very large amplitude case (Case VI, $k = .5$, $\epsilon = 0.4$). It is clear in this case that the damping is not simply exponential as may be judged from the γ vs t graph. Damping ceases quite soon ($t < 10$), and regrowth of E_2 (t) starts at $t \sim 10$. This case is clearly dominated by the initial conditions.

In order to check that the form of the results obtained in the preceding cases was not peculiar to the value $k = 0.5$, we ran cases for several other values of k, namely $k = 1.0$, 0.375, and 0.35. The first of these, Case VII ($k = 1.0$, $\epsilon = .1$), is shown in Figure 23. The electric field in this case is exponentially damped in accordance with the linear theory for as long as we can follow it. Case VIII ($k = 1.0$, $\epsilon = 0.2$) deviates from the linear result for $t \sim 5$ to 10, as shown in Figure 24. The amplitude of E_1 falls below the linear value and damps to too small a value too soon to determine an asymptotic rate of damping. The curve of γ vs t for Case VIII is included for reference in Figure 25.

Case IX is shown in Figure 26. This case is identical to Knorr's Case VI, i.e., $k = 0.375$, $\epsilon = 0.05$. During the time we followed the solution, there was no deviation from the linear

prediction. For $k = 0.35$, $\epsilon = 0.175$, Case X, however, we observed a marked decrease in the damping decrement at $t \tilde{=} 12$. The coefficients Z_{01}, Z_{02} for Case X are plotted in Figure 27, and the γ versus t curve is given in Figure 28.

Upon examination of the preceding non-linear cases which were run, it became evident that the changes in damping rate were associated with changes in the uniform part, f_o (v, t), of the distribution function. As a further test of this hypothesis, a case herein called "quasi" was run. The "quasi" system is described in section 2.5. Figure 29 shows the result of calculations on the "quasi" system for $k = 0.5$, $\epsilon = .01$. The amplitude of the first harmonic in "quasi" follows closely that in the full second order calculation until $t \gtrsim 25$ where "quasi" is slightly above "second". The change in the damping decrement is still present in the "quasi" system as evidenced in Figure 30 where γ versus t is plotted for "quasi". In order to facilitate comparison of the results of "quasi" with the results of linear and second order systems, Figure 31 is included to show the Z_{01} (t) for the initial conditions $k = 0.5$, $\epsilon = 0.1$ in each of the systems.

As a final summary graph on the results of integrating stable cases, Figure 32 is included. Figure 32 shows the envelope of Z_{01} (t) for k = 0.5, ϵ = 0.04, 0.1, 0.25, thereby illustrating in a convenient form the effect on E_1 (t) of the non-linearity introduced by increasing ϵ while keeping k constant.

4.2 Numerical Results for Unstable Initial Conditions

Several sets of strongly unstable initial conditions of the form given in (2.62) were integrated in order to determine, if possible, the asymptotic form of the solutions for the electric fields. The major difficulty encountered in numerically integrating the unstable cases was in finding initial conditions for which the growth rate was large enough to produce a limiting amplitude in 20 to 30 plasma periods, and also for which the first two Fourier harmonics represent the solution accurately. It was desired that the fundamental k be unstable but that the 2k wave-number in the solution not be unstable; therefore, several preliminary runs were made to find suitable initial conditions to use.

The first unstable case which was computed, Case XII, was for b = 0, k = 0.5, ϵ = 0.01. The results for Case XII are shown

in Figure 33. After $t \tilde{=} 5$ the solutions for E_1 and E_2 were observed to grow exponentially with growth rates of $\gamma_1 = -0.245$ and $\gamma_2 = 2\gamma_1$. The growth of the 2k wave was interpreted to be simply the feeding of energy from the k wave into the 2k wave through the $E_1 \partial f_1/\partial v$ term, because a perturbation with wave number 2k only was found in a preliminary test to exhibit no growth for these initial conditions. The growth of E_1 ceased at t = 24, after which E_1 underwent a long period fluctuation in magnitude (but not sign) until the integration was stopped at t = 60. E_2, on the other hand, stopped growing at around t = 21 and then underwent several changes of sign between t = 21 and t = 60. The second harmonic was always smaller in magnitude than the first by at least a factor of 2 and usually more. Note here that the solutions Z_{01} and Z_{02} must be multiplied by

$$\frac{i\,(2\pi)^{1/4}}{k} \qquad \text{and} \qquad \frac{i\,(2\pi)^{1/4}}{2k},$$

respectively, to correspond to E_1 and E_2.

The $f_o^{(2)}(v, t)$ and $f_o(v, t)$ for Case XII are shown in Figures 34a and 34b for t = 10; Figures 35a and 35b for t = 20; and Figures 36a and 36b for t = 30. The most obvious effect to be seen in Figures 34-36 is the filling in of the "hole" near the minimum (v = 0) of $f_o(v, t)$ as time advances.

A third order calculation, Case XIII, was performed on the same set ($k_o = 0.5$, $\epsilon = 0.01$, $b = 0$) of initial conditions in order to determine how well the second order system represented the full solution to the non-linear Vlasov equation in this case. As can be seen by comparing Figures 33 and 37, the solutions for the first and second harmonic are substantially the same in the second and third order versions of the unstable ($k = 0.5$, $\epsilon = 0.01$, $b = 0$) case. The initial growth rate of E_3 is $\tilde{=} 3\gamma_1$ and E_3 ceased growing at $t \tilde{=} 18$.

A run was attempted using the initial conditions $b = 0$, $k = 0.4$, $\epsilon = 0.01$. The growth rate γ was nearly equal to that for $k = 0.5$; however, the second harmonic soon grew to a value as large as the first, and this case was abandoned.

Figure 38 shows still another unstable case which was computed, namely, Case XIV for $k = 0.6$, $\epsilon = 0.01$, and $b = 0$. The numerical results for Case XIV are very similar to Case XIII except that the growth rate ($\gamma_1 = -0.237$) was slightly smaller in Case XIV and the E_2 did not increase to as large an amplitude. The property of the E_1 approaching a quasi-static value does not seem to be strongly dependent upon the choice of k in the initial conditions.

V. INTERPRETATION OF NUMERICAL RESULTS: COMPARISON WITH NON-LINEAR THEORIES

5.1 Stable Initial Conditions: Time Dependence of Damping

At the outset of this discussion, it should be emphasized that the numerical results obtained in this study pertaining to the time development of the non-linear first order damping decrement are in substantial agreement with the results obtained by Knorr [1963 a, b]. It has been possible in this study to extend these results and to investigate in detail the nature of the changes in the spatially averaged distribution function f_o (v, t) which are associated with deviations from exponential damping. Furthermore, we have obtained numerical results which illuminate the range of applicability of recently developed theories of non-linear damping.

The first non-linear theory we consider is that of O'Neil [1965] as outlined in section 1.4. We find that Case X ($k = 0.35$, $\epsilon = 0.175$) for which $\gamma_L = 0.035$ and $\tau = \sqrt{2/\epsilon} = 3.4$, satisfies O'Neil's criterion ($\gamma_L \tau \ll 1$) for the applicability of his results. O'Neil's prediction is $\gamma_N \to 0$ for $t \gg \tau$. It may be seen from Figure 28 for Case X that γ_N does go to zero at about $t = 15$ in apparent agreement with O'Neil's theory. Another more general

result which bears upon the Dawson [1961]--O'Neil [1965] premise that breakdown of linearization first occurs in the region around $v = \omega/k$ is the observation that the non-linear corrections to $f_o(v)$ are in all cases largest in the neighborhood of ω/k. The amount by which $f_o(v, t)$ is changed depends on the initial electric field amplitude ϵ/k. The O'Neil result that $\gamma_N \to 0$ in the long time limit seems to be valid in the restricted case to which it may properly be applied. However, the initial conditions to which the O'Neil theory applies are highly specialized; k must be neither too small nor too large for O'Neil's time τ (given, in our dimensionless units, by $\sqrt{2/\epsilon}$) to satisfy $\gamma_L \tau \ll 1$ and simultaneously to be the time at which $|\partial f_1/\partial v|$ first becomes $\approx |\partial f_o/\partial v|$. For most of the cases computed, $\tau = \sqrt{2/\epsilon}$ was considerably shorter than the time at which large departures from the linear damping rate were observed, and the electric field characteristically fell through more than an order of magnitude before the damping stopped.

The next non-linear theory we consider is that of Gary [1966], also outlined in section 1.5. For the Gary theory, the predictions which we can test numerically are:

1. Asymptotic value of the non-linear damping decrement γ_N, with particular emphasis on the $\epsilon \leq 0.1$ cases.
2. The second order correction $f_o^{(2)}$ (v, t) to the uniform part of the distribution.

Gary's results apply in the regime $t > t_A$ where t_A is determined from the consideration that terms multiplied by $e^{-\gamma_L t_A}$ must be negligible compared to all other terms in the problem; hence $\gamma_L t_A \gg 1$. For purposes of comparison, the numerical solutions were assumed to be in Gary's asymptotic, $t > t_A$, regime when the damping decrement had attained a fairly constant value and when the v^2-moment of $f_o^{(2)}$ was approximately constant. There is some uncertainty in the numerically obtained values for the asymptotic non-linear damping decrement, because the numerical solutions could be obtained only for a limited time. For all the cases to be quoted, the numerical γ_N is estimated, using the trend of the γ_N vs t curves. We present in Table 7 a comparison of our numerical versus Gary's predicted values of two quantities, γ_N (asymptotic) and $\int_{-\infty}^{\infty} v^2 f_o^{(2)}$ (v, t) dv. The $\int_{-\infty}^{\infty} f_o^{(2)}$ (v, t_A) $\frac{v^2}{2}$ dv is, in the numerical case, nearly equal to the initial field

energy in the perturbation. The initial field energy appears in the asymptotic regime as the increase in particle kinetic energy.

A further point on which Gary's theory may be compared with the numerical data which is in the detailed shape in velocity space of $f_o^{(2)}(v, t_A)$. Gary computes an $f_o^{(2)}(v, t_A)$ for $k = 0.5$, $\epsilon = 0.1$ which may be compared with Figures 12a, 13a, and 14a from this paper. By considering the development of $f_o^{(2)}(v, t)$ in time from the numerical data, it may be concluded that its asymptotic form will be quite near the form predicted by Gary and Gorman. A graphical comparison of $f_o^{(2)}(v, 20)$ from Case III and $f_o^{(2)}(v, t_A)$ for $k = 0.5$, $\epsilon = 0.1$ from Gary and Gorman [1966], as shown in Figure 39, illustrates the agreement of the theoretical and numerical results.

5.2 Stable Initial Conditions: Regrowth of the Second Harmonic

It is observed that, if the initial electric field amplitude is large enough, as in Case V, $k = 0.5$, $\epsilon = 0.25$, the uniform part of the distribution function, $f_o(v, t)$, develops a region of positive derivative near ω/k, as can be seen in Figure 24. It is also noted that when the "bump" appeared at about $t = 15$ the damping of E_1 ceased and E_2 began to grow. However, when the

f_o (v, 15) from Case V was used as an initial distribution for k = 1.0, ϵ = 0.01, the k wave did not grow but began damping away. Hence, the cause of the growth of E_2 in Case V was not that the f_o (v, 15) became unstable to perturbations of wave number 2k; the presence of the lower order wave is apparently required to produce the growth of E_2.

A similar regrowth of the second harmonic may be seen in Knorr's Figure 13e [Knorr, 1963a] for k = 0.5, ϵ = 0.5 initial conditions. Knorr does not derive the distribution function in velocity space; hence no conclusion about f_o (v, t) may be made for his case.

5.3 Unstable Initial Conditions: Tendency Towards an Inhomogeneous Equilibrium

A tentative interpretation of the numerical results obtained for the unstable initial conditions in Cases XII and XIV will now be offered. It was observed that the growing electric field reached a limiting amplitude; and after that, as long as the solution could be followed, the E_1 component of the electric field did not change sign but underwent slow variations of about a factor of 3 in amplitude. The second harmonic in Case XII did oscillate through zero after attaining its limiting amplitude,

but its variations were also very slow. The net electric field did not change sign after attaining the limiting amplitude. There seems to be no tendency for the electric fields to damp away. Rather, the indication is that the total electric field in Cases XII and XIV is settling down to a static value. If this conclusion is correct and if the numerical solutions are as accurate as they are believed to be then these results may be taken to indicate that the eventual development of a strongly unstable plasma (with an initial $f_o(v) = f_o(-v)$) is a spatially inhomogeneous equilibrium of the Bernstein-Greene-Kruskal [1957] type. This conclusion must be subjected to a much more exhaustive numerical test. The task of demonstrating analytically the correctness or incorrectness of such a conjecture is indeed formidable.

The solutions obtained in this paper for strongly unstable initial conditions are qualitatively similar to Knorr's Cases VII and VIII, although the initial conditions are quite different. Knorr's Cases VII and VIII also seem to approach a quasi-static equilibrium which is not field free; however, Knorr does not interpret his results as approaching inhomogeneous equilibria.

It is also interesting that arguments for the approach, as $t \to \infty$, to one of the spatially non-uniform equilibria can be given on the basis of the quasi-linear theory [Vedenov et al., 1962; Drummond and Pines, 1962]. However, the present strongly unstable equilibrium for which the growing modes have $\omega/k \ll V_{th}$, is not one to which the quasi-linear theory would be expected to apply. The reason for the apparent correctness of the result is not known.

APPENDIX

```
      THIS IS A TYPICAL PROGRAM WRITTEN IN FORTRAN FOUR
      TO COMPUTE THE SOLUTION OF THE NON-LINEAR VLASOV EQUATION.
$IBFTC HRMITE
C     THIS IS A PROGRAM WHICH CALCULATES THE TIME DEVELOPMENT OF THE
C     COFFICIENTS Z(M,N) IN THE REPRESENTATION OF THE ELECTRON
C     DISTRIBUTION FUNCTION.
C     THE SECOND ORDER VLASOV-HERMITE SYSTEM IS USED TO OBTAIN THE
C     DYNAMICAL EQUATIONS FOR THE Z(M,N).
C     GILL'S METHOD IS USED FOR THE NUMERICAL INTEGRATION.
C     THE Z(M,N) ARE REPRESENTED BY A DOUBLY SUBSCRIPTED VARIABLE
C     AA(I,J).
C     I IS THE FOURIER INDEX, I = 1 IS THE N=0 FOURIER MODE.
C     J IS THE HERMITE INDEX, J = 1 IS THE M = 0 COEFFICIENT.
C     RESERVE STORAGE AREA FOR VARIABLES.
        DIMENSION AA(3,1201),AKAP(3,1201,4),ROOTS(1201),DELROT(1201)
C     AKAP IS DELTAT TIMES THE DERIVATIVE OF THE AA WITH RESPECT TO TIME.
C     AA IS THE FOURIER-HERMITE COEFFICIENT.
C     ROOTS(J)=SQUARE ROOT OF J-1.
C     DELROT(J)=(FOURTH ROOTS OF 2 PI TIMES ROOTS(J) DIVIDED BY K)
C     TIMES (-DELTAT)
C     VARIABLE TYPE SPECIFICATIONS
        REAL K0
        LOGICAL L1
C     CALL A SUBROUTINE WHICH ALLOWS FOR UNDERFLOWS.
        CALL TRAPS(10,-1)
C     SET UP THE PARAMETERS OF THE PROBLEM.
        K0=0.5
        EPSLON=0.1
        DELTAT=0.025
C     SPECIFY THE NUMBER OF FOURIER HARMONICS.
        NF=3
C     SPECIFY MAXIMUM HERMITE INDEX.
        NH=1199
        NHL=NH-1
        DELTK0=DELTAT*K0
        DELTK2=2.0*DELTK0
        P0K=((2.0*3.14159265)**0.25)/K0
        DELP0K=-DELTAT*P0K
        R4P02=0.5*((2.0*3.14159265)**0.25)
        RECIPK=(SQRT(2.0*3.14159265))/(K0*K0)
        TWOCON=SQRT(2.0)
        L1=.TRUE.
C     WRITE OUT PARAMETERS
        WRITE(6,8999)
        WRITE(6,9000)NF,NH,DELTAT,K0,EPSLON
        DO99J=1,NH
        Z=FLOAT(J)
     98 ROOTS(J)=SQRT(Z)
        DELROT(J)=ROOTS(J)*DELP0K
     99 CONTINUE
C     SET UP INITIAL VALUES FOR AA(I,J).
        DO 101 I=1,NF
        DO 101 J=1,NH
```

```
  101 AA(I,J)=0.0
      AA(1,1)=1.0/((2.0*3.14159265)**0.25)
      AA(2,1)=(EPSLON*AA(1,1)/2.0)
C     INITIALIZE TIME
      TIME=0.0
C     WRITE OUT INITIAL CONDITIONS
      WRITE(6,9002)TIME
      WRITE(6,9001)((AA(I,J),I=1,NF),J=1,5)
C     SPECIFY DESIRED NUMBER OF ITERATIONS.
      ITIME=1800
C     INITIALIZE VARIABLES WHICH SPECIFY TIME AND THE INTERVALS FOR
C     WRITING OUT THE RESULTS.
      MCOUNT=0
      ICOUNT=0
C     INITIAL NUMBER OF HERMITE COEFFICIENTS
      NH=49
C     MAXIMUM NUMBER OF HERMITE COEFFICIENTS.
      NG=1185
C     TIME TO BEGIN DECREASING THE MATRIX SIXE IN THE HERMITE DIRECTION.
      DOWN=(ROOTS(NG-10)/(2.0*KO))
C     ENTER FIRST DO LOOP FOR ITERATION IN TIME.
      DO 7050 MT=1,ITIME
C     DURING THE INITIAL 142 ITERATIONS WE INCREASE THE MATRIX SIZE IN THE
C     HERMITE DIRECTION.
      IF(MT.LE.142)
     1GO TO 558
      GO TO 559
  558 NH=NH+8
      NHL=NH-1
  559 CONTINUE
C     INCREMENT VARIABLES FOR SPECIFYING INTERVALS FOR WRITING OUT RESULTS.
      L1=.NOT.L1
      MCOUNT=MCOUNT+1
      ICOUNT=ICOUNT+1
      TIME=TIME+DELTAT
C     ENTER DO LOOP FOR THE FOUR STEPS OF GILL'S METHOD.
      DO 7000 IG=1,4
C     EVALUATE ALL DERIVATIVES FOR I=1, UNIFORM PART.
      DO7090J=3,NH,2
 7090 AKAP(1,J,IG)=DELROT(J-1)*(2.0*AA(2,1)*AA(2,J-1)+AA(3,1)*AA(3,J-1))
C     EVALUATE DERIVATIVES FOR I=2, FIRST HARMONIC.
 8002 AKAP(2,1,IG)= DELTKO*AA(2,2)
      DO8003J=2,NHL,2
 8003 AKAP(2,J,IG)=-DELTKO*(AA(2,J-1)*ROOTS(J-1)+ROOTS(J)*AA(2,J+1))
     1+DELROT(J-1)*(AA(2,1)*AA(1,J-1)+AA(3,1)*AA(2,J-1)*0.5
     2-AA(2,1)*AA(3,J-1))
      DO 8009J=3,NHL,2
 8009 AKAP(2,J,IG)= DELTKO*(AA(2,J-1)*ROOTS(J-1)+AA(2,J+1)*ROOTS(J))
     1+DELROT(J-1)*(AA(3,1)*AA(2,J-1)*0.5+AA(2,1)*AA(3,J-1))
      AKAP(2,NH,IG)= DELTKO*AA(2,NHL)*ROOTS(NHL)
     1+DELROT(NHL)*(AA(3,1)*AA(2,NHL)*0.5+AA(2,1)*AA(3,NHL))
      IF(TIME.GE.(DOWN+DELTAT)) GO TO 70
      IF(ABS(AA(2,NH)).LE.1.0E-10)
     1 GO TO 6991
      X=ALOG(ABS(AA(2,NHL-4)))
```

```
      Y=ALOG(ABS(AA(2,NHL-2)))
      Z=ALOG(ABS(AA(2,NHL)))
      R=2.5*Z-2.0*Y+0.5*X
      S=EXP(R)
      Q=SIGN(S,-AA(2,NHL))
      AKAP(2,NH,IG)=AKAP(2,NH,IG)+DELTKO*Q*ROOTS(NH)
      GO TO 6991
   70 AKAP(2,NH,IG)=AKAP(2,NH,IG)+DELTKO*AA(2,NH+1)*ROOTS(NH)
 6991 CONTINUE
C    EVALUATE DERIVATIVES FOR I=3, SECOND HARMONIC.
      AKAP(3,1,IG)= DELTK2*AA(3,2)
      DO 8020J=2,NHL,2
 8020 AKAP(3,J,IG)=-DELTK2*(AA(3,J-1)*ROOTS(J-1)+AA(3,J+1)*ROOTS(J))
     1+DELROT(J-1)*(AA(3,1)*AA(1,J-1)*0.5+AA(2,1)*AA(2,J-1))
      DO 8021J=3,NHL,2
 8021 AKAP(3,J,IG)= DELTK2*(AA(3,J-1)*ROOTS(J-1)+AA(3,J+1)*ROOTS(J))
     1-DELROT(J-1)*AA(2,1)*AA(2,J-1)
      AKAP(3,NH,IG)= DELTK2*AA(3,NHL)*ROOTS(NHL)
     1-DELROT(NHL)*AA(2,1)*AA(2,NHL)
      IF(TIME.GE.(DOWN+DELTAT)) GO TO 80
      IF(ABS(AA(3,NH)).LE.1.0E-10)
     1 GO TO 6992
      X=ALOG(ABS(AA(3,NHL-4)))
      Y=ALOG(ABS(AA(3,NHL-2)))
      Z=ALOG(ABS(AA(3,NHL)))
      R=2.5*Z-2.0*Y+0.5*X
      S=EXP(R)
      Q=SIGN(S,-AA(3,NHL))
      AKAP(3,NH,IG)=AKAP(3,NH,IG)+DELTK2*Q*ROOTS(NH)
      GO TO 6992
   80 AKAP(3,NH,IG)=AKAP(3,NH,IG)+DELTK2*AA(3,NH+1)*ROOTS(NH)
 6992 CONTINUE
C    NOW ADVANCE THE SOLUTIONS USING GILL'S FORMULAE.
      GO TO (7001,7002,7003,7004),IG
 7001 CONTINUE
      DO7022I=1,NF
      DO7022J=1,NH
 7022 AA(I,J)=AA(I,J)+0.5*AKAP(I,J,IG)
      GO TO 7000
 7002 CONTINUE
      DO7032I=1,NF
      DO7032J=1,NH
 7032 AA(I,J)=AA(I,J)-.29289322*(AKAP(I,J,1)-AKAP(I,J,2))
      GO TO 7000
 7003 CONTINUE
      DO7042I=1,NF
      DO7042J=1,NH
 7042 AA(I,J)=AA(I,J)-.20710682*AKAP(I,J,1)-AKAP(I,J,2)
     1+1.7071068*AKAP(I,J,3)
      GO TO 7000
 7004 CONTINUE
      DO7062I=1,NF
      DO7062J=1,NH
 7062 AA(I,J)=AA(I,J)+0.16666667*(AKAP(I,J,1)+AKAP(I,J,4))
     1+0.80473785 *AKAP(I,J,2)
```

```
     2-1.1380712*AKAP(I,J,3)
 7000 CONTINUE
C    CHECK TIME AND DECIDE WHETHER TO REDUCE THE MATRIX SIZE.
       IF(TIME.GE.DOWN)
      1GO TO 555
       GO TO 556
  555 IF(L1) NH=NH-2
      NHL=NH-1
      WRITE(6,9011) NH
  556 CONTINUE
C    CHECK VARIABLE AND DECIDE WHETHER TO WRITE OUT RESULTS.
       IF(ICOUNT.NE.4) GO TO 7050
C    RESET VARIABLE.
       ICOUNT=0
C    COMPUTE ELECTRON KINETIC ENERGY.
       PENRGY=R4PO2*(TWOCON*AA(1,3)+AA(1,1))
C    COMPUTE FIELD ENERGY.
       FENRGY=0.0
       DO6999I=2,NF
 6999 FENRGY=FENRGY+(AA(I,1)/(FLOAT(I-1)))**2
       FENRGY=FENRGY*RECIPK
C    COMPUTE TOTAL ENERGY.
       TENRGY=FENRGY+PENRGY
       WRITE(6,9002)TIME
C    DECIDE WHETHER TO LIST FULL OR ABBREVIATED MATRIX AA(I,J).
       IF(MCOUNT.EQ.400) GO TO 6998
C    WRITE ABBREVIATED MATRIX.
       DO7044MZ=1,5
       J=MZ
       WRITE(6,9001)(AA(I,J),I=1,NF)
 7044 CONTINUE
C    WRITE LABELS FOR ENERGIES.
       WRITE(6,9004)
C    WRITE ENERGIES.
       WRITE(6,9005)FENRGY,PENRGY,TENRGY
C    CHECK TO SEE IS OPERATOR WANTS TO END EXECUTION OF PROGRAM.
       CALL SSWTCH(2,KTEST)
       IF(KTEST.EQ.1) GO TO 17
       GO TO 7050
 6998 CONTINUE
C    RESET COUNTER.
       MCOUNT=0
C    WRITE FULL MATRIX.
       WRITE(6,9010)((AA(I,J),I=1,NF),J=1,NH)
C    WRITE ENERGY LABELS.
       WRITE(6,9004)
C    WRITE ENERGIES.
       WRITE(6,9005) FENRGY,PENRGY,TENRGY
 7050 CONTINUE
   17 CONTINUE
C    PUNCH OUT INFORMATION FOR RELOADING PROGRAM.
       WRITE(7,9013) TIME
       DO401I=1,NF
       DO400 K=1,NH,5
  400 WRITE(7,9012)I,K,AA(I,K),AA(I,K+1),AA(I,K+2),AA(I,K+3),AA(I,K+4)
```

```
  401 CONTINUE
 8999 FORMAT(1H1,11X,2HNF,11X,2HNH,10X,6HDELTAT,18X,2HKO,9X,6HEPSLON)
 9000 FORMAT(1H0,10X,I3,8X,I5,10X,F6.3,10X,F10.6,10X,F6.3)
 9001 FORMAT(1H ,8(1X,E15.8))
 9002 FORMAT(1H0,23H       MATRIX AT TIME =,3X,F10.3)
 9003 FORMAT(1H0,21HSINE MATRIX AT TIME =,3X,F10.3)
 9004 FORMAT(1H0,8X,12HFIELD ENERGY,5X,15HPARTICLE ENERGY,8X,
     112HTOTAL ENERGY)
 9005 FORMAT(1H ,3(9X,F11.8))
 9006 FORMAT(1H0,18HINCREMENTAL TIME =,3X,F10.3)
 9007 FORMAT(1H0,F10.3,1X,I3,10(1X,E10.3))
 9008 FORMAT(1H0,10(3X,E10.3))
 9009 FORMAT(1H ,16X,7(1X,E15.8))
 9010 FORMAT(1H0,6(4X,E15.8))
 9011 FORMAT(1H ,I5)
 9012 FORMAT(I1,I4,5(E15.8))
 9013 FORMAT(F8.3)
      CALL EXIT
      END
$ENTRY HRMITE
```

240

TABLE 1

Comparison of Analytic and Numerical
Free-Streaming Solutions

Time	Z_{01} Numerical	Z_{01} Analytic	Deviation	Iterations
0	$.31580938 \times 10^{-1}$	$.31580938 \times 10^{-1}$	0.00	0
2	$.19154749 \times 10^{-1}$	$.191548077 \times 10^{-1}$	-5.87×10^{-8}	80
4	$.42739932 \times 10^{-2}$	$.42740153 \times 10^{-2}$	-2.21×10^{-8}	160
6	$.35082764 \times 10^{-3}$	$.35083254 \times 10^{-3}$	-4.90×10^{-9}	240
8	$.10592985 \times 10^{-4}$	$.10595225 \times 10^{-4}$	-1.24×10^{-9}	320
10	$.11814119 \times 10^{-6}$	$.1176920 \times 10^{-6}$	$+4.50 \times 10^{-10}$	400
12	$.10854431 \times 10^{-8}$	$.48097706 \times 10^{-9}$	$+6.04 \times 10^{-9}$	480

TABLE 2

Comparison of Z_{01} Obtained with Different Δt for $k = 0.5$, $\epsilon = 0.1$

Time	Z_{01}		Deviation %
	$\Delta t = 0.025$	$\Delta t = 0.0125$	
0	$.31580938 \times 10^{-1}$	$0.31580938 \times 10^{-1}$	0.0
5	$.10228778 \times 10^{-1}$	0.1022896×10^{-1}	0.00080
10	$.23269353 \times 10^{-2}$	$0.23268939 \times 10^{-2}$	0.0017
15	$-.18966850 \times 10^{-3}$	$-0.18967476 \times 10^{-3}$	0.0033
20	$-.35462848 \times 10^{-3}$	$-0.35463134 \times 10^{-3}$	0.000806
25	$-.33775979 \times 10^{-3}$	$-0.33774903 \times 10^{-3}$	0.0032

TABLE 3

Conservation of Energy for Stable
$k = 0.5$, $\epsilon = 0.1$ Case

Time	W_p	W_E	W_{tot}
0	0.50000000	0.0099999995	0.5099999995
5	0.5089508437	0.001049075	0.5099999187
10	0.5099454681	0.000054294	0.5099997621
15	0.5099993128	0.000000351	0.5099996638
20	0.5099983083	0.000001253	0.5099995613
25	0.5099983230	0.000001153	0.5099994760
30	0.5099979577	0.000001403	0.5099993607
35	0.5099981054	0.000001153	0.5099992584
40	0.5099984337	0.000000701	0.5099991347
45	0.5099986821	0.000000350	0.5099990321
50	0.5099988311	0.000000100	0.5099988411

TABLE 4

Comparison of Z_{01} and Z_{02} With and Without $E_2\ \partial f_{-2}/\partial v + E_{-2}\ \partial f_2/\partial v$ Terms in $\partial f_o\ (v,t)/\partial t$

	Z_{01}			Z_{02}		
Time	With	Without	% Dev	With	Without	% Dev
0	$.31580938 \times 10^{-1}$	$.31580938 \times 10^{-1}$	0.0	0.0	0.0	0.0
5	$.10228778 \times 10^{-1}$	$.10228705 \times 10^{-1}$	0.00071	$.68835078 \times 10^{-4}$	$0.68851453 \times 10^{-4}$	0.0238
10	$.23269353 \times 10^{-2}$	$.23259702 \times 10^{-2}$	0.0414	$-.28314711 \times 10^{-4}$	$-0.28216602 \times 10^{-4}$	0.348
15	$-.18966850 \times 10^{-3}$	$-.19202516 \times 10^{-3}$	1.23	$-.95812813 \times 10^{-5}$	$-0.94723775 \times 10^{-5}$	1.15
20	$-.35462848 \times 10^{-3}$	$-.35614695 \times 10^{-3}$	0.426	$.25748446 \times 10^{-5}$	$0.25117150 \times 10^{-5}$	2.51
25	$-.33775979 \times 10^{-3}$	$-.33711603 \times 10^{-3}$	0.201	$.25647253 \times 10^{-5}$	$0.24808875 \times 10^{-5}$	3.38
30	$-.37409606 \times 10^{-3}$	$-.37177997 \times 10^{-3}$	0.623	$.11226868 \times 10^{-5}$	$0.10838695 \times 10^{-5}$	3.58
35	$-.3826795 \times 10^{-3}$	$-.33507153 \times 10^{-3}$	0.954	$.26137679 \times 10^{-6}$	$0.21727006 \times 10^{-6}$	7.31

TABLE 5

Comparison of Second and Third Order Results
$k = 0.5$, $\epsilon = 0.25$

	Z_{01}			Z_{02}	
Time	Second	Third	% Dev	Second	Third
0	$0.78952347 \times 10^{-1}$	$0.78952347 \times 10^{-1}$	0.0	0.0	0.0
5	$0.22993276 \times 10^{-1}$	$.22987347 \times 10^{-1}$	0.026	$0.34944769 \times 10^{-3}$	$0.33626417 \times 10^{-3}$
10	$0.45308043 \times 10^{-2}$	$.45328011 \times 10^{-2}$	0.044	$0.58144960 \times 10^{-4}$	$-0.64013374 \times 10^{-4}$
15	$0.31100715 \times 10^{-2}$	$.31371019 \times 10^{-2}$	0.861	$0.73193859 \times 10^{-5}$	$0.26057195 \times 10^{-4}$

TABLE 6

Summary of Stable Cases

Case	Order of System Used	k	ϵ
I	Second	0.5	0.025
II	Second	0.5	0.04
III	Second	0.5	0.1
IV	Second	0.5	0.25
V	Third	0.5	0.25
VI	Third	0.5	0.40
VII	Second	1.0	0.1
VIII	Second	1.0	0.2
IX	Second	0.375	0.05
X	Second	0.35	0.175

TABLE 7

Comparison of Numerical Results with Theoretical Results of Gary and Gorman, k = 0.5

ϵ	γ_N		$\int_{-\infty}^{\infty} f_o^{(2)}(v, t)\, v^2\, dv$	
	Numerical	Theoretical	Numerical	Theoretical
0.025	$\gtrsim$ .11	.0995	0.00125	0.00125
0.04	.08	.0850	0.0032	0.0032
0.10	.048	.0449	0.020	0.020
0.25	0.0	--	0.125	0.125
0.4	0.0	--	0.320	0.32

REFERENCES

Armstrong, T., and D. Montgomery, Non-Uniform Plasma Equilibria and the Penrose Stability Law, to be published, 1966.

Backus, G., Linearized Plasma Oscillations in an Arbitrary Electron Velocity Distribution, Journal of Mathematical Physics, 1, 178-191, 1960.

Bernstein, I., J. Greene, and M. Kruskal, Exact Non-Linear Plasma Oscillations, Phys. Rev., 108, 546-550, 1957.

Bodner, S., and E. Frieman, The Quasi-Linear Theory of Plasma Oscillations and Instabilities, Propagation and Instabilities in Plasmas, ed. W. I. Futterman, Stanford University Press, 1963.

Buneman, O., Dissipation of Currents in Ionized Media, Phys. Rev., 115, 503-517, 1959.

_____. Maintenance of Equilibrium by Instabilities, J. Nucl. Energy, Part C, Plasma Physics, 119, 1963.

Burger, P., Theory of Large-Amplitude Oscillations in the One-Dimensional Low Pressure Cesium Thermionic Converter, J. Appl. Phys., 36, 1938, 1965.

Dawson, J., Nonlinear Electron Oscillations in a Cold Plasma, Phys. Rev., 113, 383-387, 1959.

Dawson, J., One Dimensional Plasma Model, Phys. Fluids, 5, 445-459, 1962.

Dawson, J., On Landau Damping, Phys. Fluids, 4, 869-874, 1961.

Drummond, W. E., and D. Pines, Non-Linear Stability of Plasma Oscillations, Nuclear Fusion, Pt. 3, 1049-1057, 1962 Sup.

Engelmann, F., M. Feix, E. Minardi, and J. Oxenius, Non-Linear Effects from Vlasov's Equation, Phys. Fluids, 6, 266-275, 1963.

Gartenhaus, S., Particle Dynamics in a Bounded Region, Phys. Fluids, 6, 451-452, 1963.

Gary, S. P., Third Order Oscillations in a Maxwellian Plasma, to be published, 1966.

Gill, S., A Process for the Step Integration of Differential in an Automatic Digital Computing Machine, Proc. Camb. Phil. Soc., 47, 96-108, 1951.

Hayes, J. N., Damping of Plasma Oscillations in the Linear Theory, Phys. Fluids, 4, 1387-1392, 1961.

Jackson, D., Fourier Series and Orthogonal Polynomials, Open Court Publ. Co., La Salle, Illinois, 1961.

Jackson, J. D., Longitudinal Plasma Oscillations, J. Nuc. Energy, Pt. C., 1, 171-189, 1960.

Kellogg, P. J., Some Properties of the Two Stream Instability at Large Amplitudes, Phys. Fluids, 8, 102-110, 1965.

Knorr, G., Beiträge zür Lösung der Nichtlinearen Vlasov-Gleichung, Thesis, Max Planck Institut für Physik und Astrophysik, München, 1963a.

Knorr, G., Zür Lösung der Nicht-linearen Vlasov-Gleichung, Zeits. für Naturforschung, 18a, 1304-1315, 1963b.

Krall, N., and M. Rosenbluth, Stability of a Slightly Inhomogeneous Plasma, Phys. Fluids, 4, 163-172, 1961.

Landau, L., On the Vibrations of the Electronic Plasma, J. Phys. USSR, X, 25-34, 1946.

Low, F., Persistence of Stability in Lagrangian Systems, Phys. Fluids, 4, 842-846, 1961.

Montgomery, D., Comments on "Non-Linear Landau Damping of Oscillations in a Bounded Plasma", Phys. Fluids, 7, 447-448, 1964.

_____. Stability of Large Amplitude Waves in the One-Dimensional Plasma, Phys. Fluids, 3, 274-277, 1960.

Montgomery, D., and D. Gorman, Boltzmann-Vlasov Equation in a Bounded Region, Phys. Fluids, 5, 947-949, 1962.

Montgomery, D., and D. Tidman, Plasma Kinetic Theory, McGraw-Hill, New York, 1964.

O'Neil, T., Collisionless Damping of Non-Linear Plasma Oscillations, Phys. Fluids, 8, 2255-2262, 1965.

Pearlstein, L., Longitudinal Instability in a Semi-Infinite Inhomogeneous Plasma, Phys. Fluids, 7, 1461-1467, 1964.

Penrose, O., Electrostatic Instabilities of a Uniform Non-Maxwellian Plasma, Phys. Fluids, 3, 258-265, 1960.

Saenz, A. W., Long-Time Behavior of the Electric Potential and Stability in Linearized Vlasov Theory, J. Math. Phys., 6, 859-875, 1965.

Smith, C., and J. Dawson, Some Computer Experiments with a One-Dimensional Plasma Model (Princeton Plasma Lab Report Matt-151, 1963).

Taylor, E. C., Landau Solution of the Plasma Oscillation Problem, Phys. Fluids, 8, 2250-2254, 1965.

Vedenov, A., E. Velikhov, and R. Sagdeev, Quasi-Linear Theory of Plasma Oscillations, Nuclear Fusion, Pt. 2, 465-475, 1962 Sup.

Weitzner, H., Plasma Oscillations and Landau Damping, Phys. Fluids, 6, 1123-1127, 1963.

Wilhelmsson, H., Stationary Nonlinear Plasma Oscillations, Phys. Fluids, 4, 335-340, 1961.

FIGURE CAPTIONS

Figure 1. Geometry for a plasma slab confined between perfectly reflecting boundaries.

Figure 2. Numerical versus analytic solution of the free streaming equation.

Figure 3. Numerical integration of the linearized Vlasov equation for $k = 0.5$, $\epsilon = 0.1$.

Figure 4. Numerical integration of the second order system for $k = 0.5$, $\epsilon = 0.025$, Case I.

Figure 5. Damping decrement versus time, Case I.

Figure 6. Numerical integration of the second order system for $k = 0.5$, $\epsilon = 0.04$, Case II.

Figure 7. Damping decrement versus time, Case II.

Figures 8a, 8b. Plot of $f_o^{(2)}(v, t)$ and $f_o(v, t)$ for Case II, $t = 20$.

Figures 9a, 9b. Same as Figures 8a, 8b except $t = 35$.

Figure 10. Numerical integration of the second order system for $k = 0.5$, $\epsilon = 0.1$, Case III.

Figure 11. Damping decrement versus time for Case III.

Figures 12a, 12b. Plot of $f_o^{(2)}(v, t)$ and $f_o(v, t)$ for Case III, $t = 10$.

Figures 13a, 13b. Same as Figures 12a, 12b except $t = 20$.

Figures 14a, 14b. Same as Figures 12a, 12b except t = 30.

Figure 15. Numerical integration of the second order system for $k = 0.5$, $\epsilon = 0.25$, Case IV.

Figure 16. Damping decrement versus time for Case IV.

Figures 17a, 17b. Plot of $f_o^{(2)}(v, t)$ and $f_o(v, t)$ for Case IV, $t = 5.0$.

Figures 18a, 18b. Same as Figures 17a, 17b except t = 10.0.

Figures 19a, 19b. Same as Figures 17a, 17b except t = 15.0.

Figure 20. Numerical integration of third order system for $k = 0.5$, $\epsilon = 0.25$, Case V.

Figure 21. Numerical integration of third order system for $k = 0.5$, $\epsilon = 0.4$, Case VI.

Figure 22. Plot of the damping decrement versus time, Case VI.

Figure 23. Numerical integration of second order system for $k = 1.0$, $\epsilon = 0.1$, Case VII.

Figure 24. Numerical integration of second order system for $k = 1.0$, $\epsilon = 0.2$, Case VIII.

Figure 25. Damping decrement versus time for Case VIII.

Figure 26. Numerical integration of second order system for $k = 0.375$, $\epsilon = 0.05$, Case IX.

Figure 27. Numerical integration of second order system for $k = 0.35$, $\epsilon = 0.175$, Case X.

Figure 28. Damping decrement versus time for Case X.

"SLAB" GEOMETRY

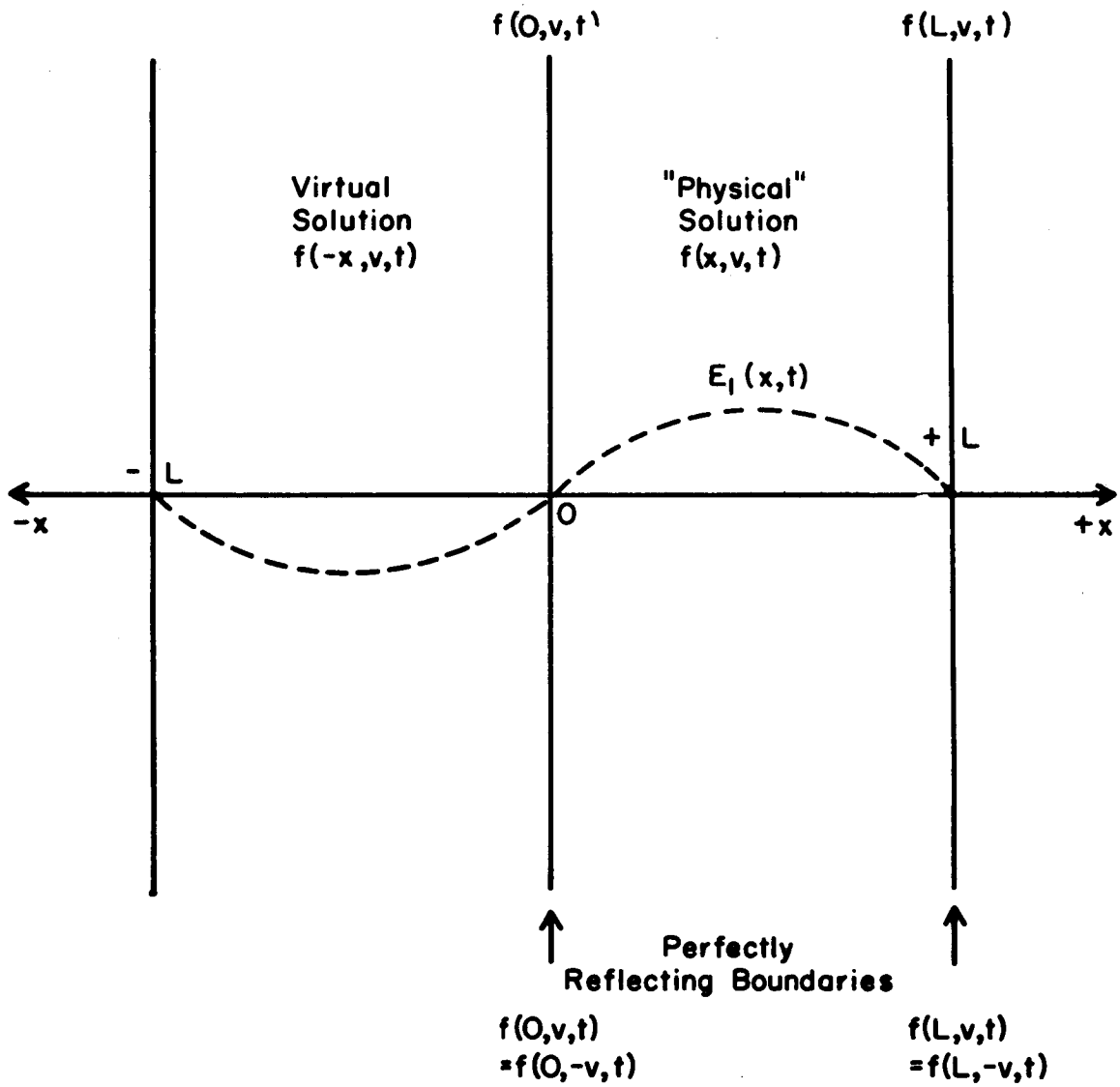

Figure 1

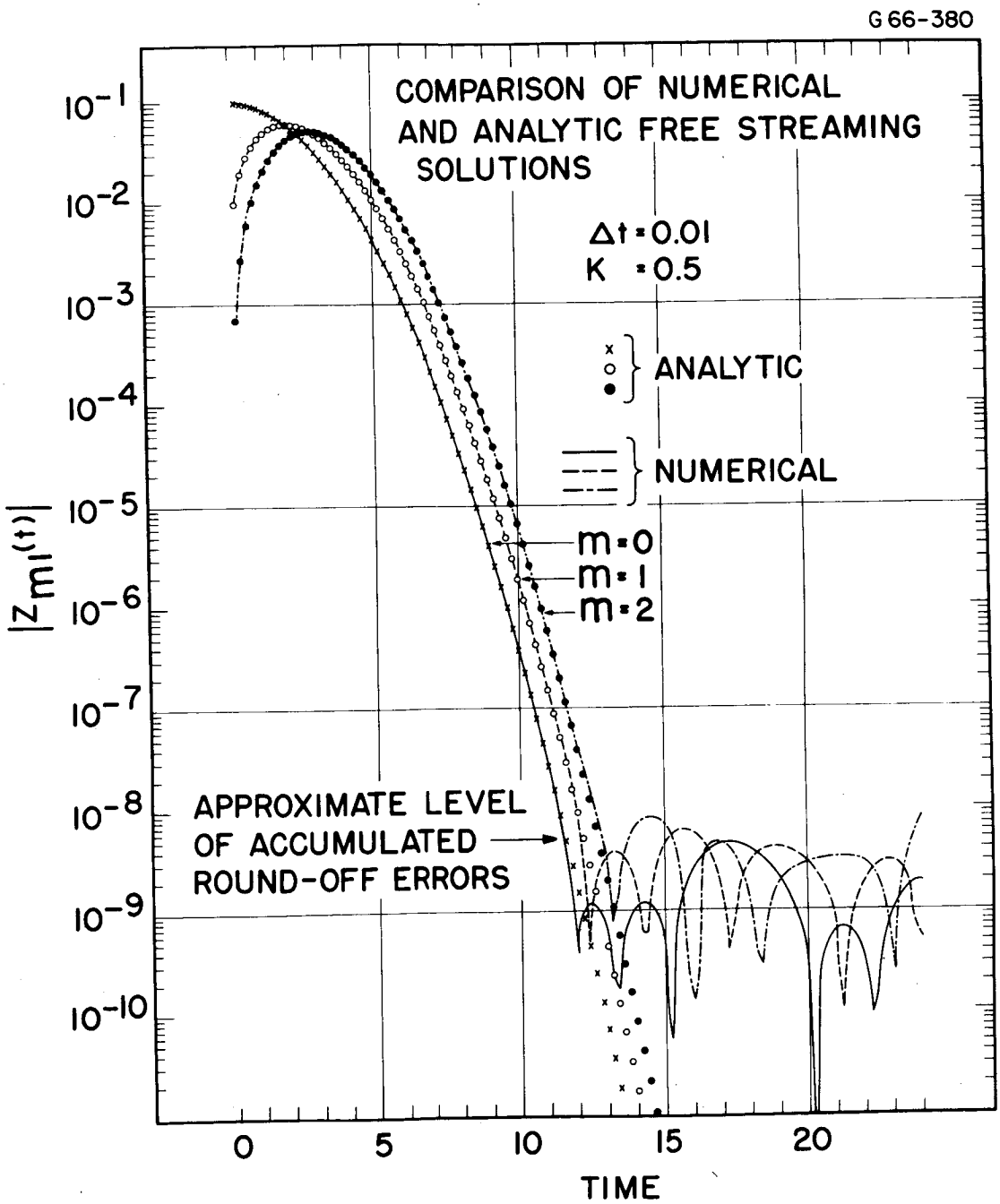
G 66-380
COMPARISON OF NUMERICAL AND ANALYTIC FREE STREAMING SOLUTIONS
Δt = 0.01
K = 0.5
ANALYTIC
NUMERICAL
m = 0
m = 1
m = 2
APPROXIMATE LEVEL OF ACCUMULATED ROUND-OFF ERRORS
$|Z_{ml}^{(t)}|$
10^{-1}
10^{-2}
10^{-3}
10^{-4}
10^{-5}
10^{-6}
10^{-7}
10^{-8}
10^{-9}
10^{-10}
0
5
10
15
20
TIME

Figure 2

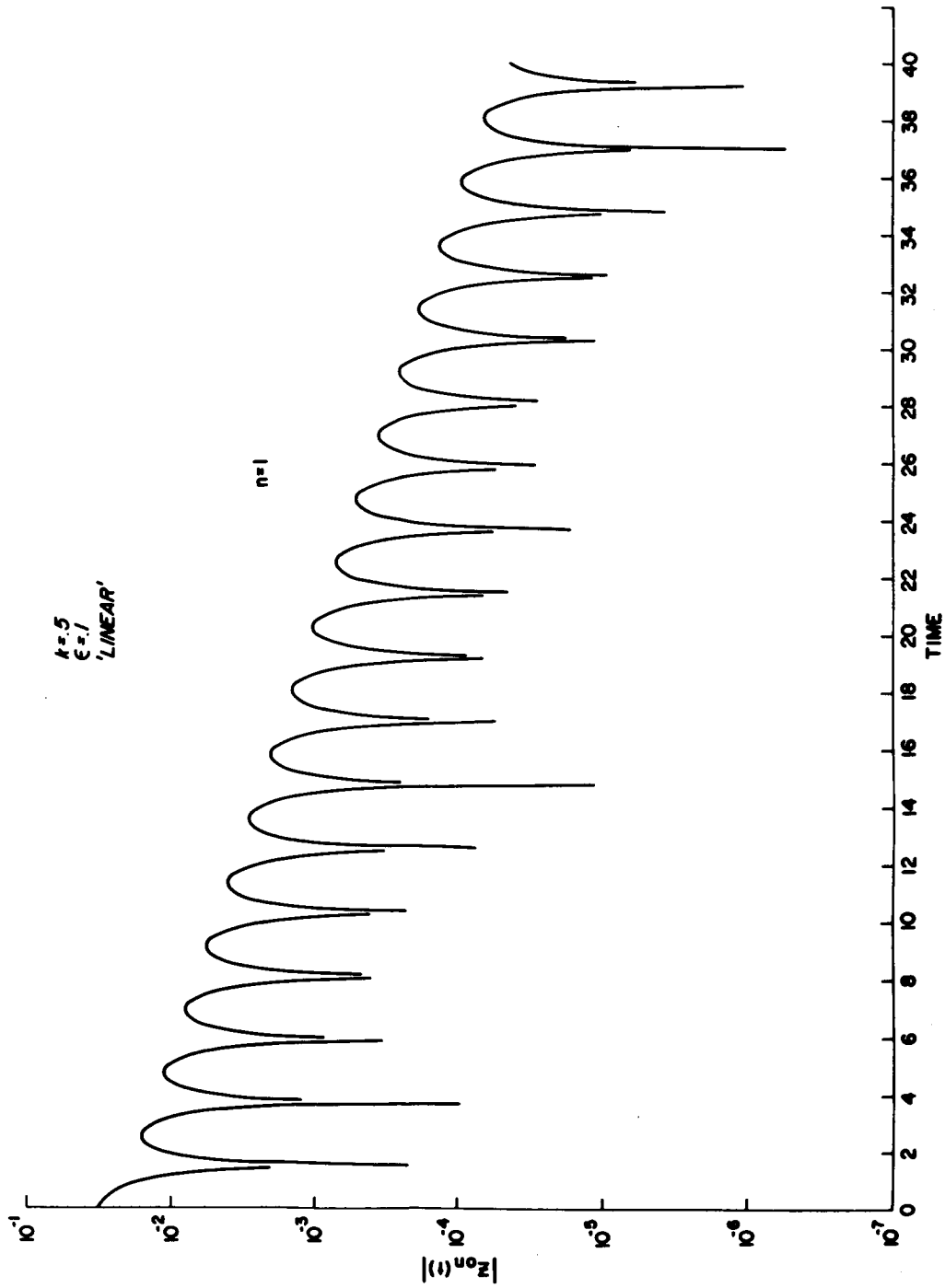
k=.5
ε=.1
'LINEAR'
n=1
10^{-1}
10^{-2}
10^{-3}
10^{-4}
10^{-5}
10^{-6}
10^{-7}
$|\tilde{n}_{on}(t)|$
0
2
4
6
8
10
12
14
16
18
20
22
24
26
28
30
32
34
36
38
40
TIME

Figure 3

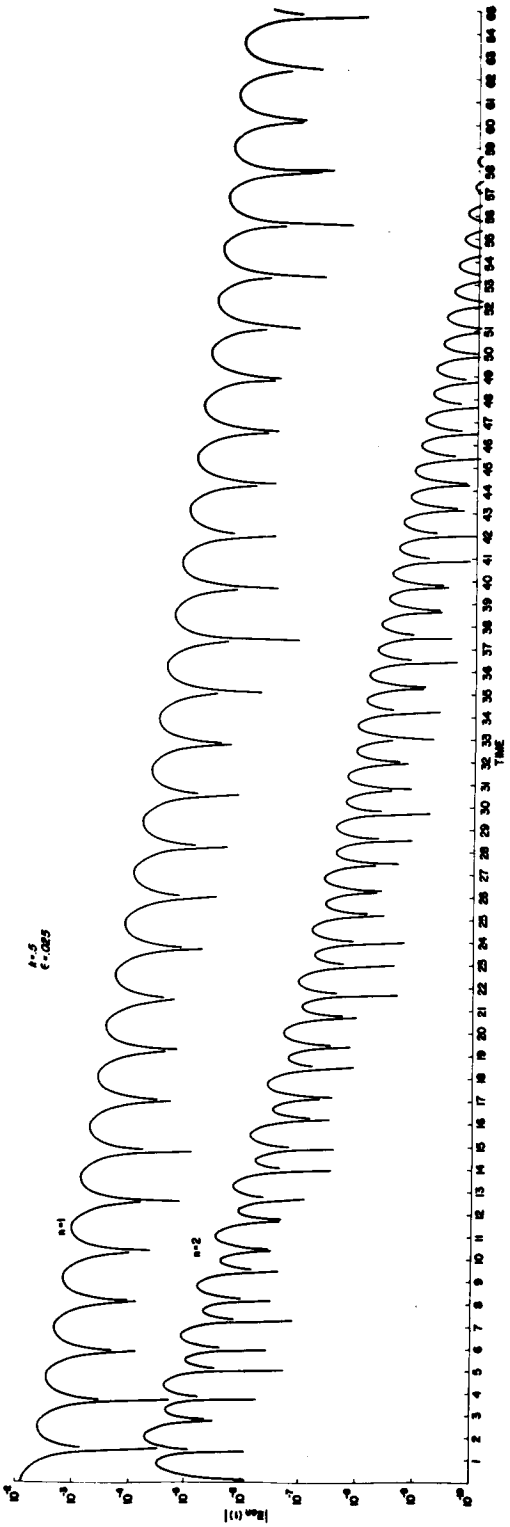

Figure 4

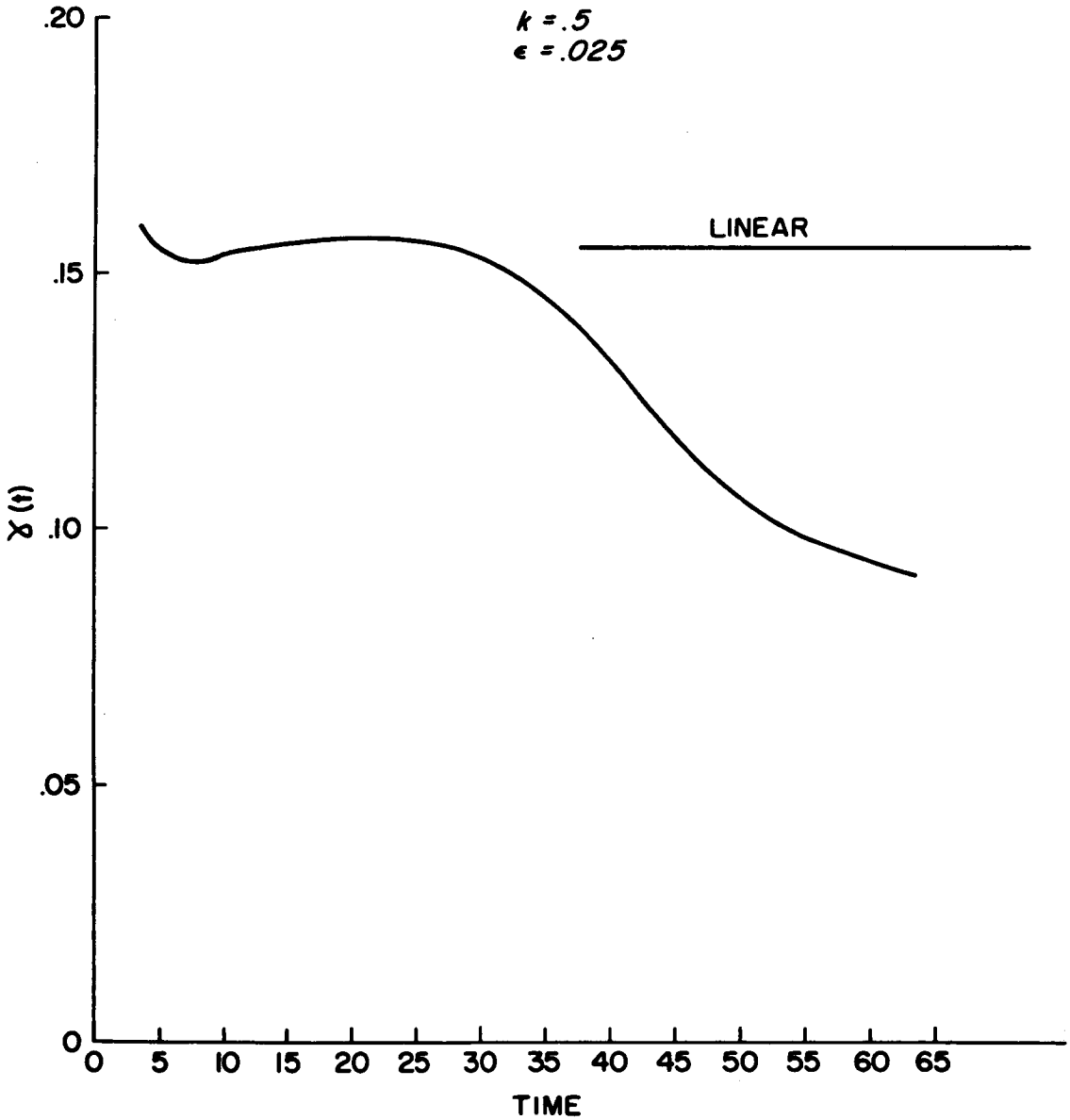
k = .5
ε = .025
LINEAR
.20
.15
.10
.05
0
γ(ε)
0
5
10
15
20
25
30
35
40
45
50
55
60
65
TIME

Figure 5

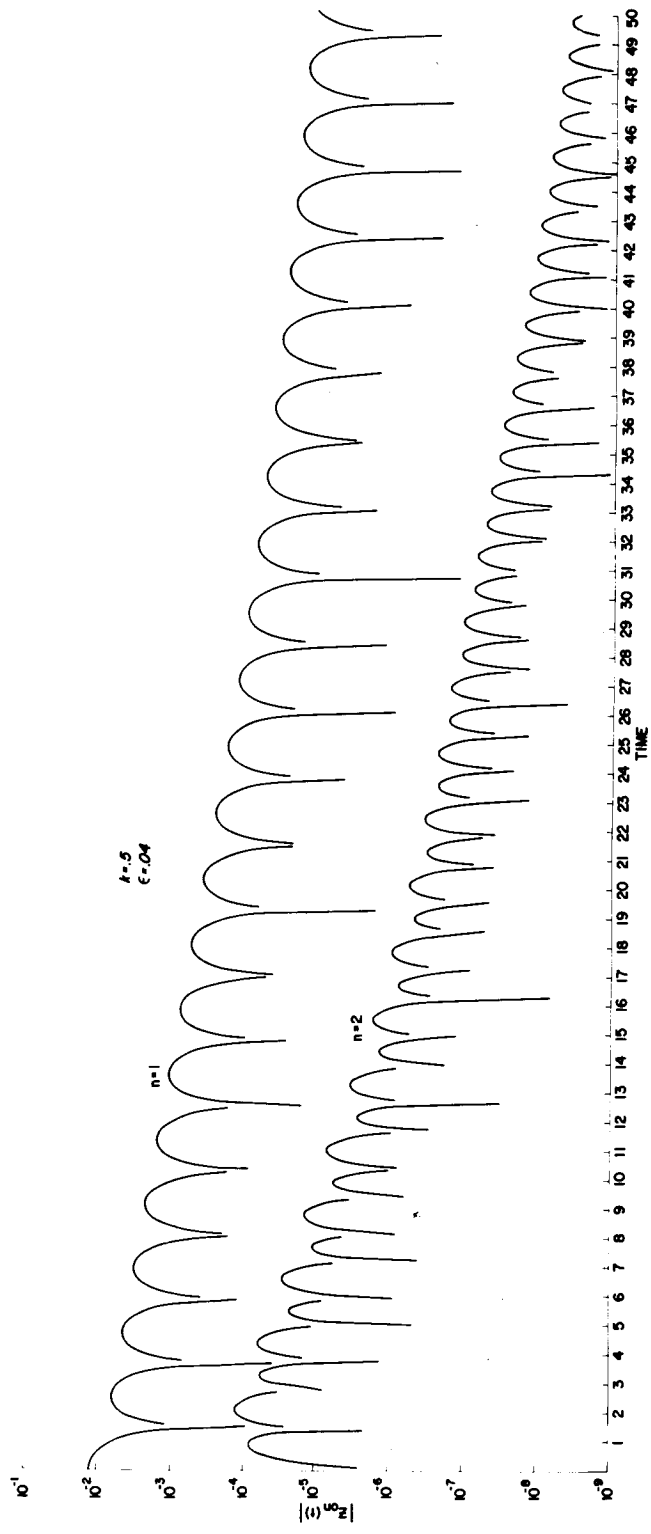

Figure 6

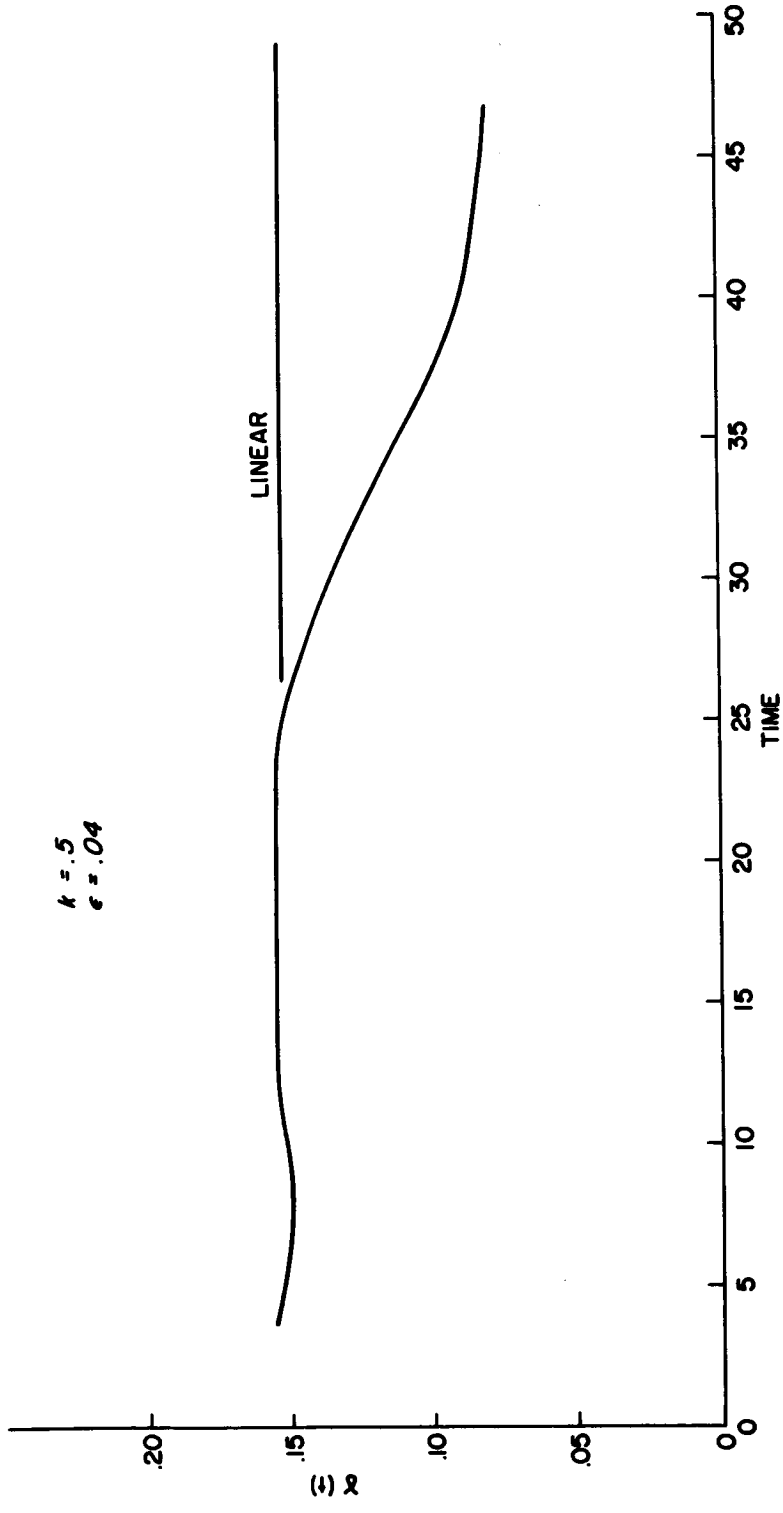

Figure 7

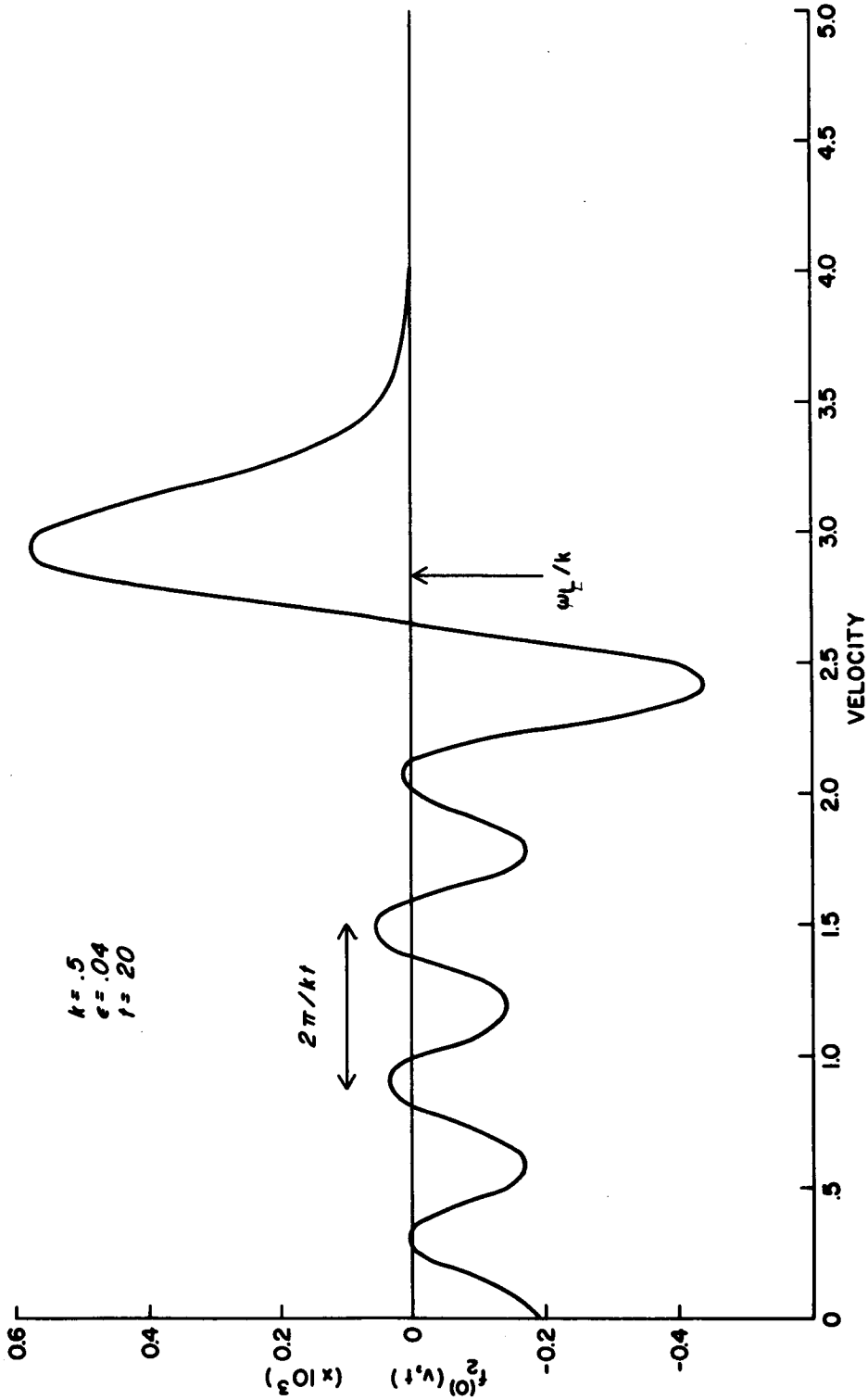
k = .5
ε = .04
t = 20
2π/kl
ω_L/k
VELOCITY
0
.5
1.0
1.5
2.0
2.5
3.0
3.5
4.0
4.5
5.0
0.6
0.4
0.2
0
-0.2
-0.4
f₂⁽⁰⁾(v,t) (x 10³)

Figure 8a.

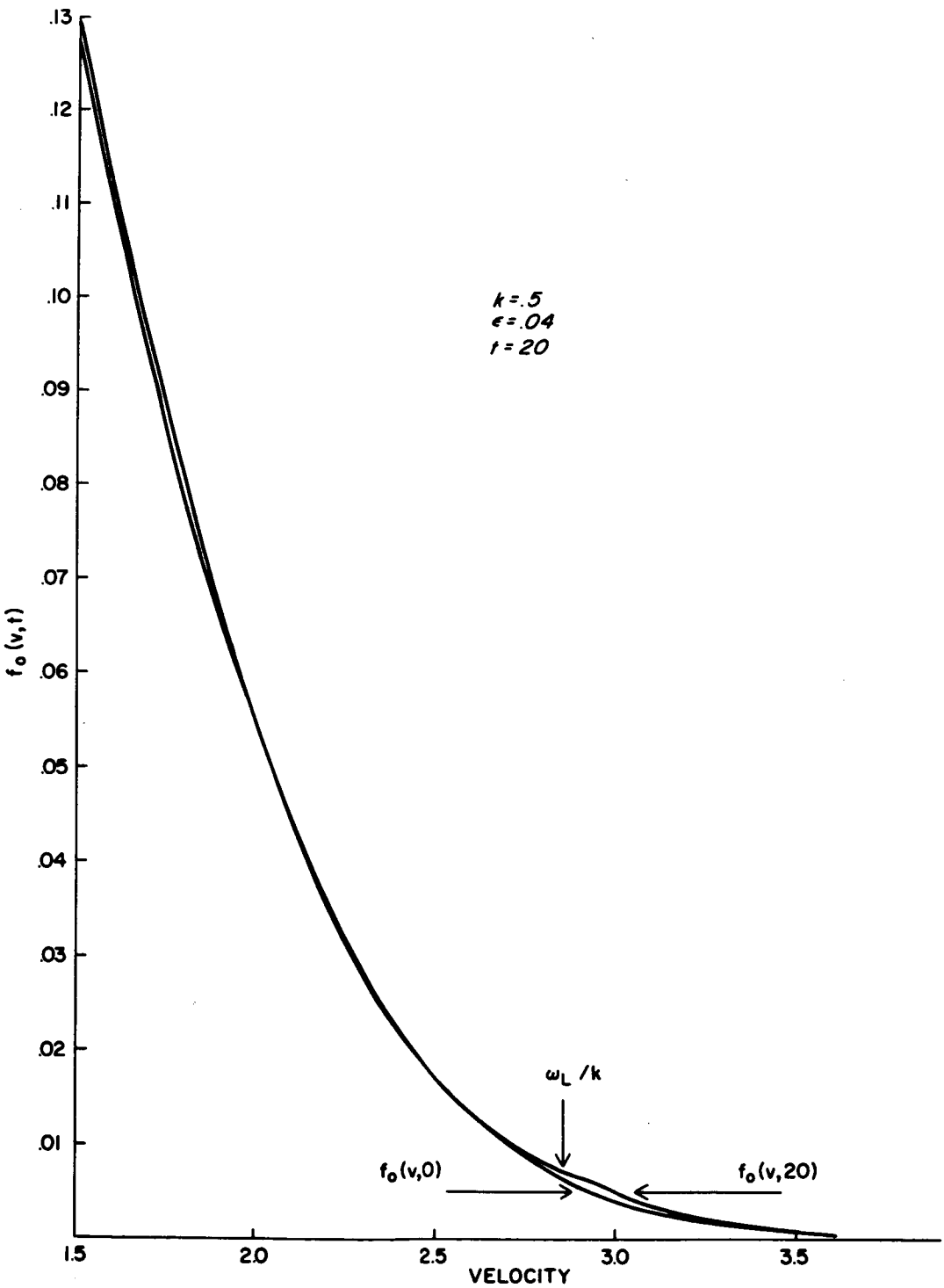
.13
.12
.11
.10
.09
.08
.07
.06
.05
.04
.03
.02
.01
$f_0(v,t)$
$k = .5$
$\epsilon = .04$
$t = 20$
ω_L / k
$f_0(v,0)$
$f_0(v,20)$
1.5
2.0
2.5
3.0
3.5
VELOCITY

Figure 8b.

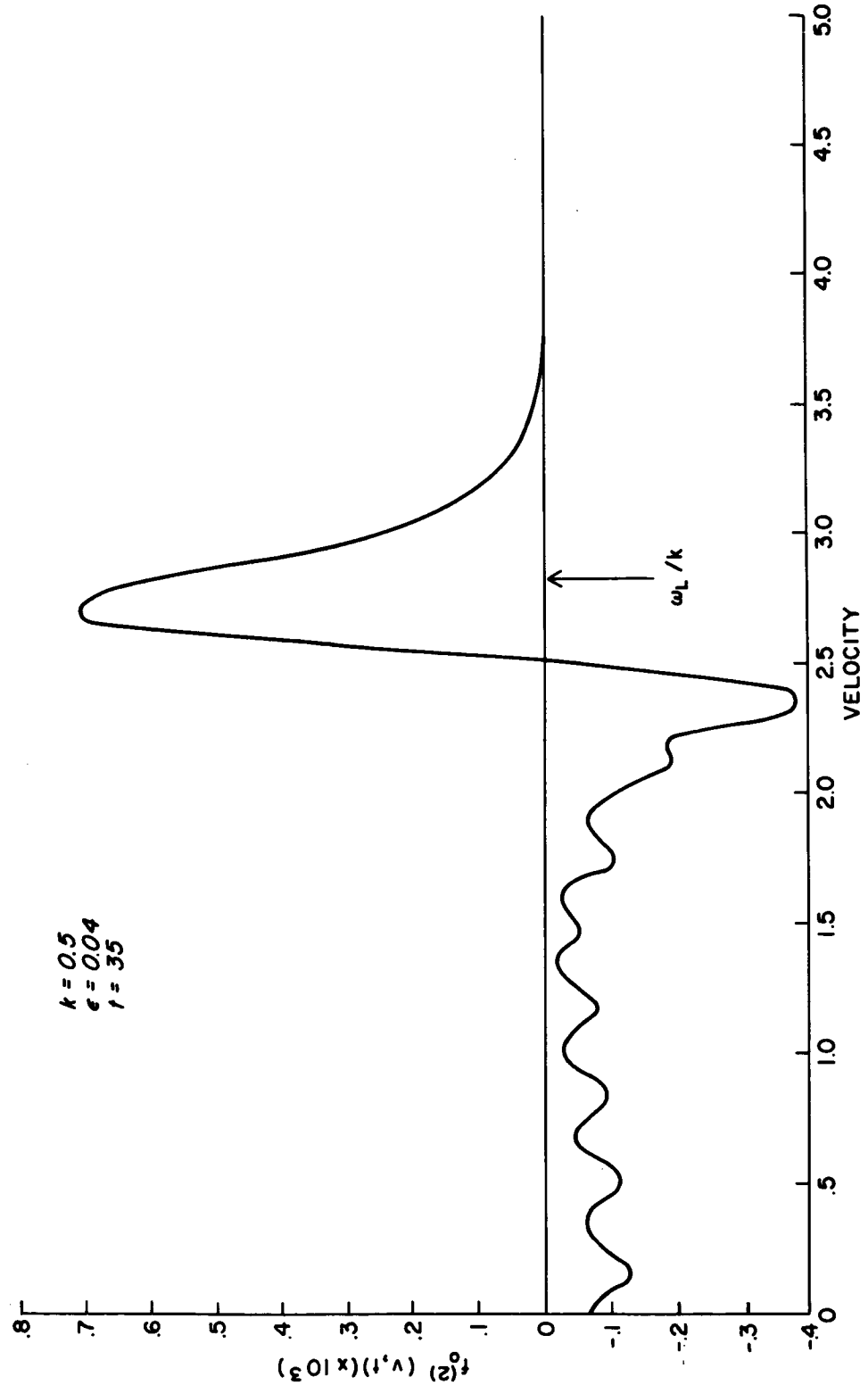
k = 0.5
ε = 0.04
t = 35
ω_L/k
VELOCITY
$f_0^{(2)}(v,t)(\times 10^3)$
.8
.7
.6
.5
.4
.3
.2
.1
0
-.1
-.2
-.3
-.4
0
.5
1.0
1.5
2.0
2.5
3.0
3.5
4.0
4.5
5.0

Figure 9a.

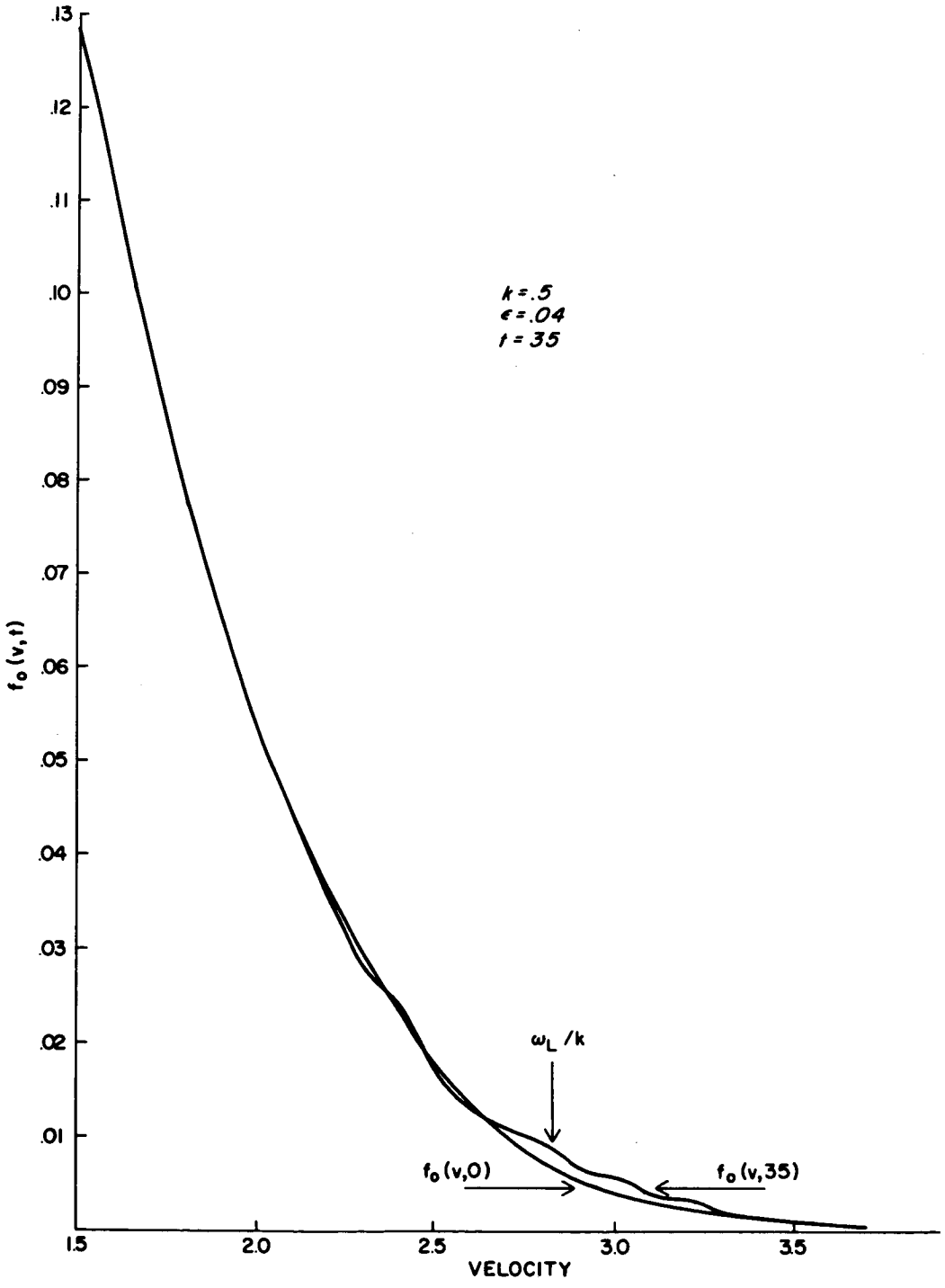
.13
.12
.11
.10
.09
.08
.07
.06
.05
.04
.03
.02
.01
$f_o(v,t)$
k = .5
ε = .04
t = 35
ω_L/k
$f_o(v,0)$
$f_o(v,35)$
1.5
2.0
2.5
3.0
3.5
VELOCITY

Figure 9b.

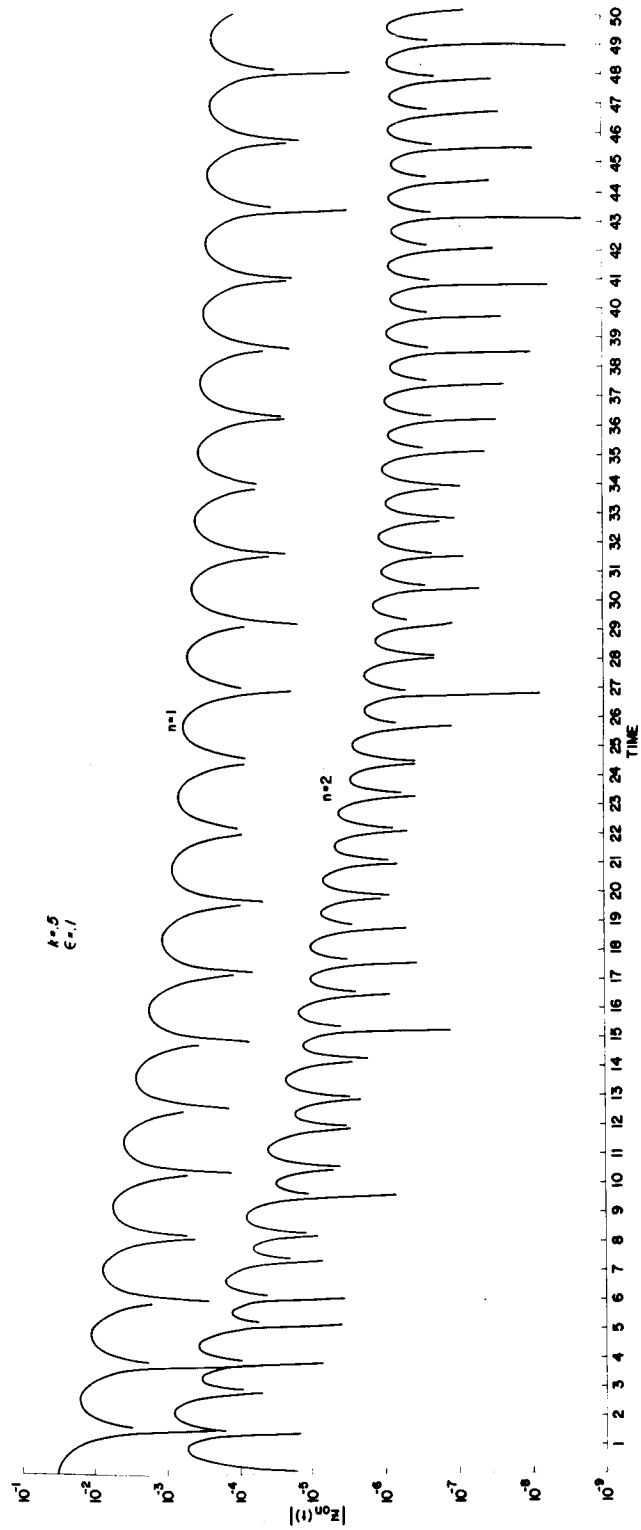

Figure 10

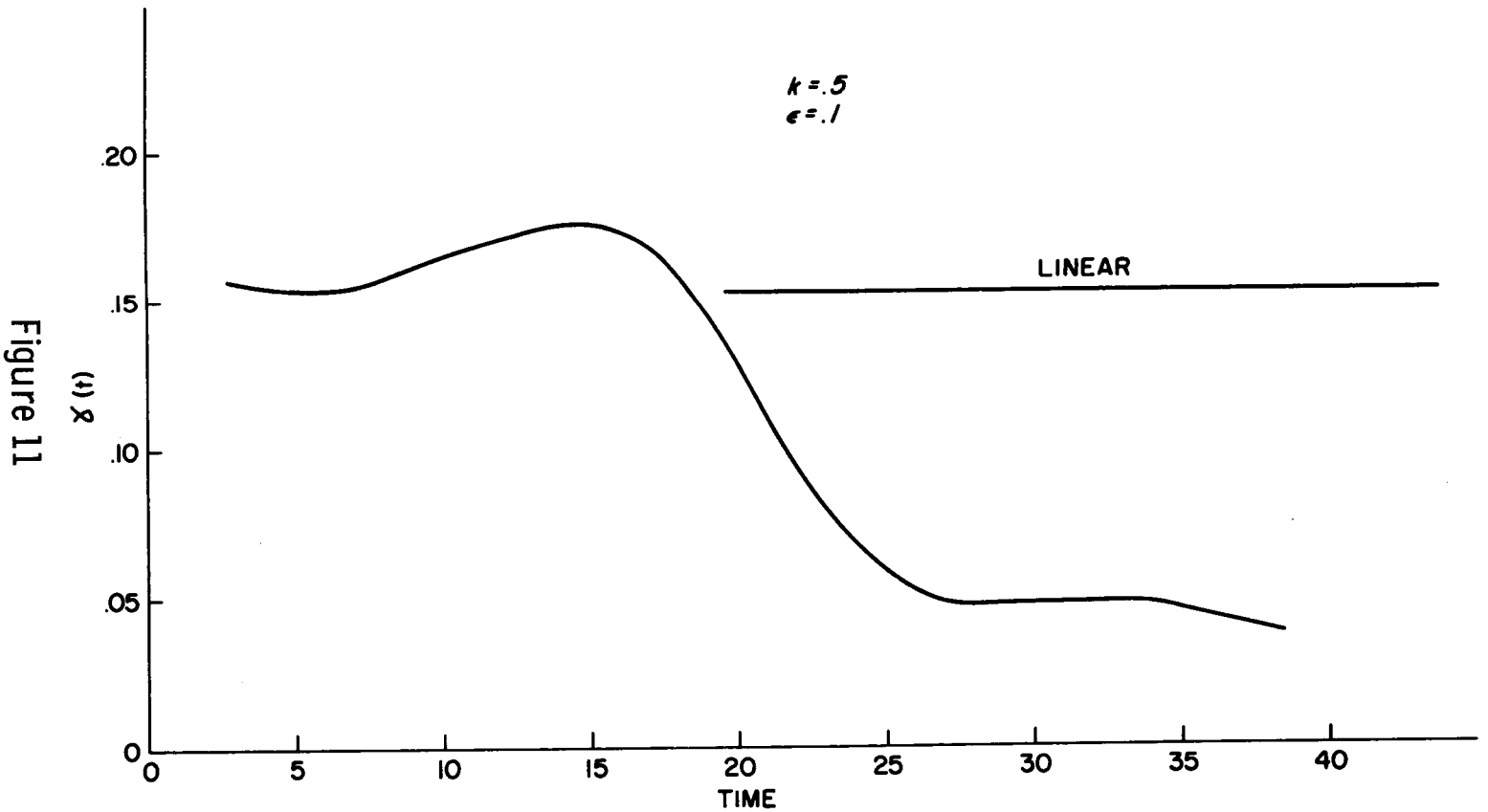

Figure 11

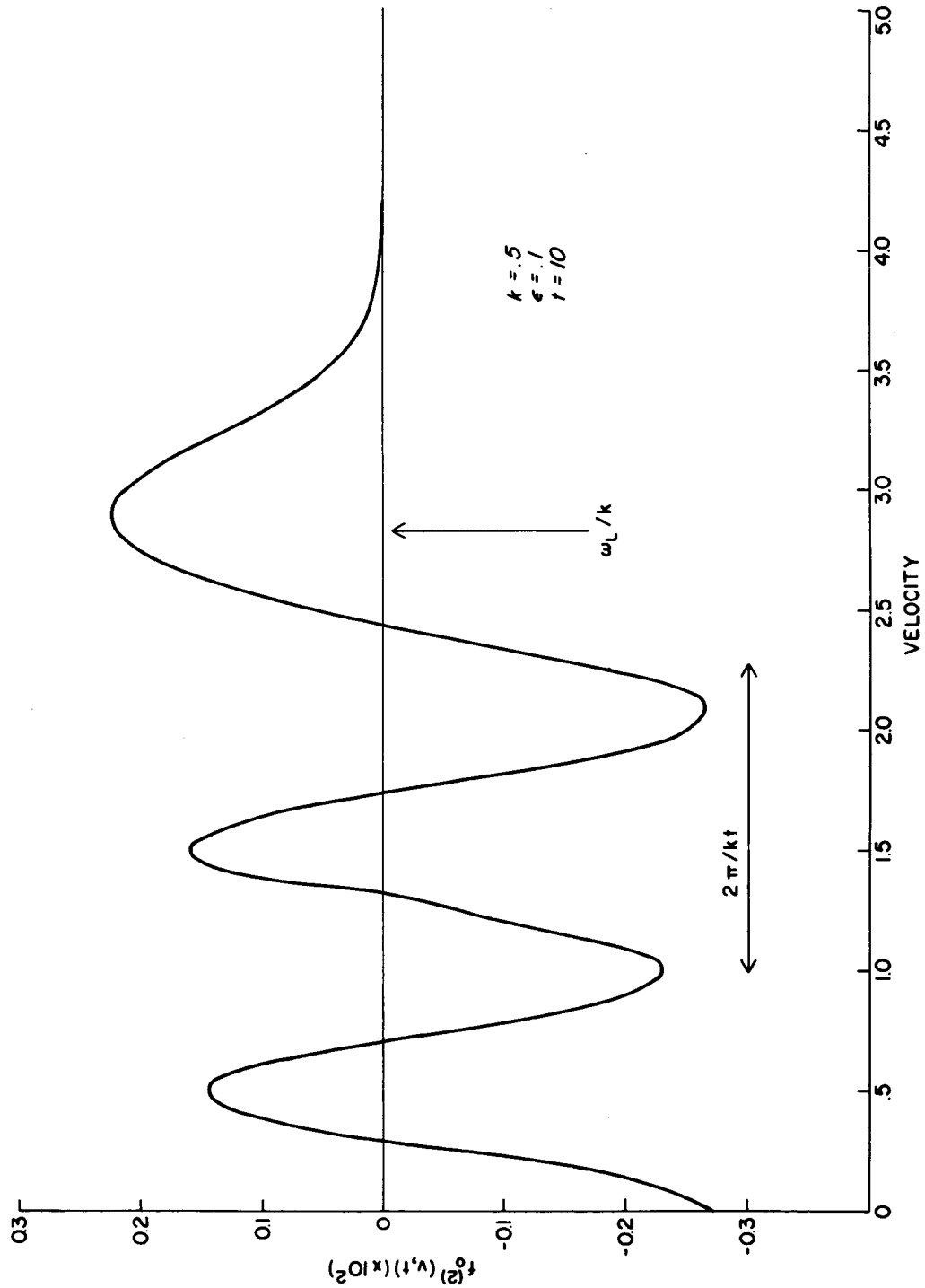
k = .5
ε = .1
t = 10
ω_L / k
2π/kt
VELOCITY
0
.5
1.0
1.5
2.0
2.5
3.0
3.5
4.0
4.5
5.0
0.3
0.2
0.1
0
-0.1
-0.2
-0.3
f_0^(2) (v,t) (x 10^2)

Figure 12a.

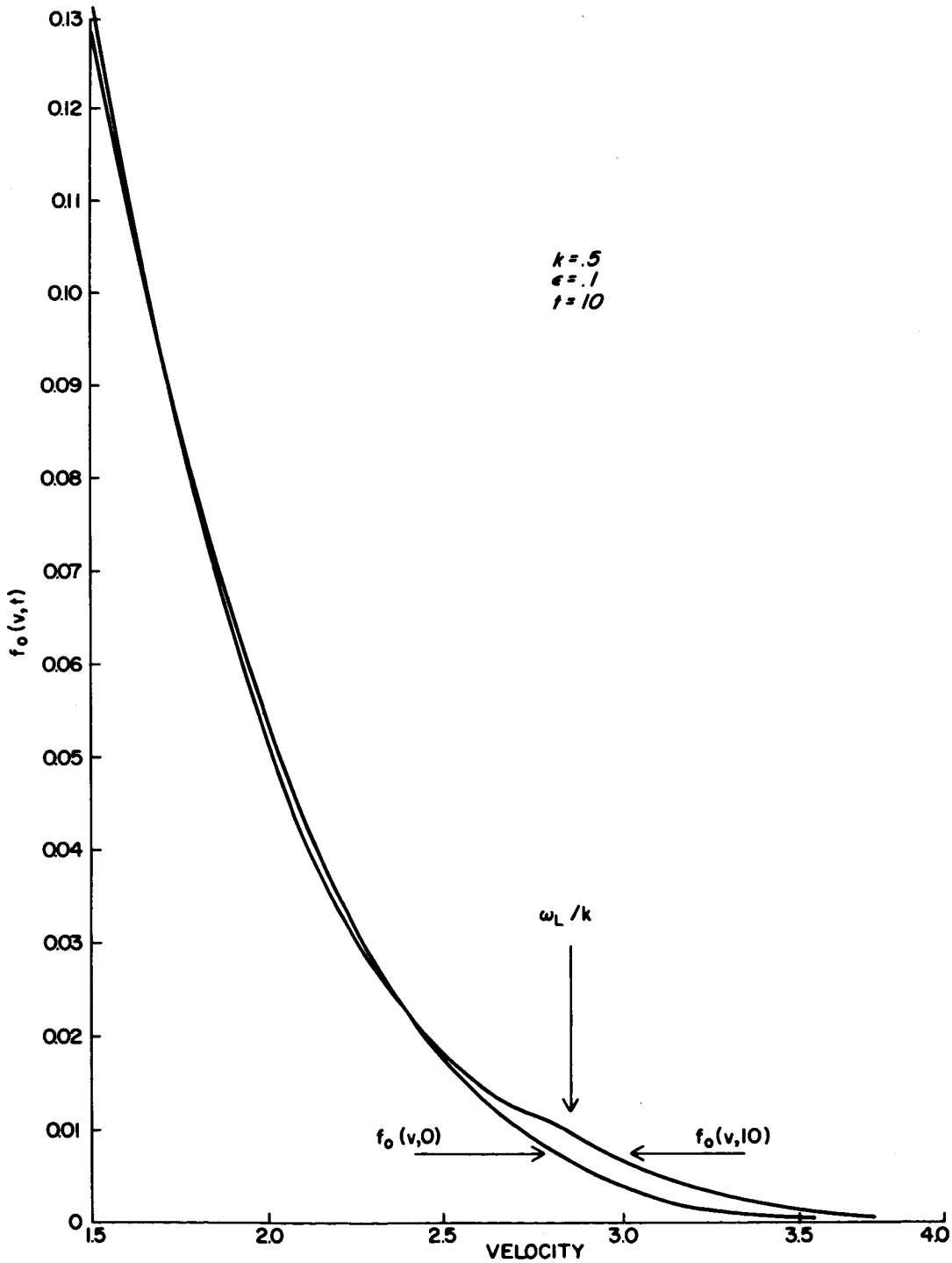
0.13
0.12
0.11
0.10
0.09
0.08
0.07
0.06
0.05
0.04
0.03
0.02
0.01
0
$f_0(v,t)$
k=.5
ε=.1
t=10
ω_L/k
$f_0(v,0)$
$f_0(v,10)$
1.5
2.0
2.5
3.0
3.5
4.0
VELOCITY

Figure 12b.

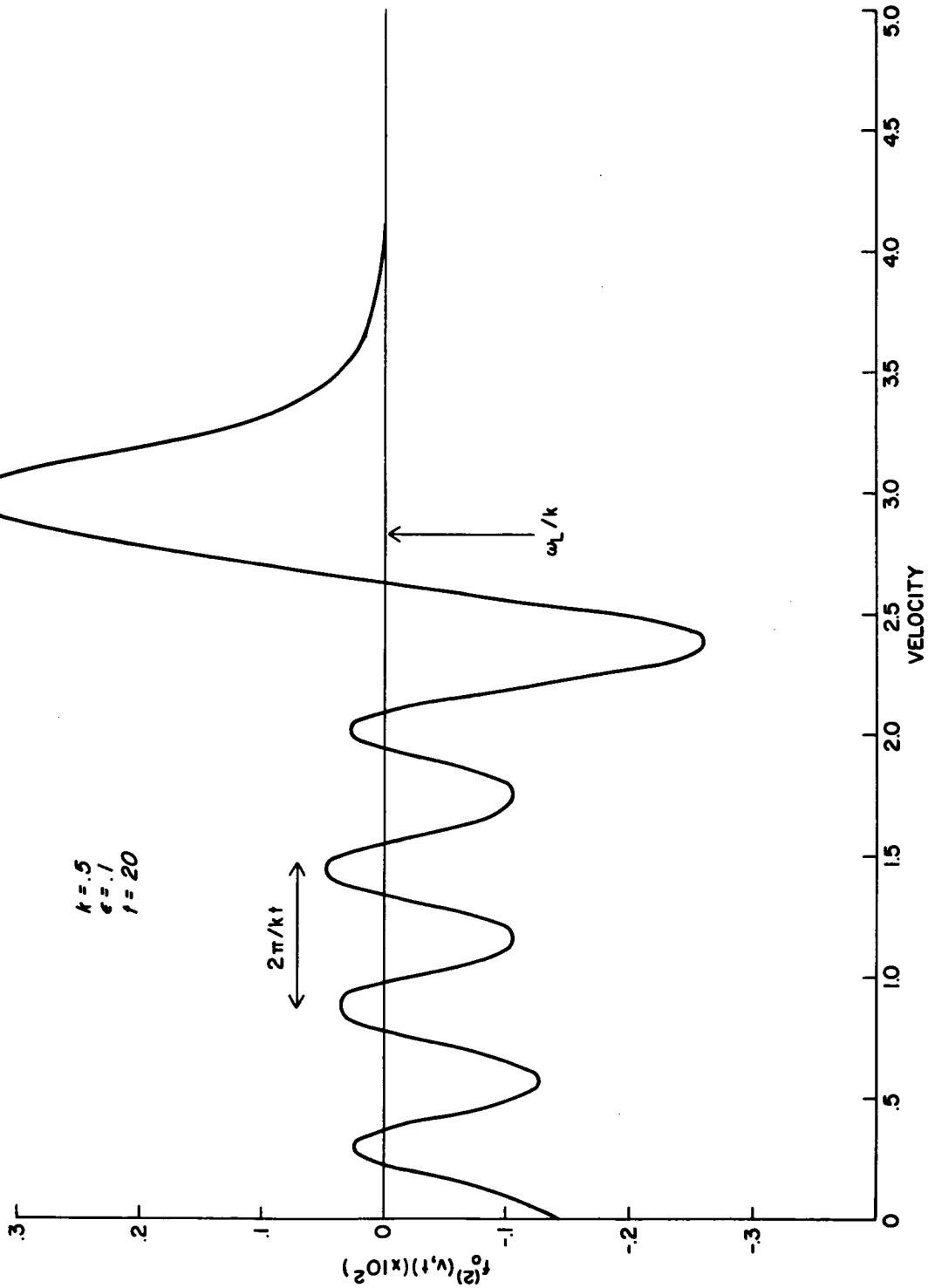
k = .5
ε = .1
t = 20
2π/kt
ω_L/k
f₀⁽²⁾(v,t)(x10²)
VELOCITY
.3
.2
.1
0
-.1
-.2
-.3
0
.5
1.0
1.5
2.0
2.5
3.0
3.5
4.0
4.5
5.0

Figure 13a.

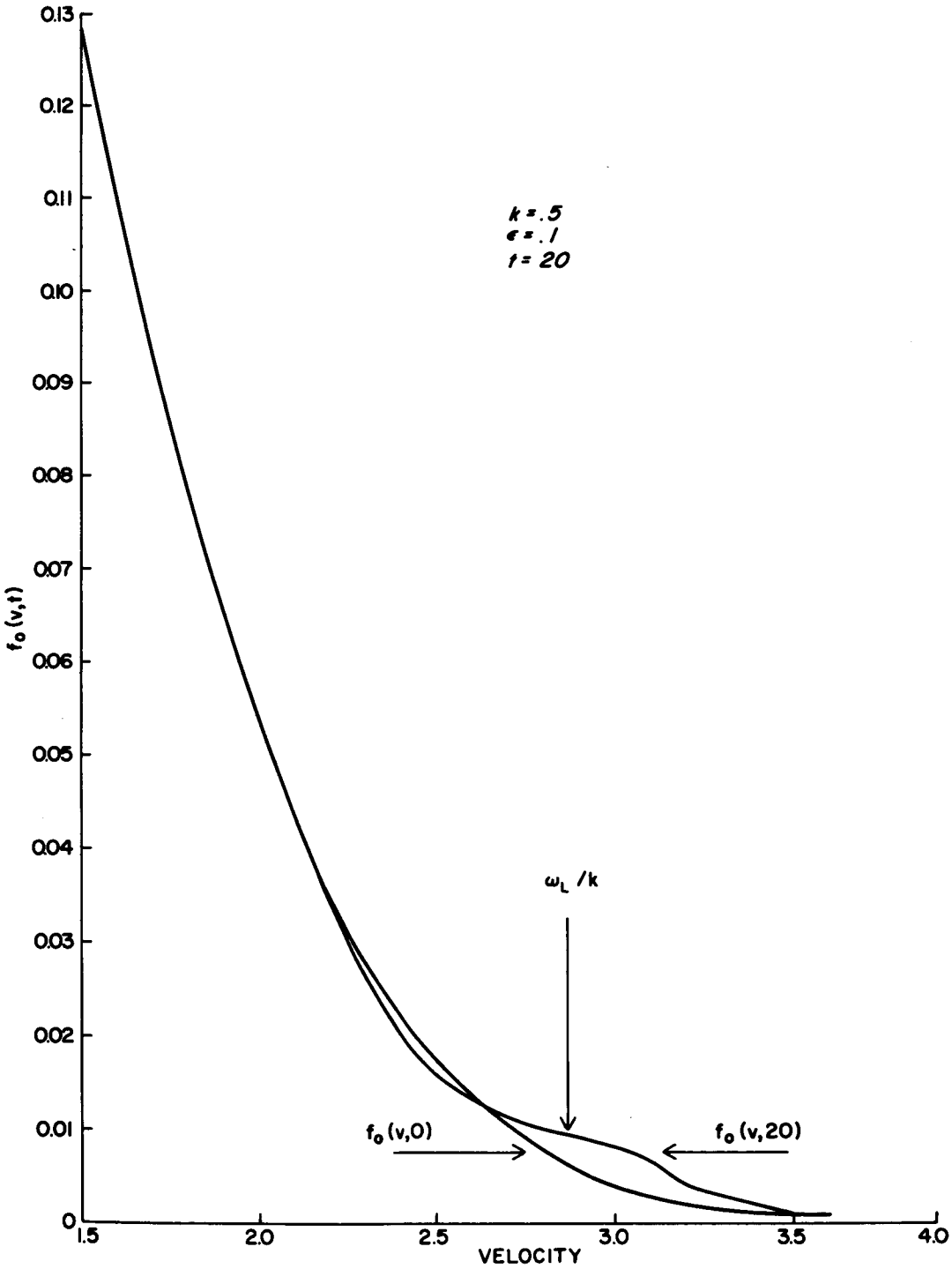
k = .5
ε = .1
t = 20
0.13
0.12
0.11
0.10
0.09
0.08
0.07
0.06
0.05
0.04
0.03
0.02
0.01
0
f₀(v,t)
ω_L /k
f₀(v,0)
f₀(v,20)
1.5
2.0
2.5
3.0
3.5
4.0
VELOCITY

Figure 13b.

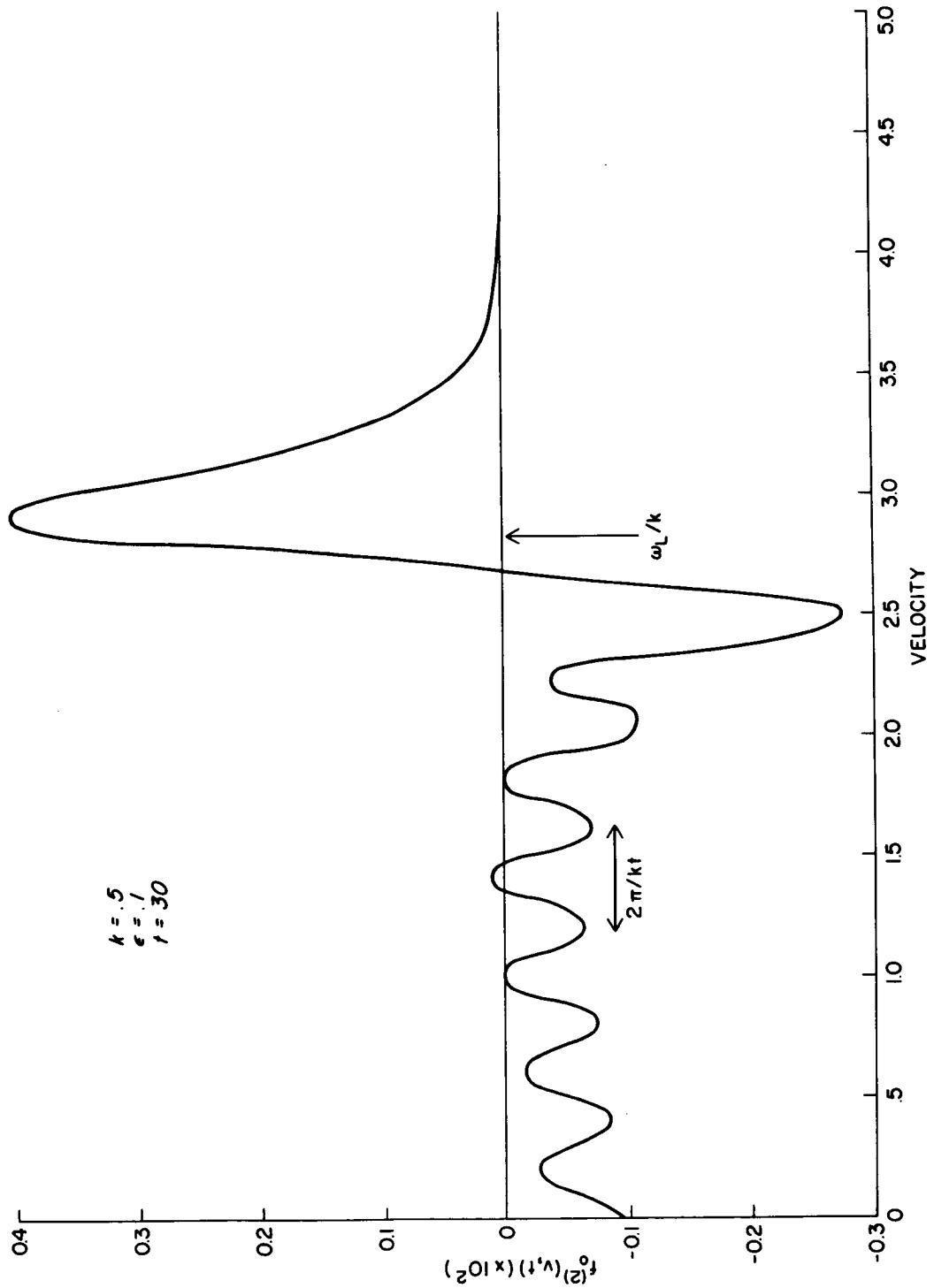
k = .5
ε = .1
t = 30
ω_L/k
$2\pi/kt$
VELOCITY
$f_0^{(2)}(v,t)$ (x 10^2)
0.4
0.3
0.2
0.1
0
-0.1
-0.2
-0.3
0
.5
1.0
1.5
2.0
2.5
3.0
3.5
4.0
4.5
5.0

Figure 14a.

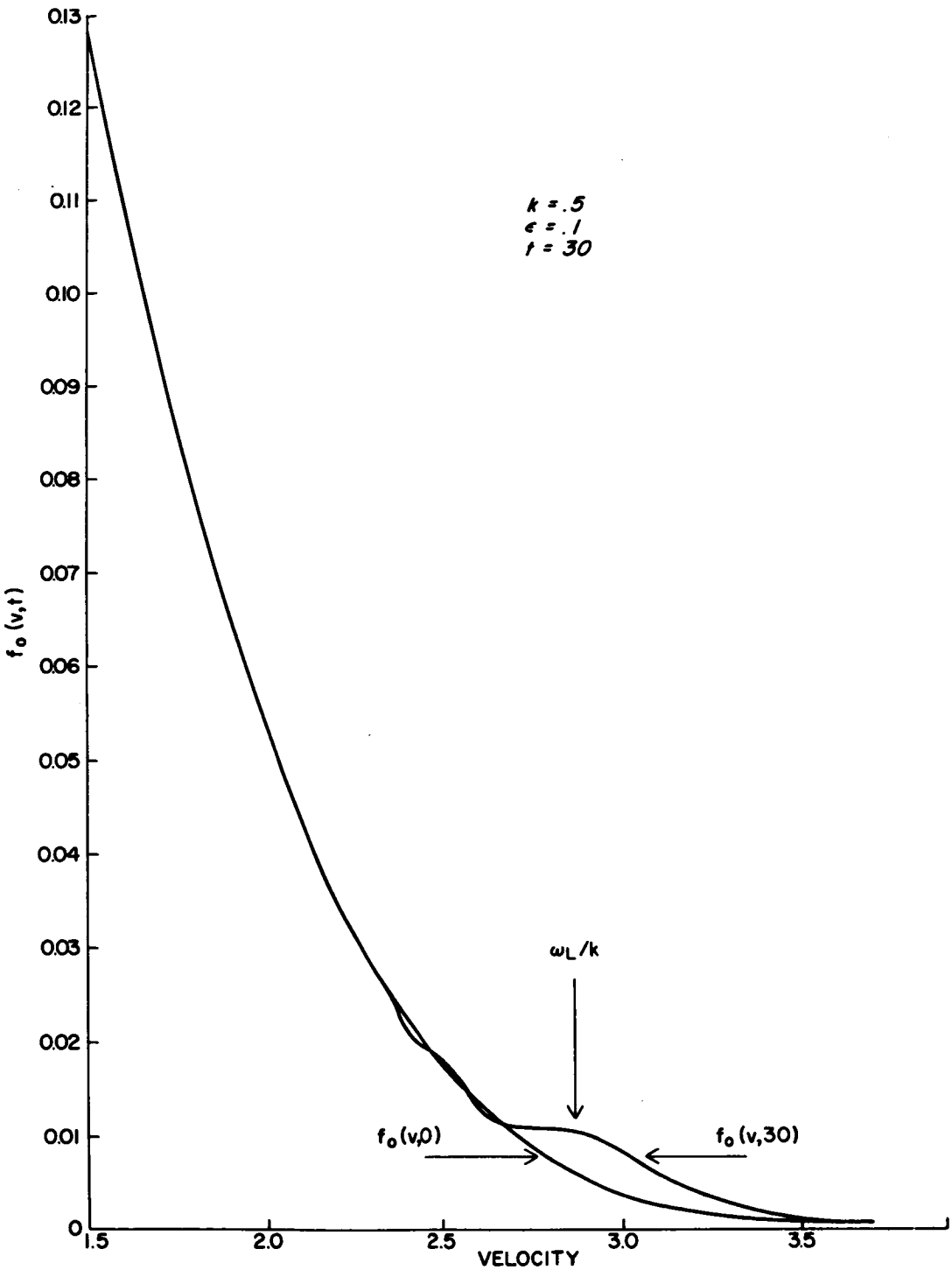
0.13
0.12
0.11
0.10
0.09
0.08
0.07
0.06
0.05
0.04
0.03
0.02
0.01
0
$f_0(v,t)$
k = .5
ϵ = .1
t = 30
ω_L/k
$f_0(v,0)$
$f_0(v,30)$
1.5
2.0
2.5
3.0
3.5
VELOCITY

Figure 14b.

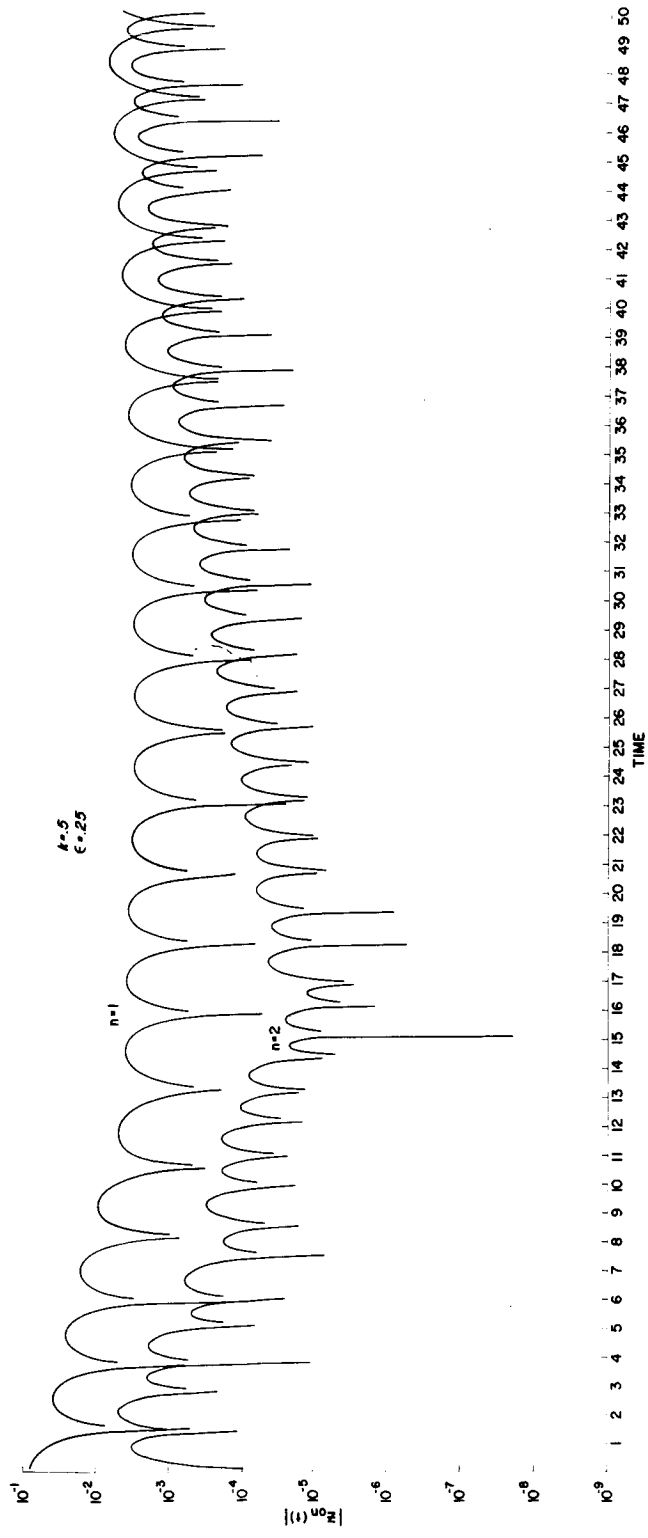

Figure 15

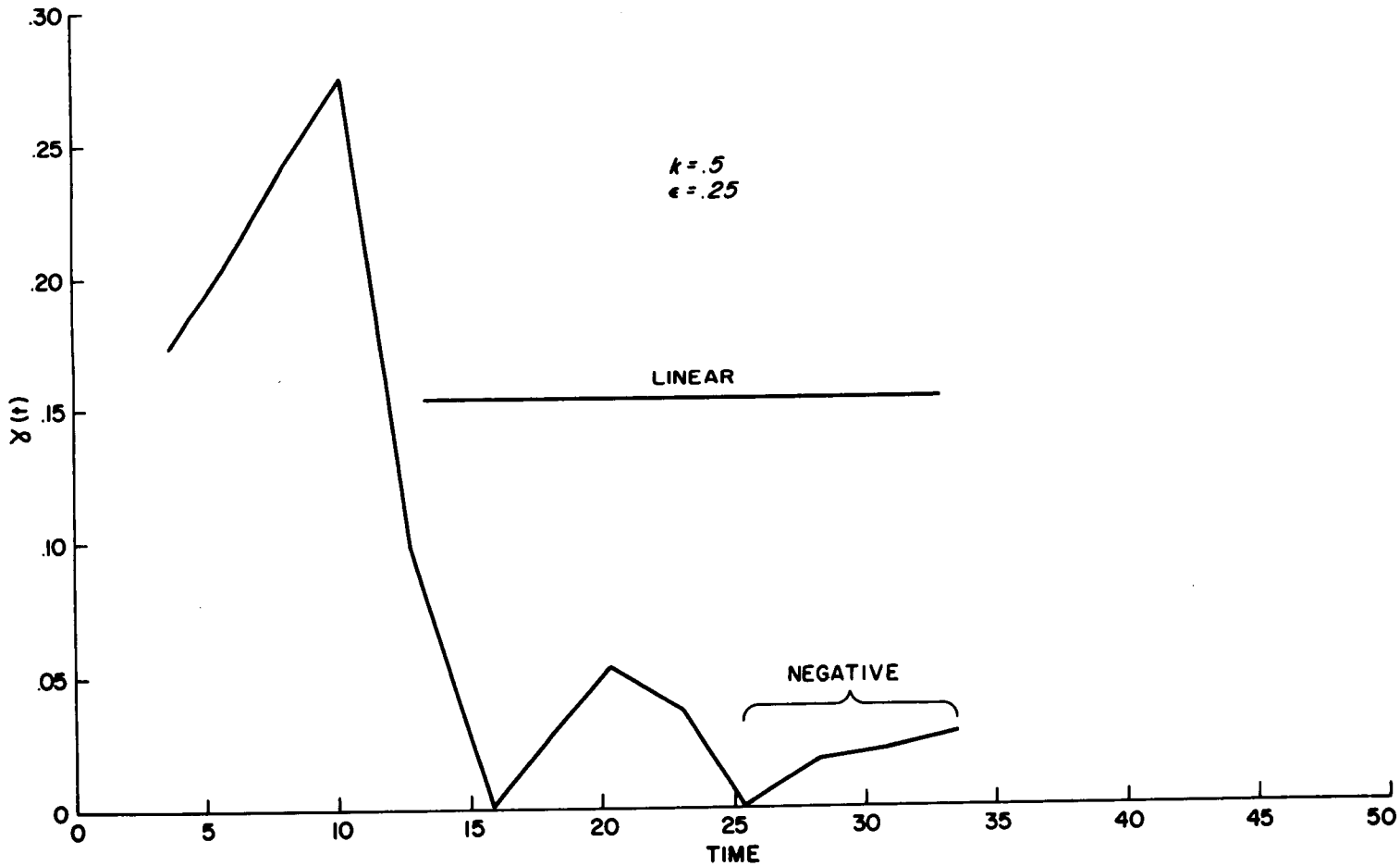
.30
.25
.20
.15
.10
.05
0
R(t)
k = .5
ε = .25
LINEAR
NEGATIVE
0
5
10
15
20
25
30
35
40
45
50
TIME

Figure 16

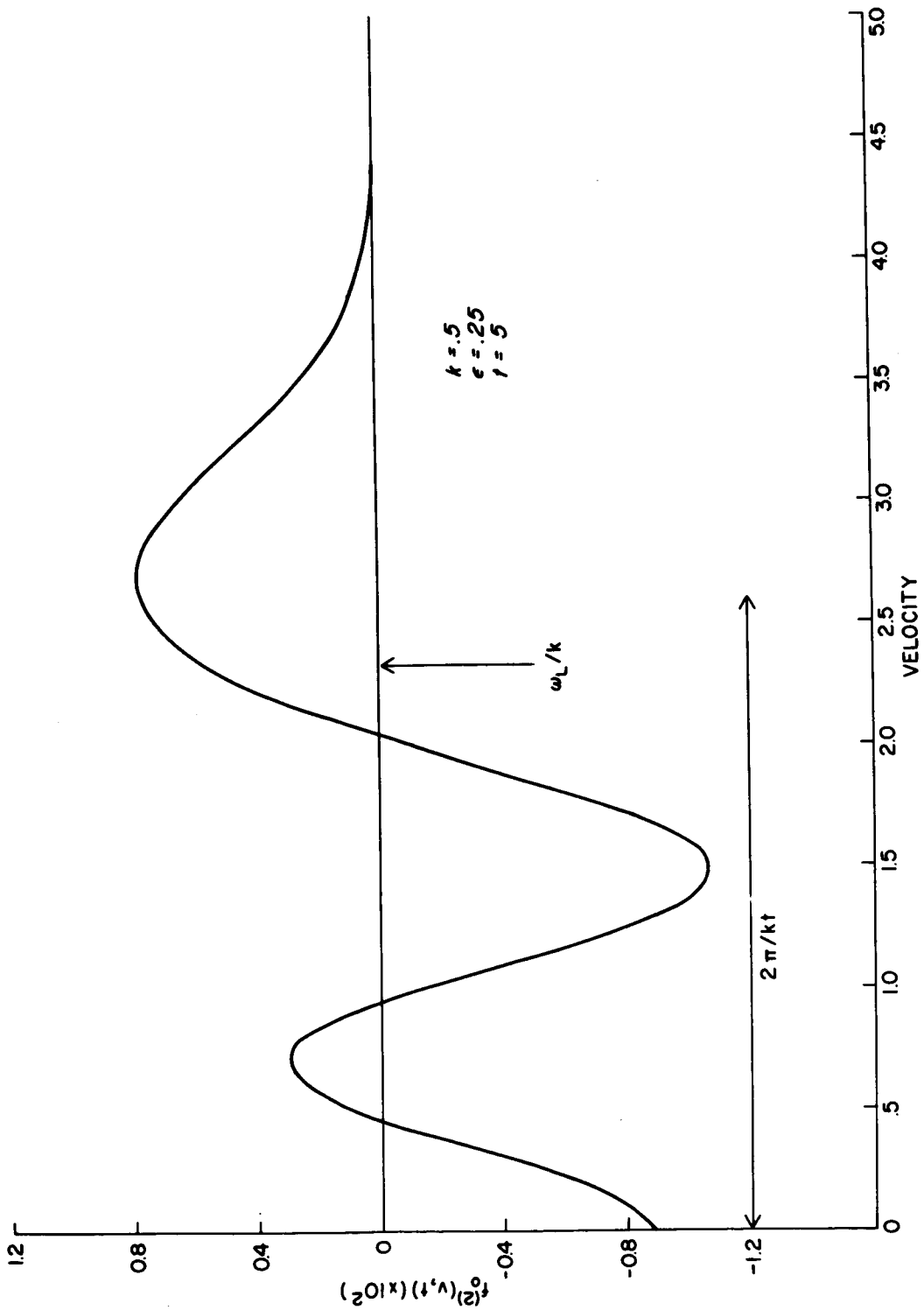
k = .5
ε = .25
t = 5
ω_L/k
2π/kt
VELOCITY
f₀⁽²⁾(v,t) (x10²)
1.2
0.8
0.4
0
-.4
-.8
-1.2
0
.5
1.0
1.5
2.0
2.5
3.0
3.5
4.0
4.5
5.0

Figure 17a.

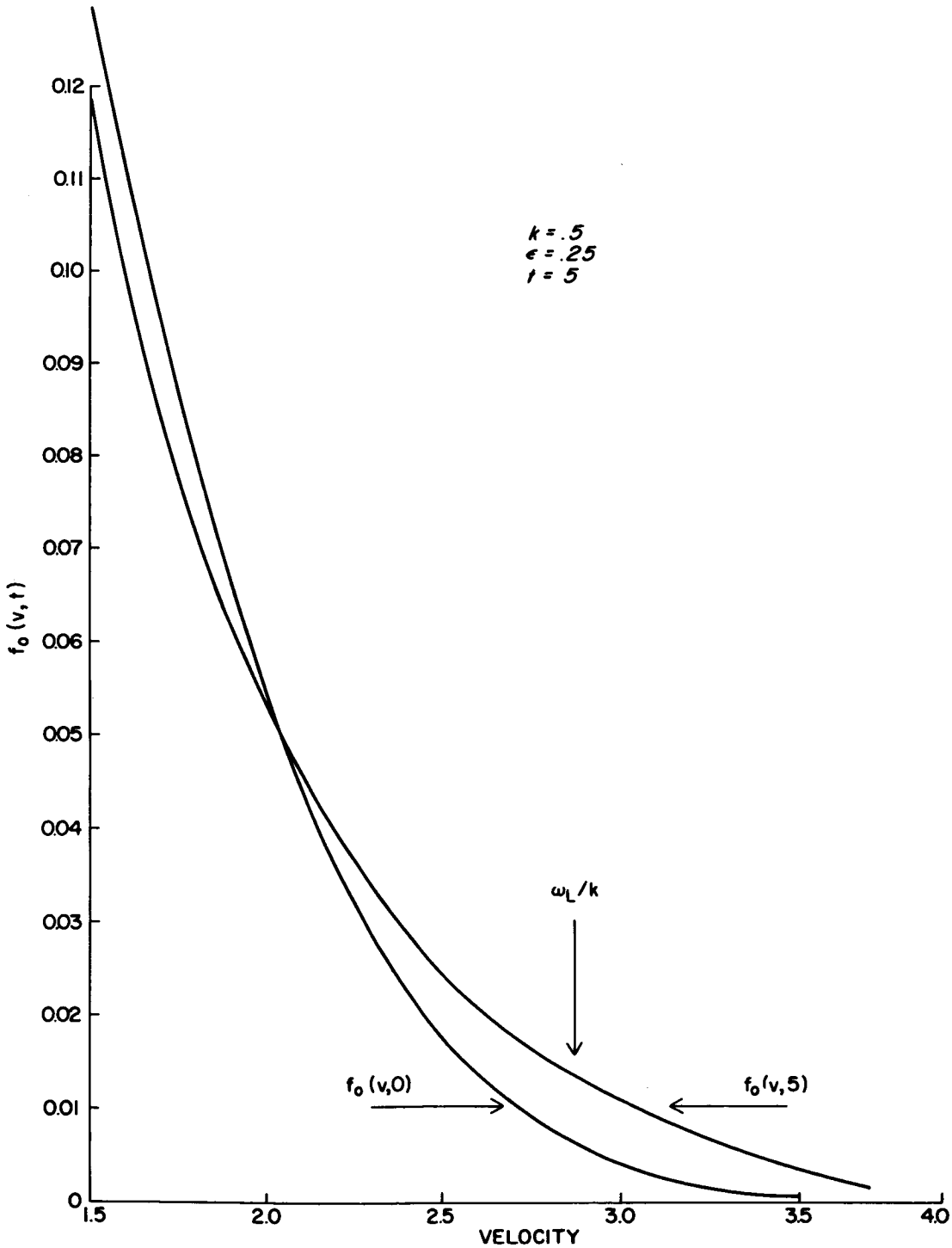
k = .5
ϵ = .25
t = 5
0.12
0.11
0.10
0.09
0.08
0.07
0.06
0.05
0.04
0.03
0.02
0.01
0
f₀ (v, t)
ωL/k
f₀ (v,0)
f₀(v,5)
1.5
2.0
2.5
3.0
3.5
4.0
VELOCITY

Figure 17b.

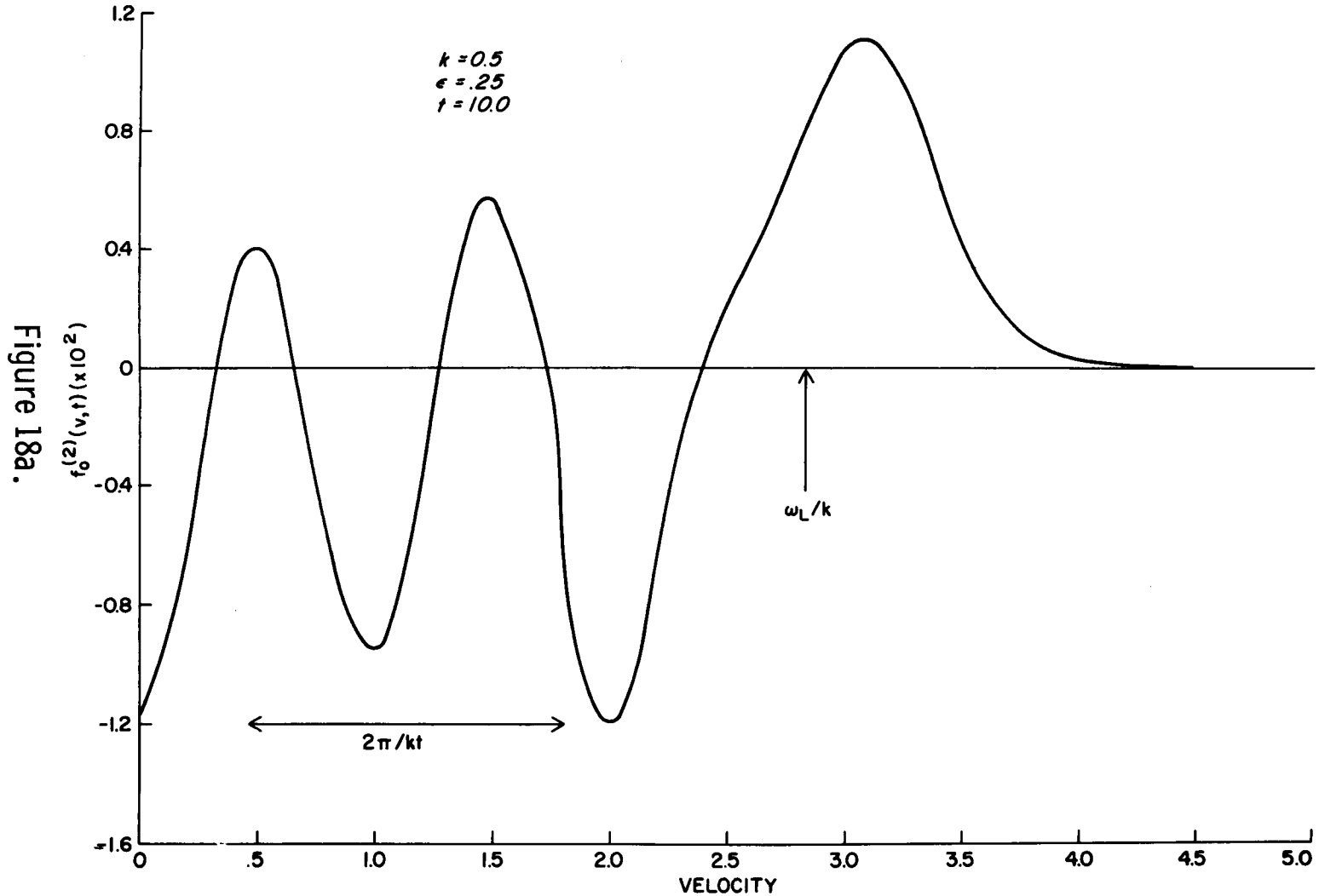
k = 0.5
ϵ = .25
t = 10.0
1.2
0.8
0.4
0
-0.4
-0.8
-1.2
-1.6
$f_0^{(2)}(v,t)(\times 10^2)$
ω_L/k
$2\pi/kt$
0
.5
1.0
1.5
2.0
2.5
3.0
3.5
4.0
4.5
5.0
VELOCITY

Figure 18a.

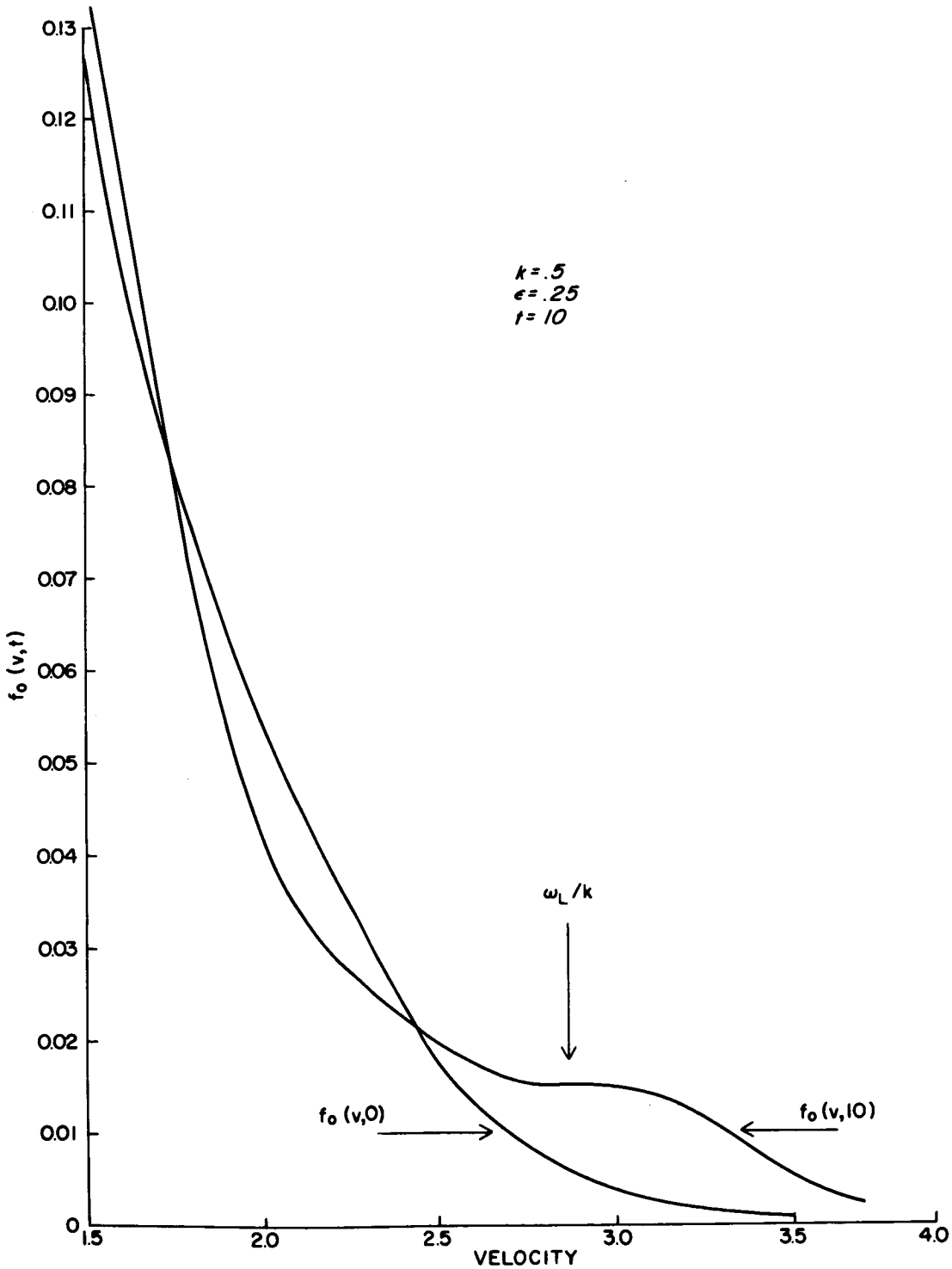
0.13
0.12
0.11
0.10
0.09
0.08
0.07
0.06
0.05
0.04
0.03
0.02
0.01
0
$f_0(v,t)$
$k = .5$
$\epsilon = .25$
$t = 10$
ω_L/k
$f_0(v,0)$
$f_0(v,10)$
1.5
2.0
2.5
3.0
3.5
4.0
VELOCITY

Figure 18b.

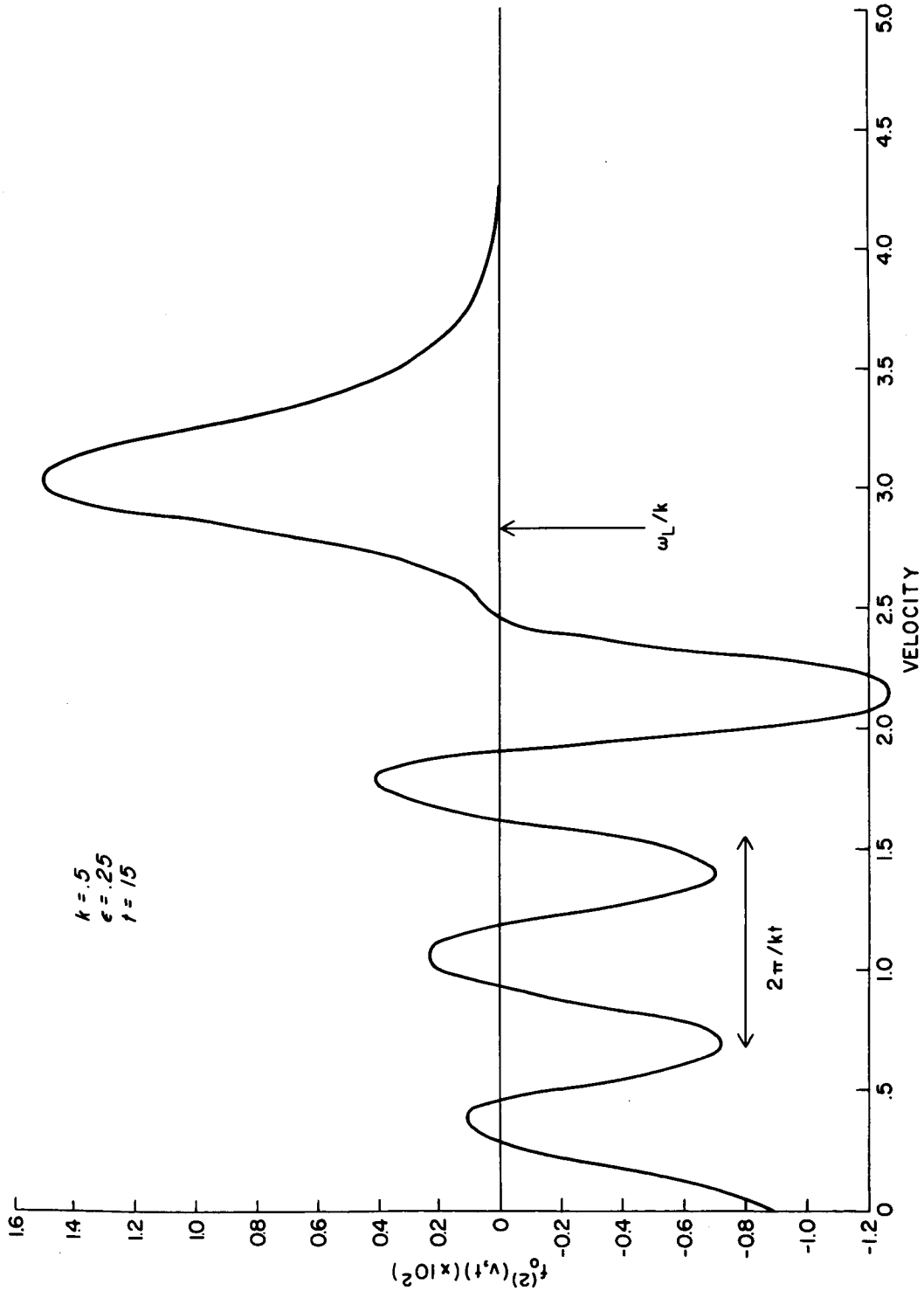
k = .5
ε = .25
t = 15
ω_L/k
$2\pi/kt$
VELOCITY
$f_0^{(2)}(v,t)(x10^2)$
1.6
1.4
1.2
1.0
0.8
0.6
0.4
0.2
0
-0.2
-0.4
-0.6
-0.8
-1.0
-1.2
0
.5
1.0
1.5
2.0
2.5
3.0
3.5
4.0
4.5
5.0

Figure 19a.

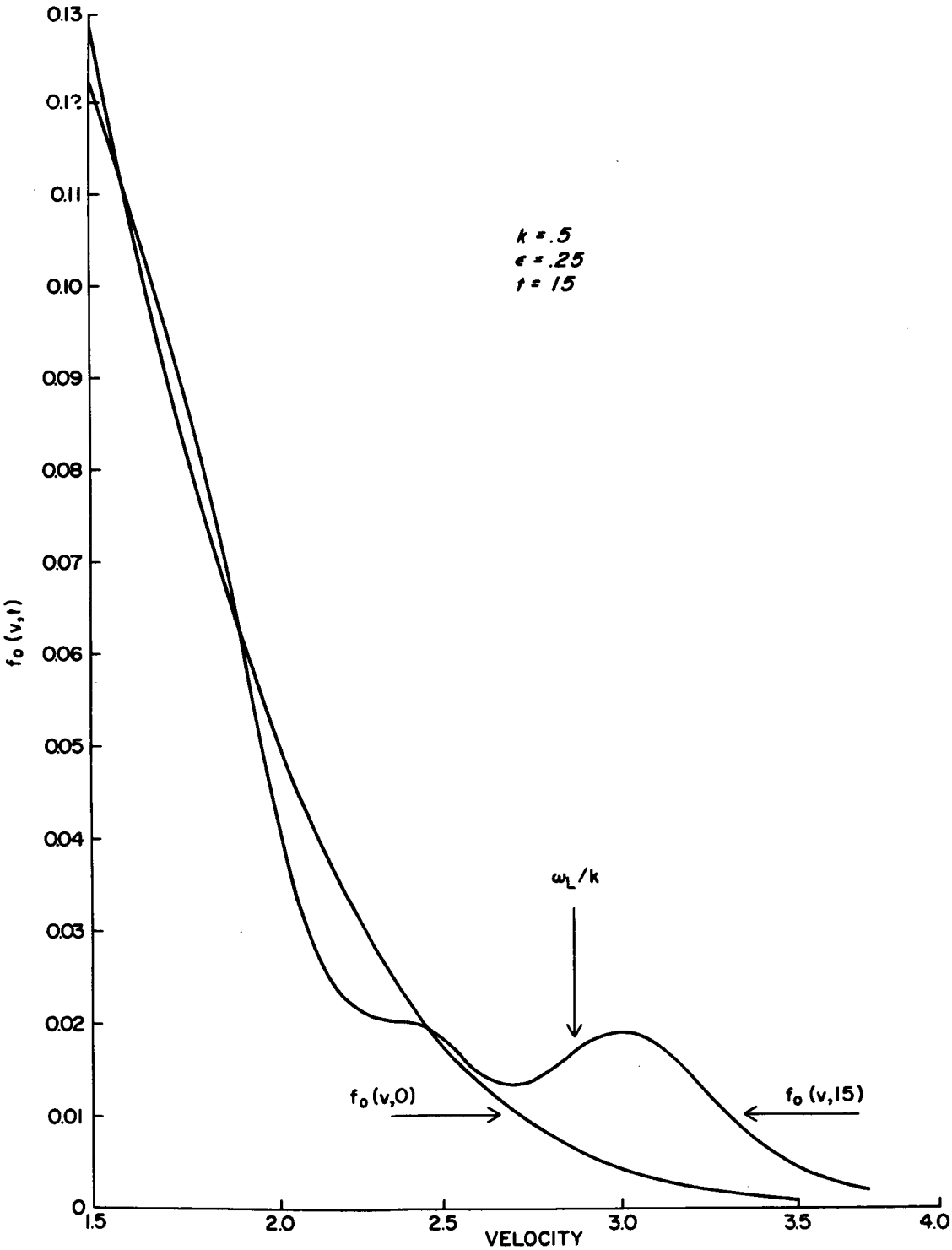
0.13
0.12
0.11
0.10
0.09
0.08
0.07
0.06
0.05
0.04
0.03
0.02
0.01
0
$f_0(v,t)$
k = .5
ϵ = .25
t = 15
ω_L/k
$f_0(v,0)$
$f_0(v,15)$
1.5
2.0
2.5
3.0
3.5
4.0
VELOCITY

Figure 19b.

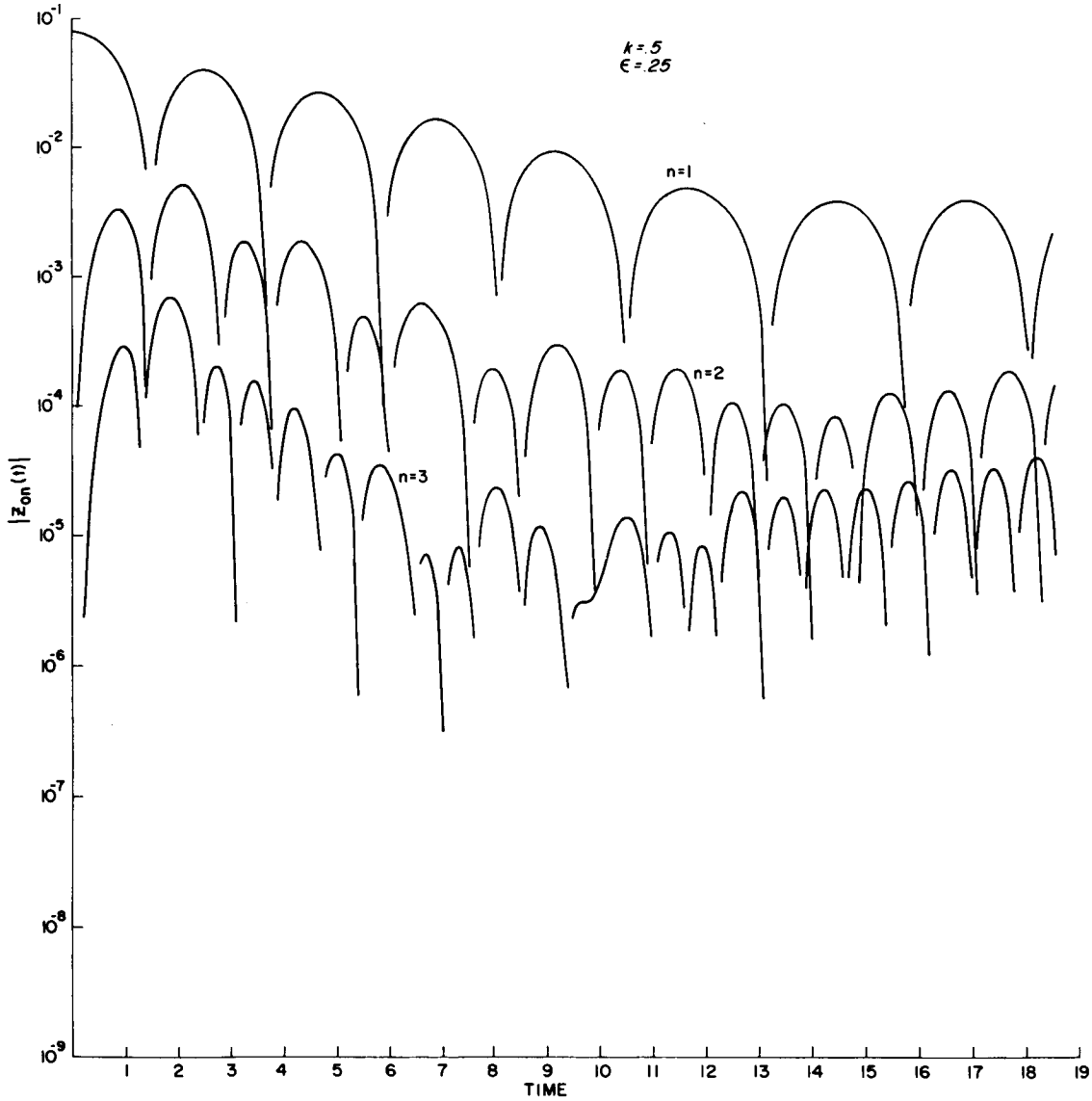
k=.5
ϵ=.25
n=1
n=2
n=3
$|z_{on}(t)|$
10^{-1}
10^{-2}
10^{-3}
10^{-4}
10^{-5}
10^{-6}
10^{-7}
10^{-8}
10^{-9}
1 2 3 4 5 6 7 8 9 10 11 12 13 14 15 16 17 18 19
TIME

Figure 20

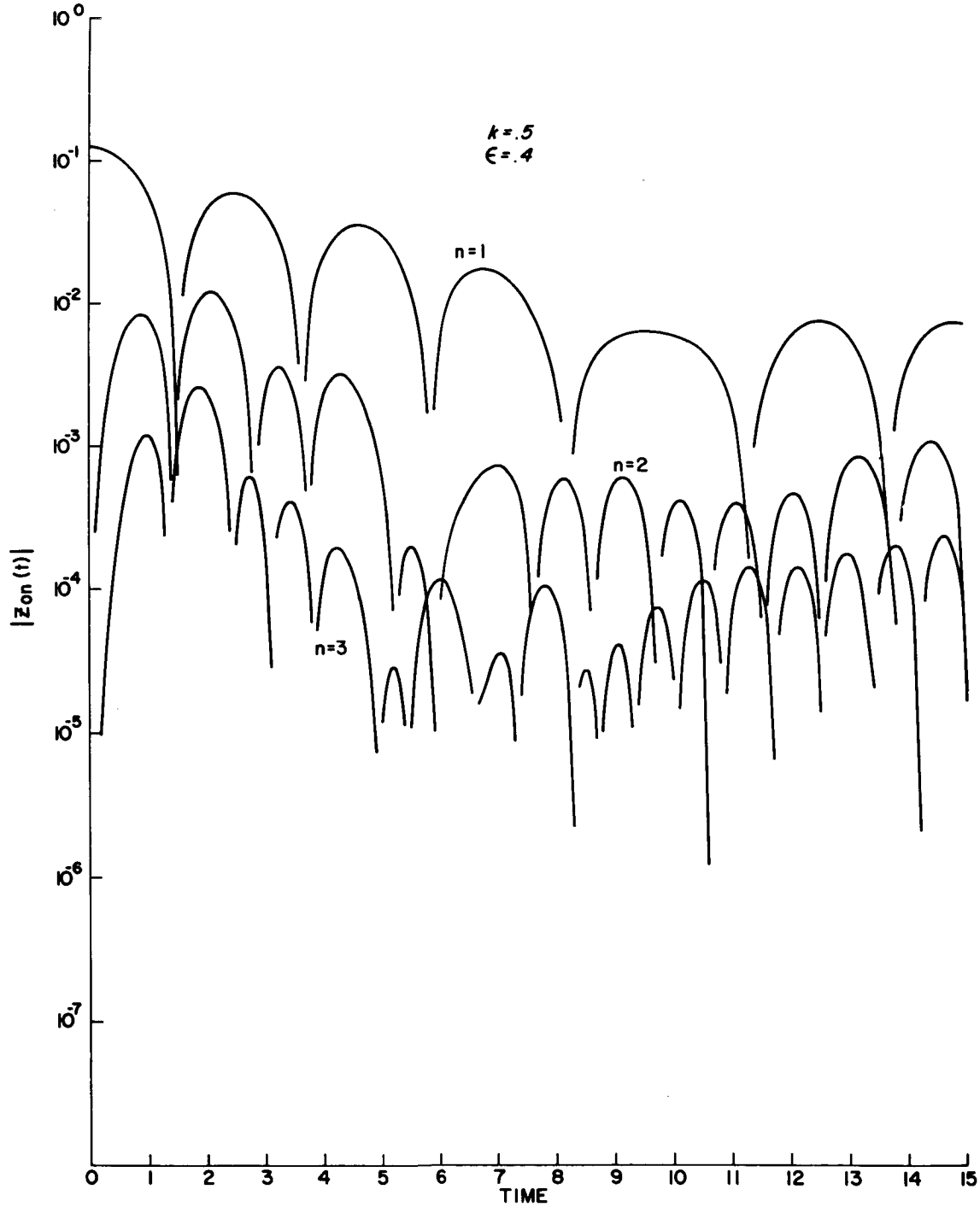
10^0
10^{-1}
10^{-2}
10^{-3}
10^{-4}
10^{-5}
10^{-6}
10^{-7}
$|Z_{on}(t)|$
k=.5
ϵ=.4
n=1
n=2
n=3
0 1 2 3 4 5 6 7 8 9 10 11 12 13 14 15
TIME

Figure 21

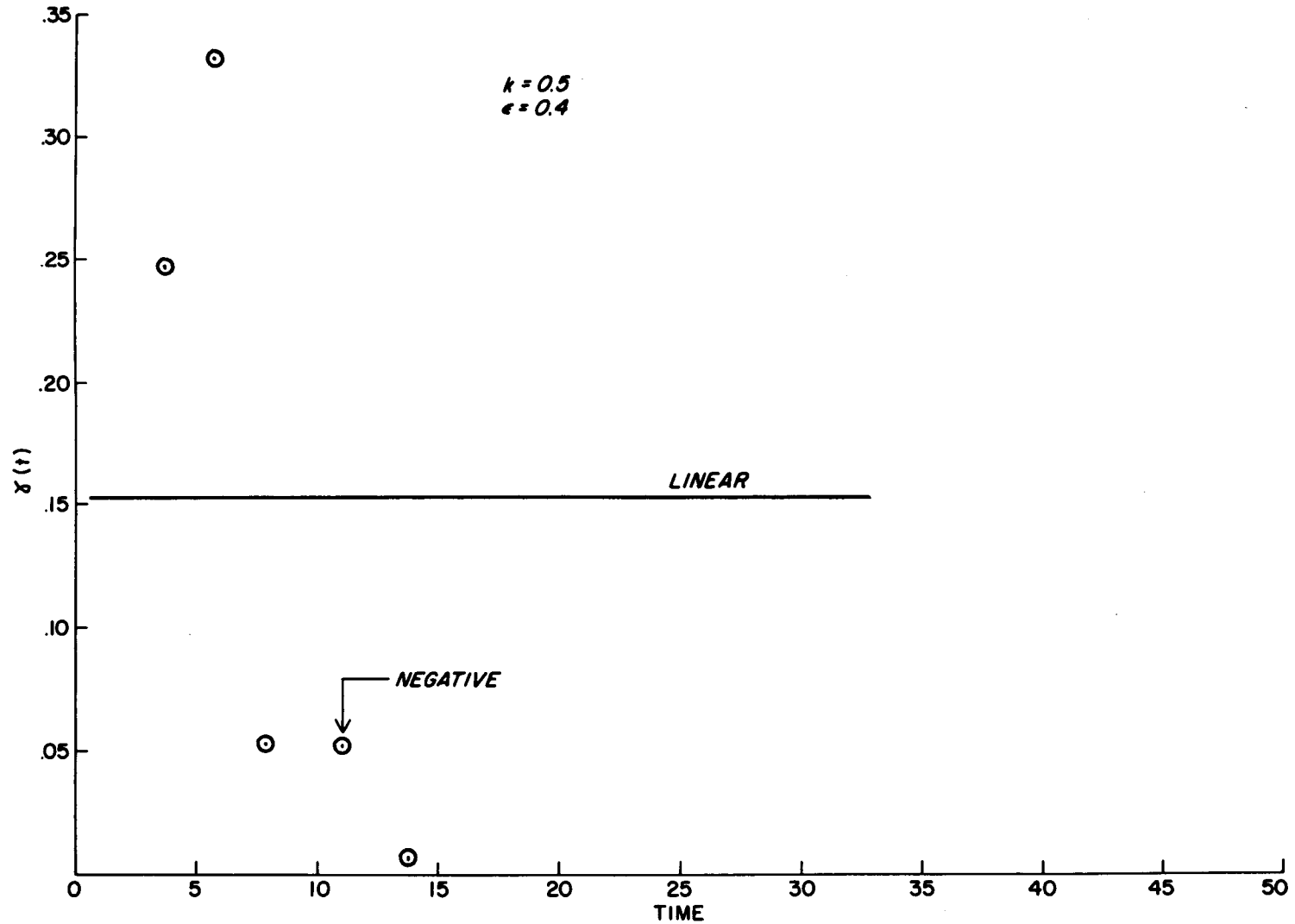
.35
.30
.25
.20
.15
.10
.05
k = 0.5
ε = 0.4
LINEAR
NEGATIVE
R (t)
0
5
10
15
20
25
30
35
40
45
50
TIME

Figure 22

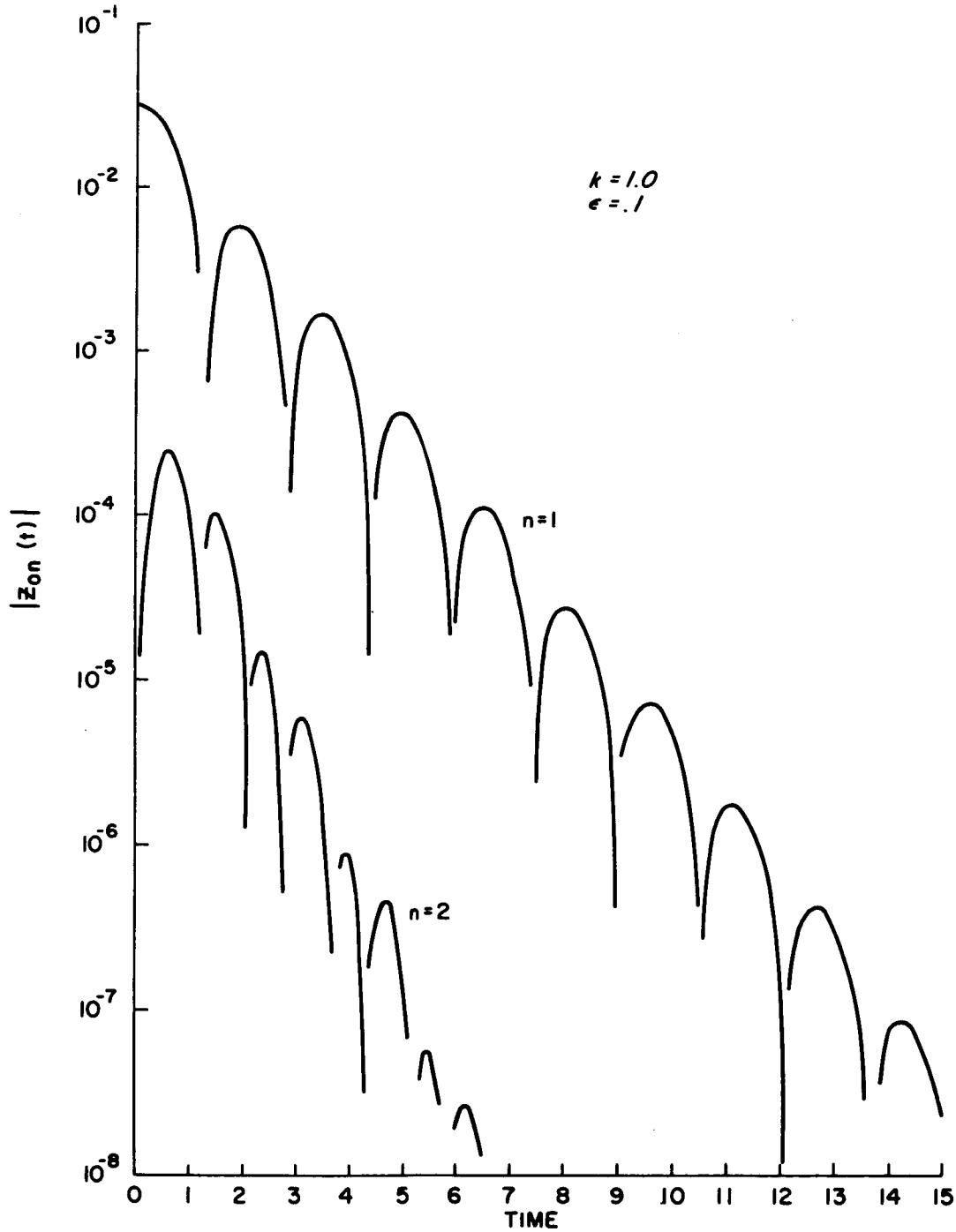
10^{-1}
10^{-2}
10^{-3}
10^{-4}
10^{-5}
10^{-6}
10^{-7}
10^{-8}
$|z_{on}(t)|$
k = 1.0
ϵ = .1
n=1
n=2
0 1 2 3 4 5 6 7 8 9 10 11 12 13 14 15
TIME

Figure 23

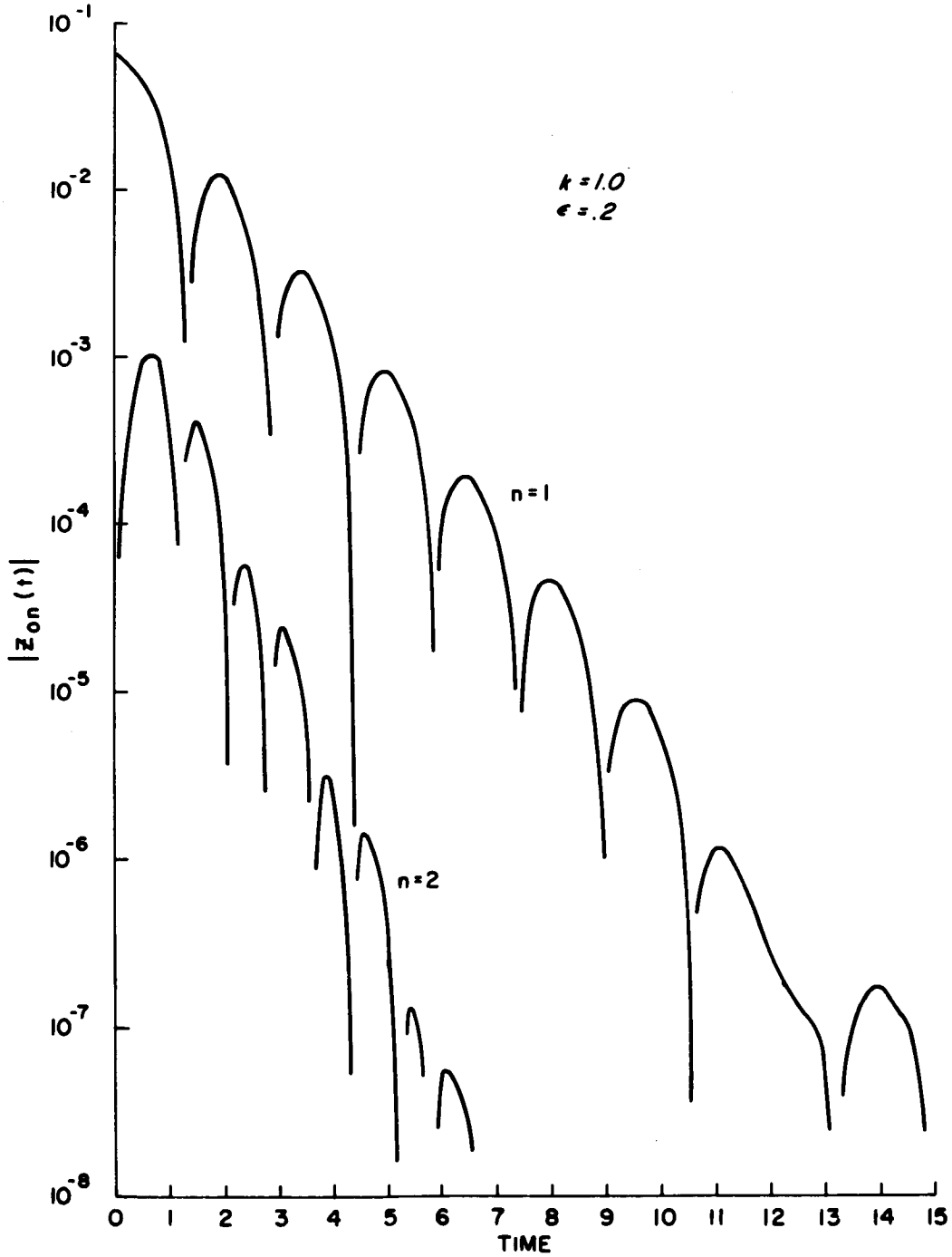
10^{-1}
10^{-2}
10^{-3}
10^{-4}
10^{-5}
10^{-6}
10^{-7}
10^{-8}
$|z_{on}(t)|$
k = 1.0
ϵ = .2
n = 1
n = 2
0 1 2 3 4 5 6 7 8 9 10 11 12 13 14 15
TIME

Figure 24

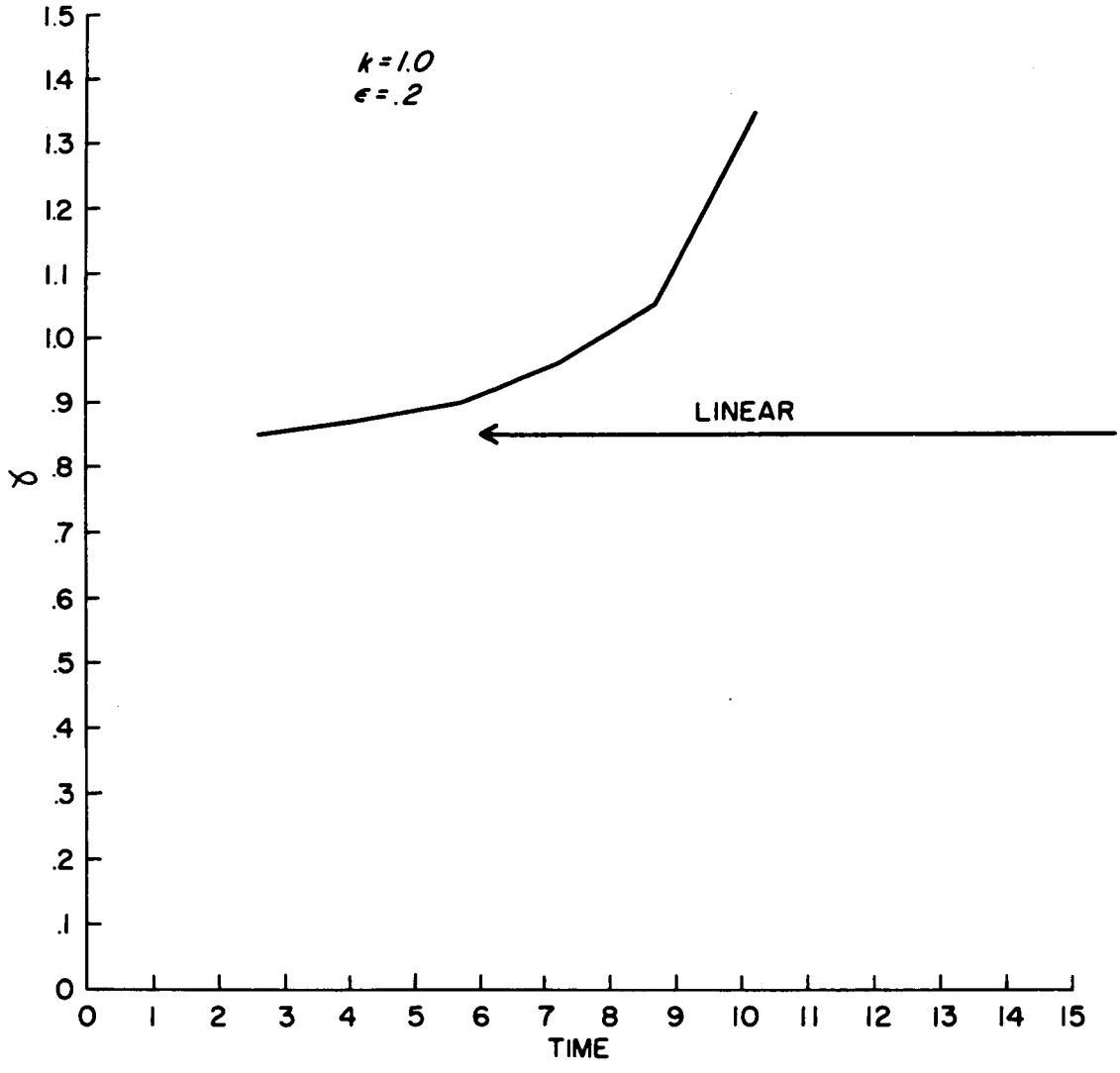
k=1.0
ε=.2
LINEAR
X
TIME
1.5
1.4
1.3
1.2
1.1
1.0
.9
.8
.7
.6
.5
.4
.3
.2
.1
0
0 1 2 3 4 5 6 7 8 9 10 11 12 13 14 15

Figure 25

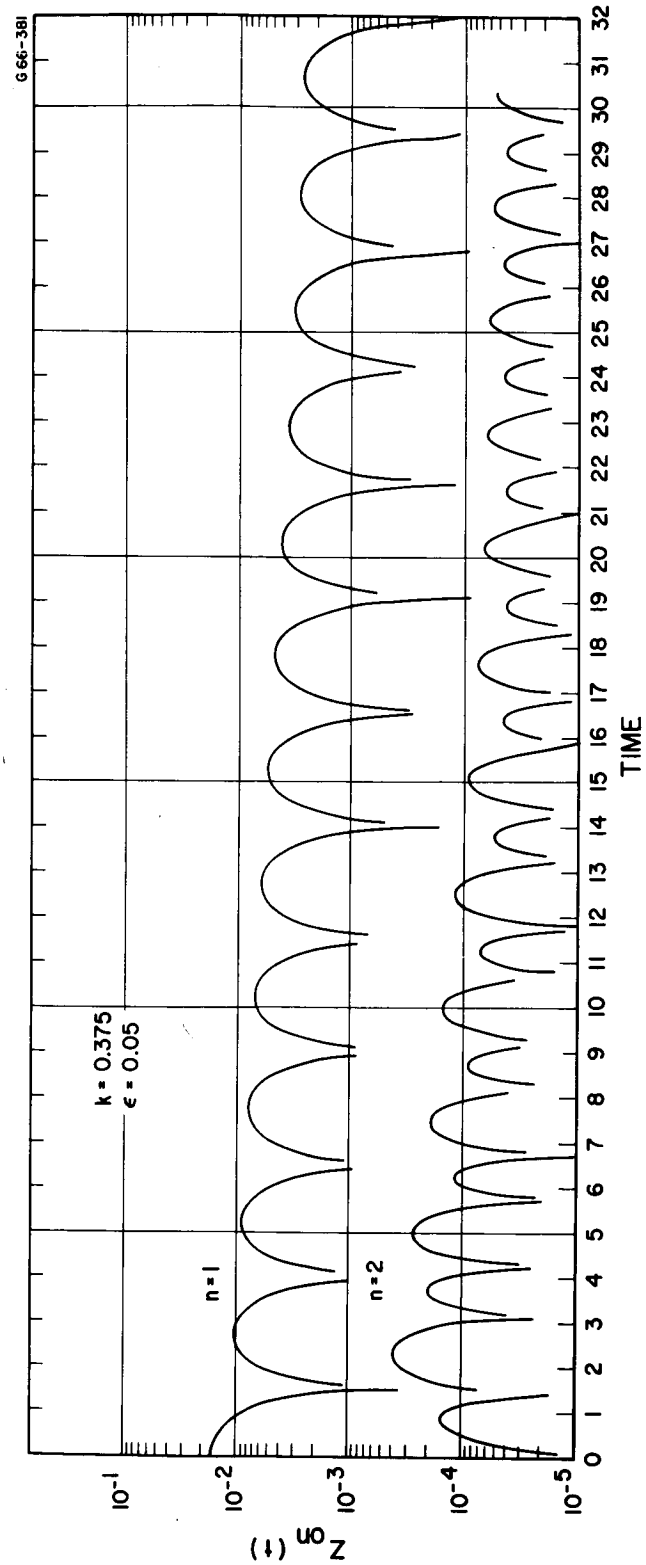
G 66-381
k = 0.375
ϵ = 0.05
n = 1
n = 2
10^{-1}
10^{-2}
10^{-3}
10^{-4}
10^{-5}
$Z_{on}(t)$
0 1 2 3 4 5 6 7 8 9 10 11 12 13 14 15 16 17 18 19 20 21 22 23 24 25 26 27 28 29 30 31 32
TIME

Figure 26

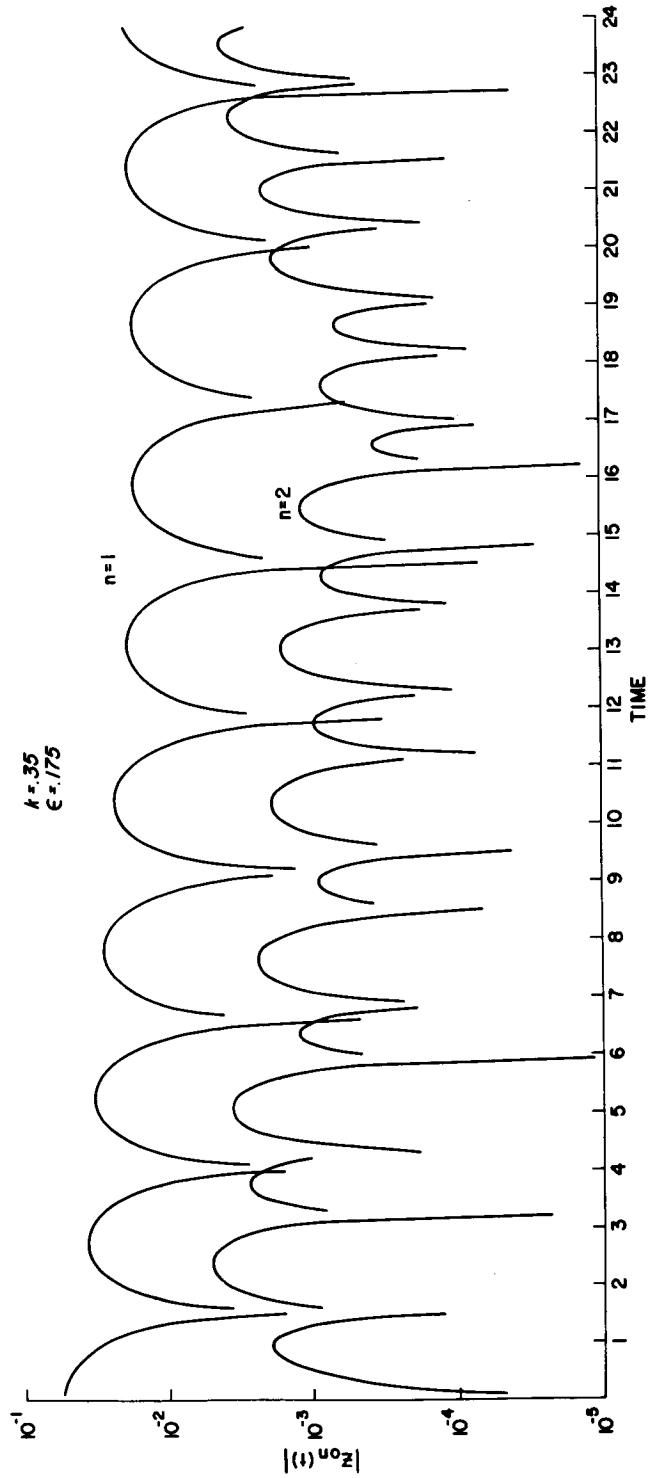
k=.35
ε=.175
n=1
n=2
TIME
$|z_{on}(t)|$
10^{-1}
10^{-2}
10^{-3}
10^{-4}
10^{-5}
1
2
3
4
5
6
7
8
9
10
11
12
13
14
15
16
17
18
19
20
21
22
23
24

Figure 27

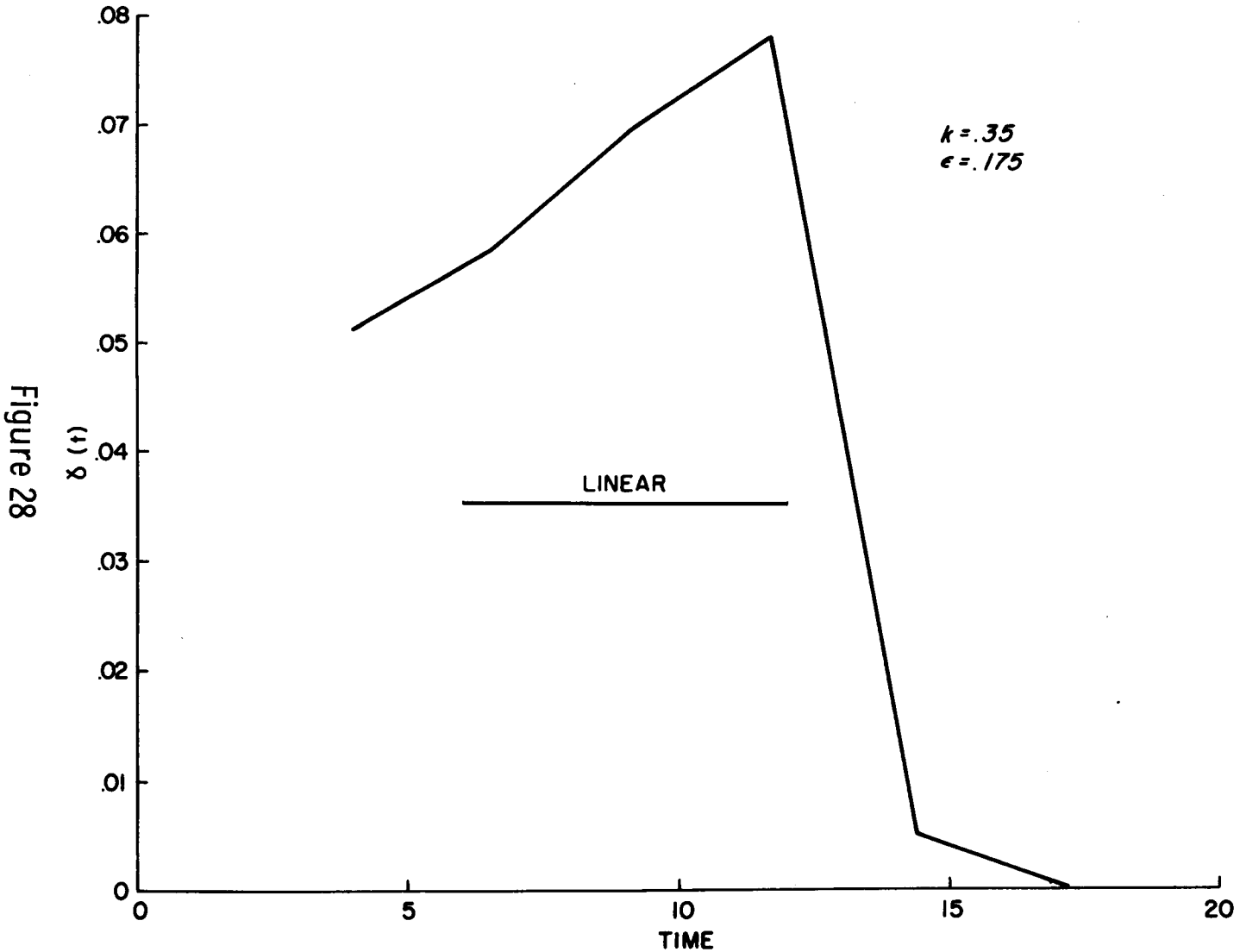

Figure 28

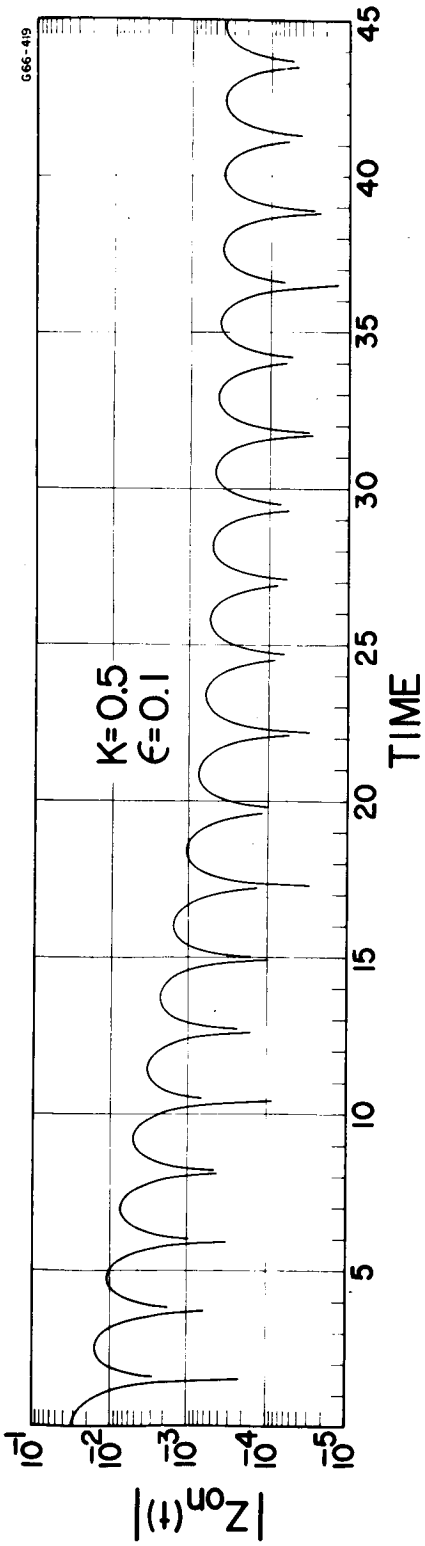
G66-419
K=0.5
ϵ=0.1
TIME
5
10
15
20
25
30
35
40
45
10^{-1}
10^{-2}
10^{-3}
10^{-4}
10^{-5}
$|Z_{on}(t)|$

Figure 29

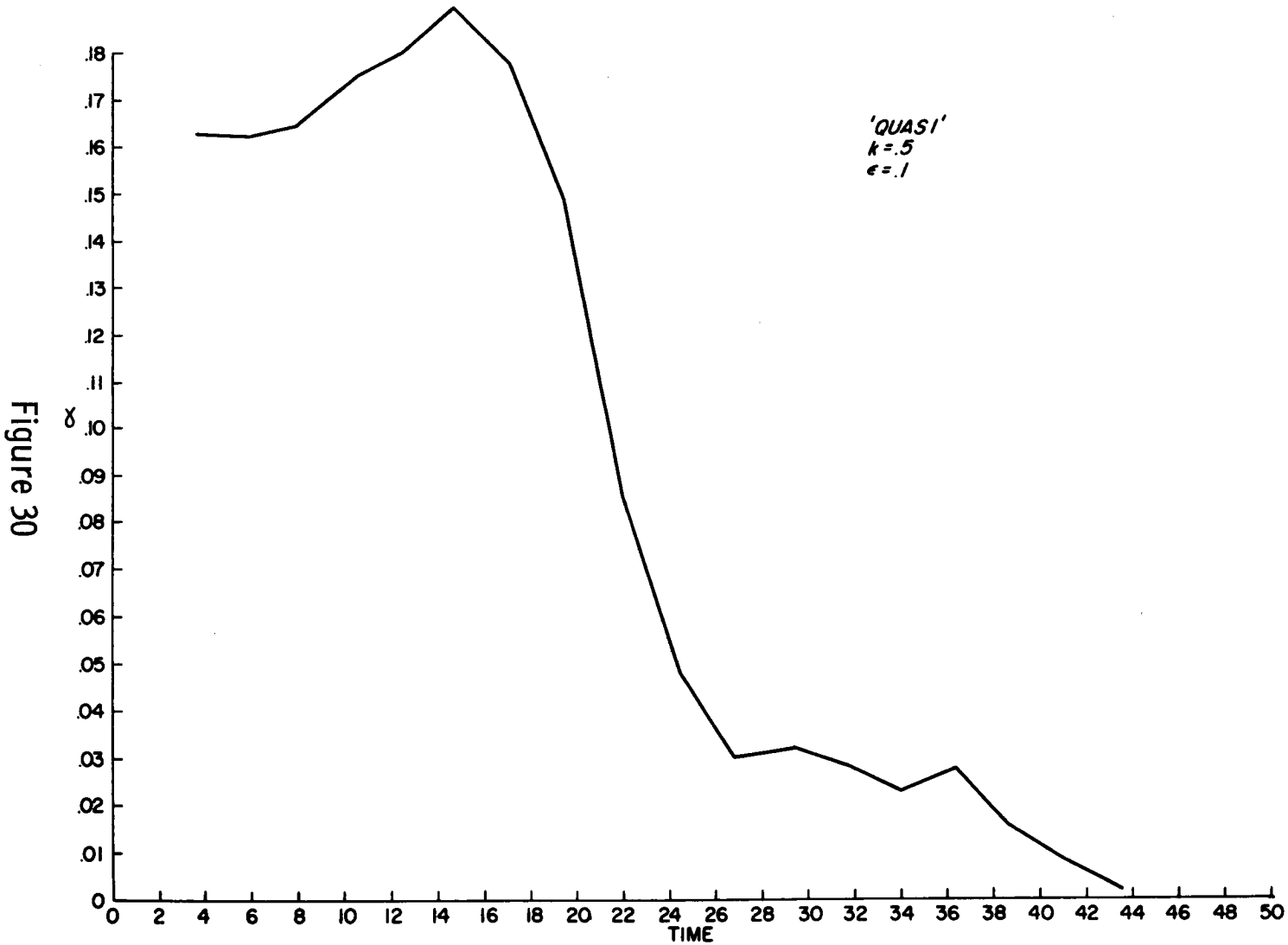
'QUASI'
k=.5
ε=.1
γ
TIME
0
.01
.02
.03
.04
.05
.06
.07
.08
.09
.10
.11
.12
.13
.14
.15
.16
.17
.18
0 2 4 6 8 10 12 14 16 18 20 22 24 26 28 30 32 34 36 38 40 42 44 46 48 50

Figure 30

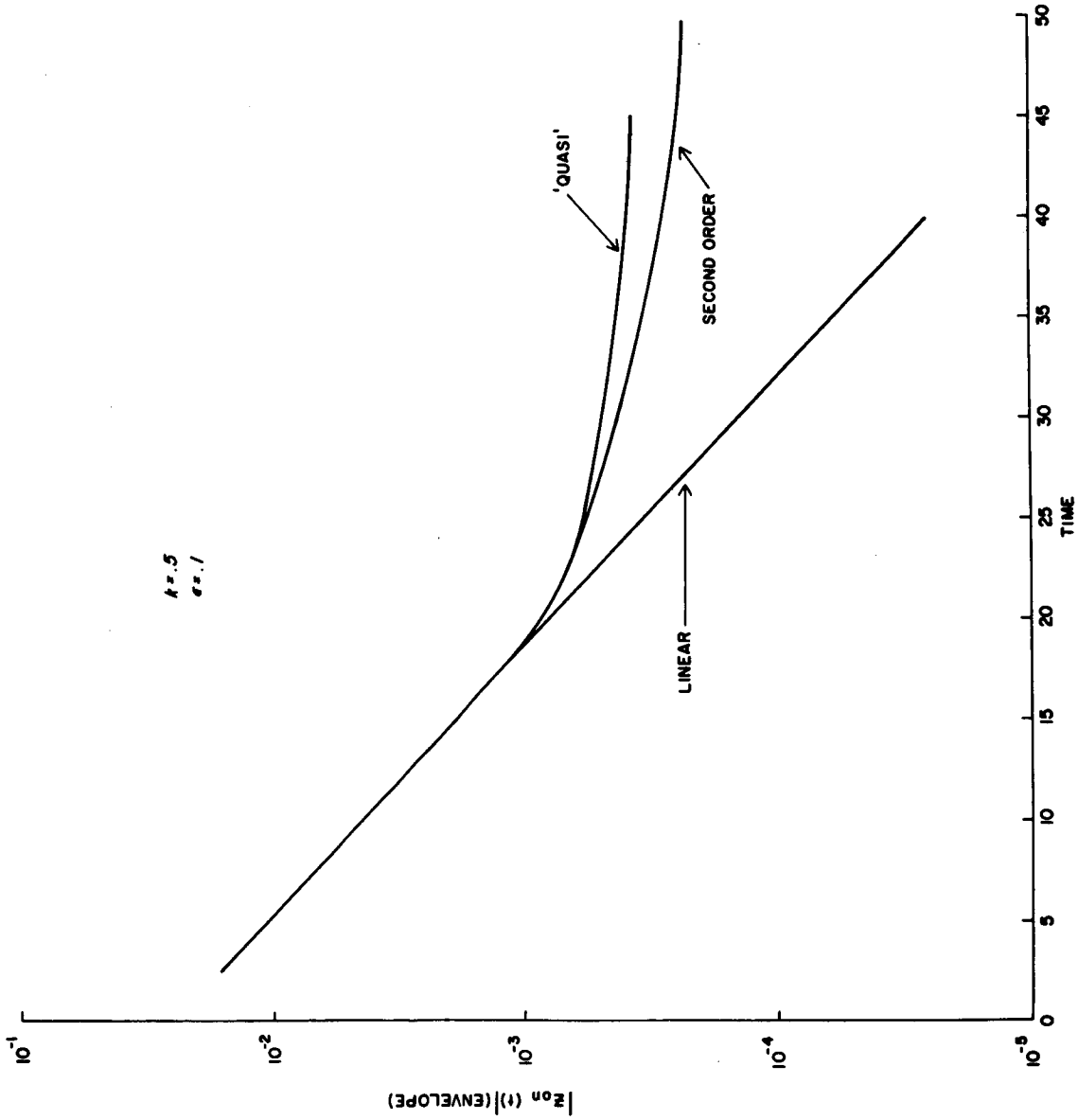
$|a_{on}(t)|$ (ENVELOPE)
10^{-1}
10^{-2}
10^{-3}
10^{-4}
10^{-5}
0
5
10
15
20
25
30
35
40
45
50
TIME
'QUASI'
SECOND ORDER
LINEAR
k=.5
ε=.1

Figure 31

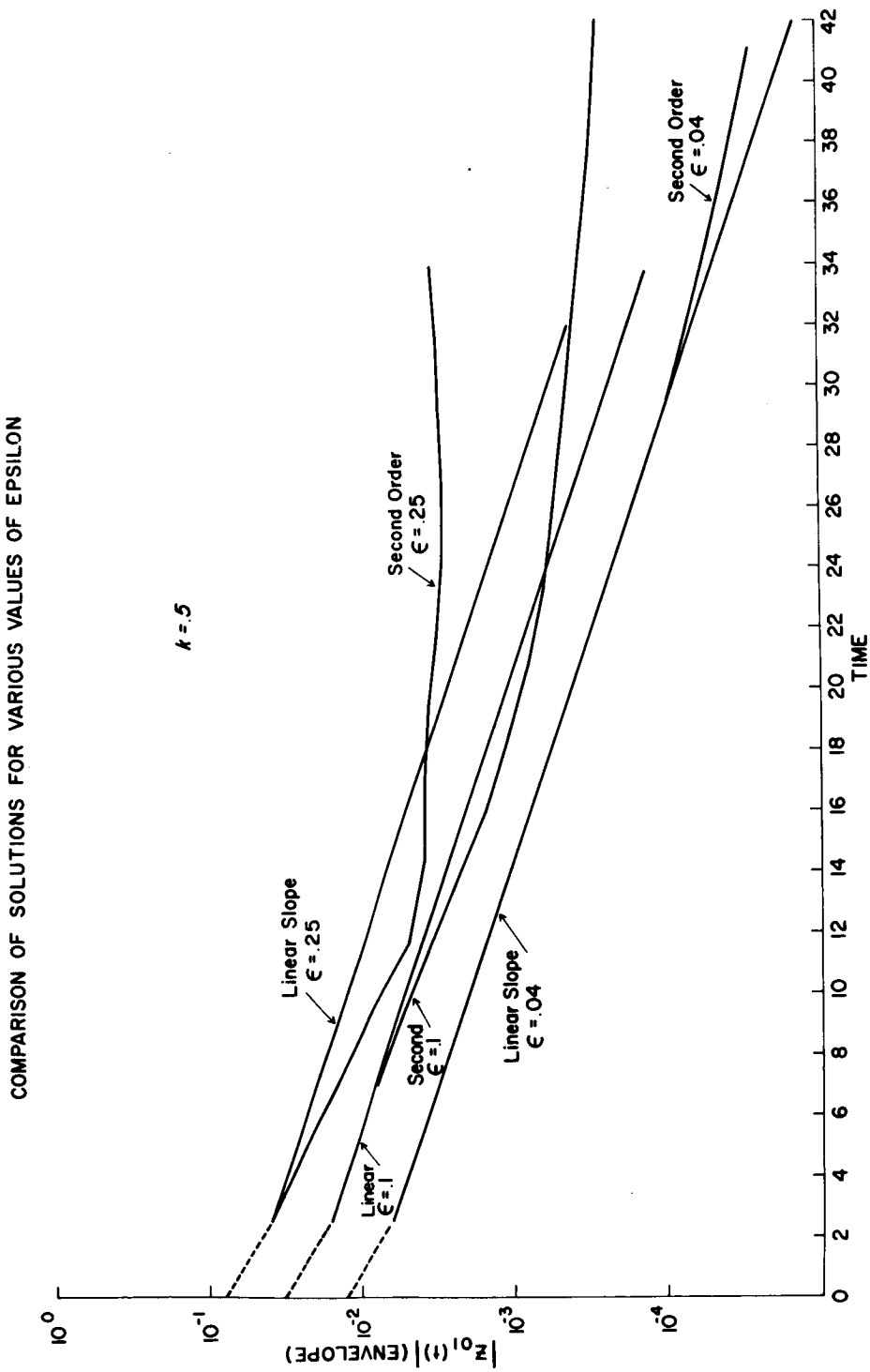
COMPARISON OF SOLUTIONS FOR VARIOUS VALUES OF EPSILON
k = .5
Linear Slope ε = .25
Second Order ε = .25
Second ε = .1
Linear ε = .1
Linear Slope ε = .04
Second Order ε = .04
$|N_{01}(t)|$ (ENVELOPE)
TIME
10^0
10^{-1}
10^{-2}
10^{-3}
10^{-4}
0 2 4 6 8 10 12 14 16 18 20 22 24 26 28 30 32 34 36 38 40 42

Figure 32

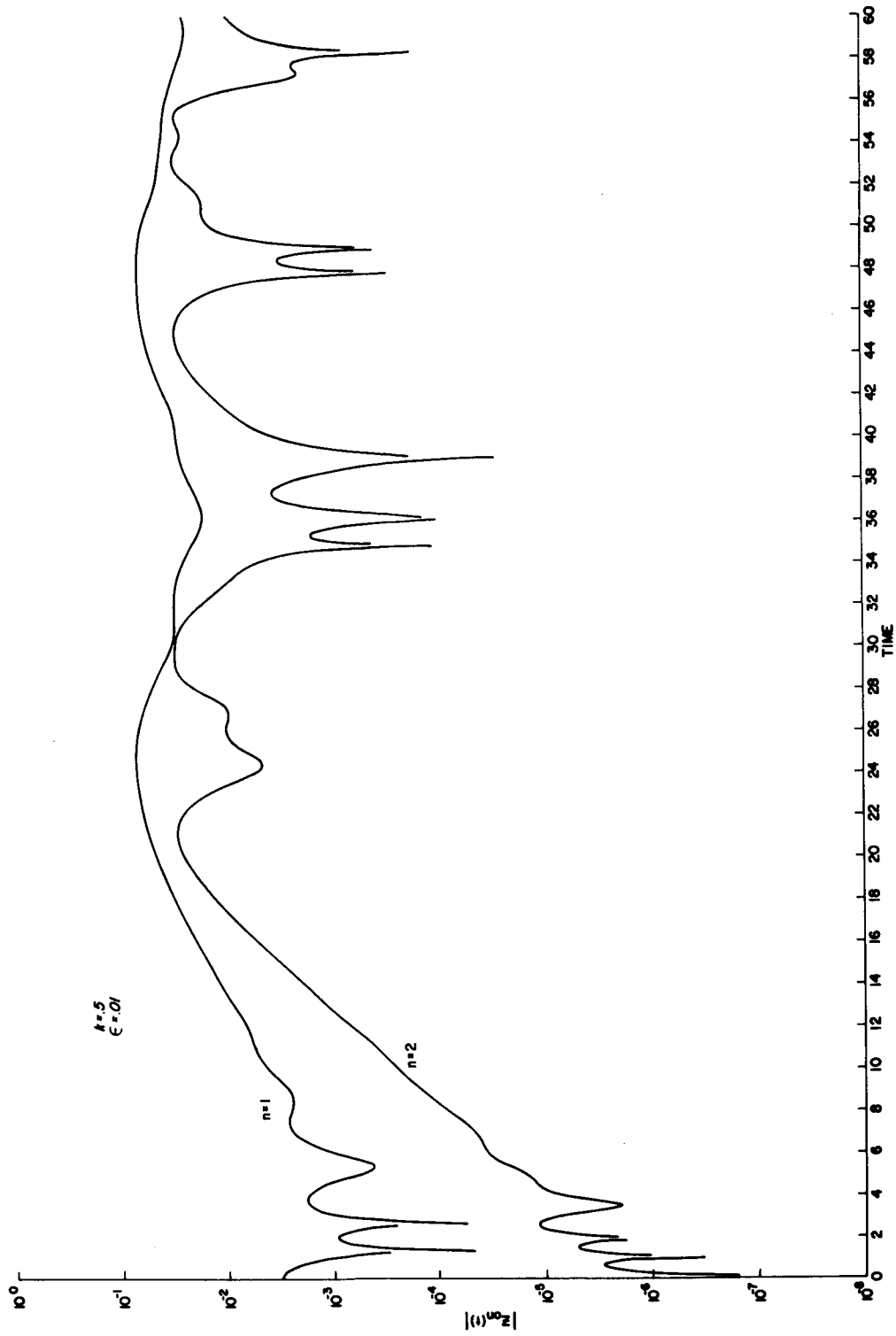

Figure 33

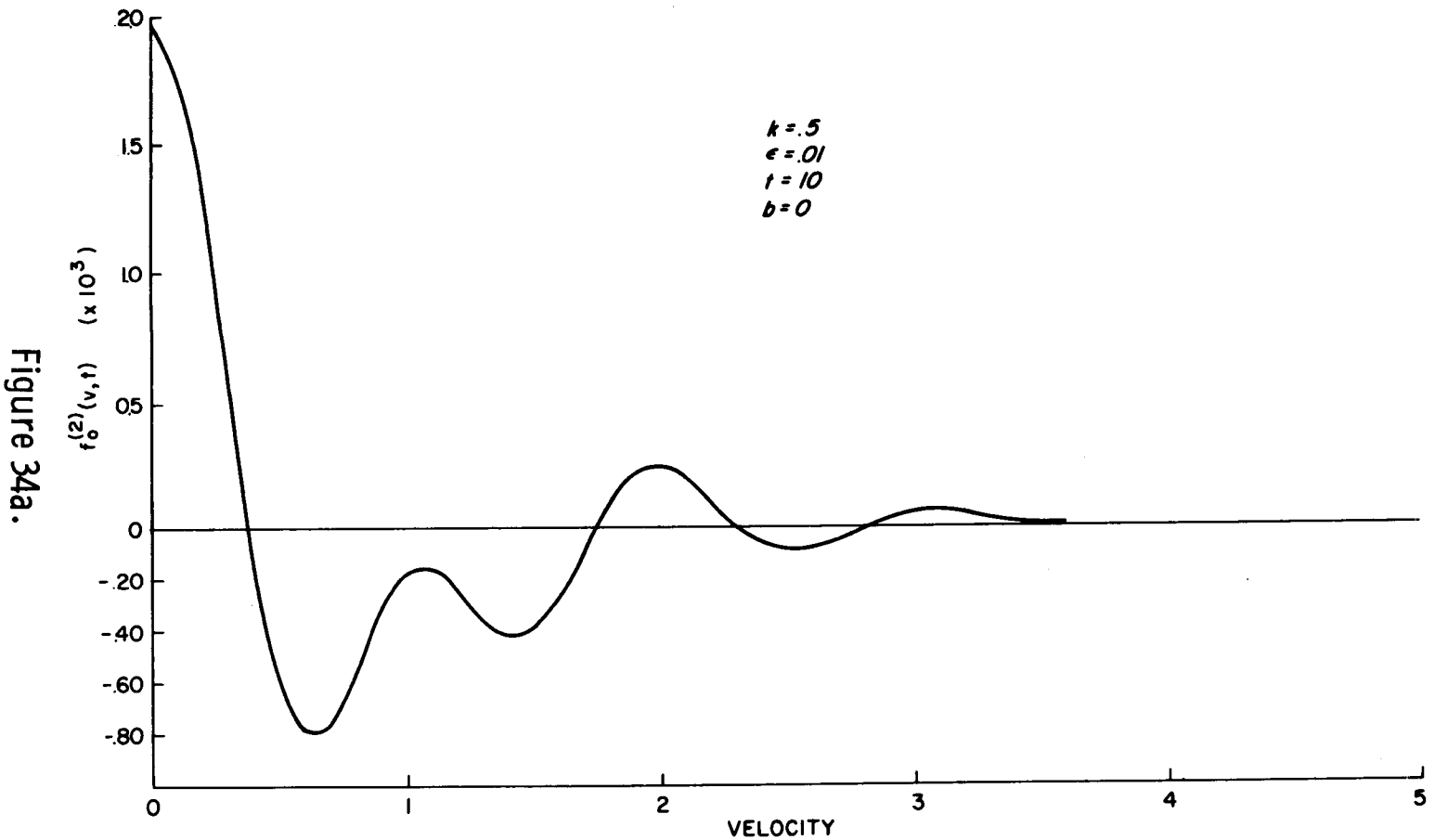
k = .5
ε = .01
t = 10
b = 0
$f_0^{(2)}(v,t)$ (x 10^3)
.20
1.5
1.0
0.5
0
-.20
-.40
-.60
-.80
0
1
2
3
4
5
VELOCITY

Figure 34a.

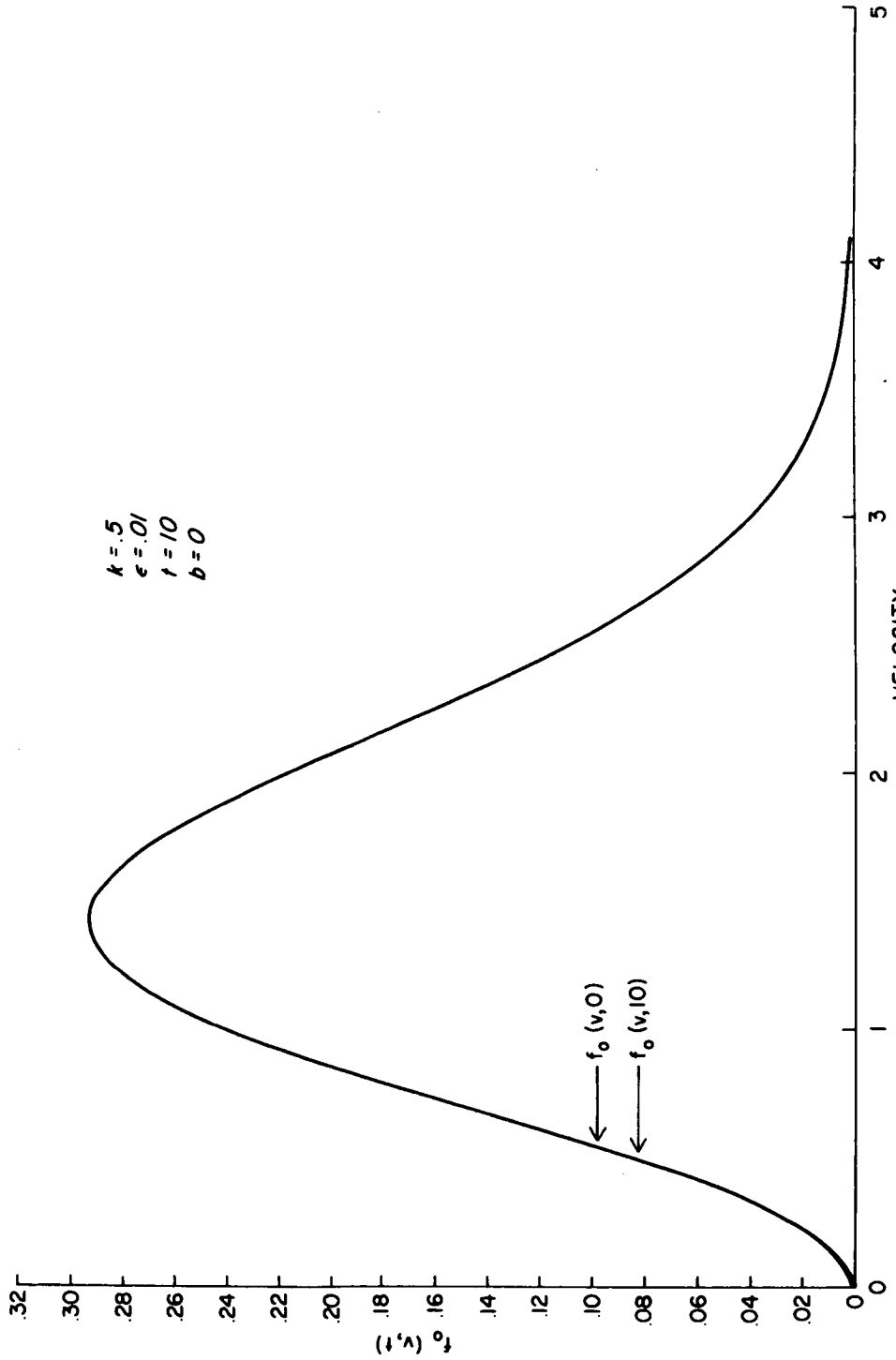
k = .5
ε = .01
τ = 10
b = 0
f_0 (v,0)
f_0 (v,10)
f_0 (v,τ)
VELOCITY
0
1
2
3
4
5
.02
.04
.06
.08
.10
.12
.14
.16
.18
.20
.22
.24
.26
.28
.30
.32

Figure 34b.

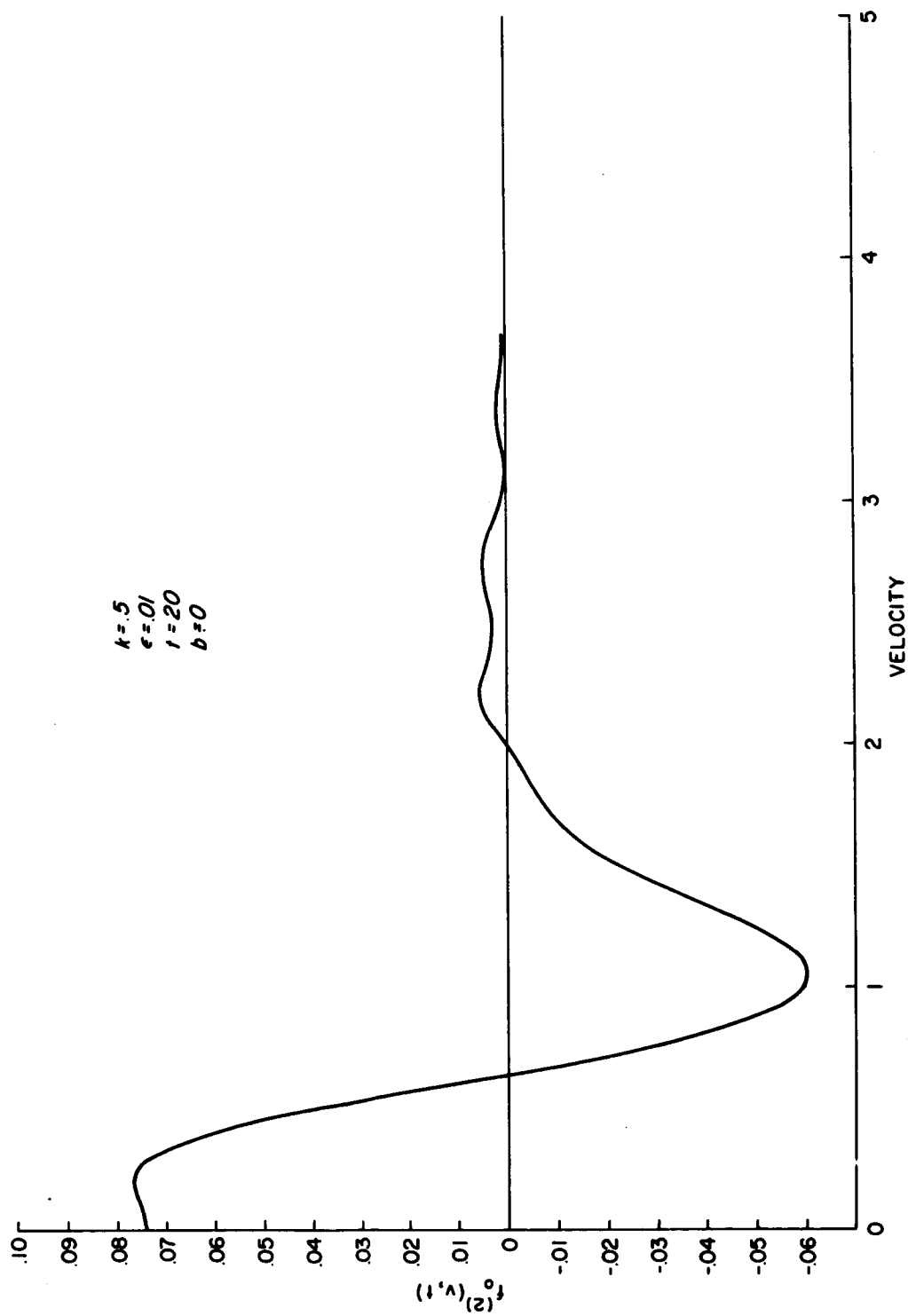

Figure 35a.

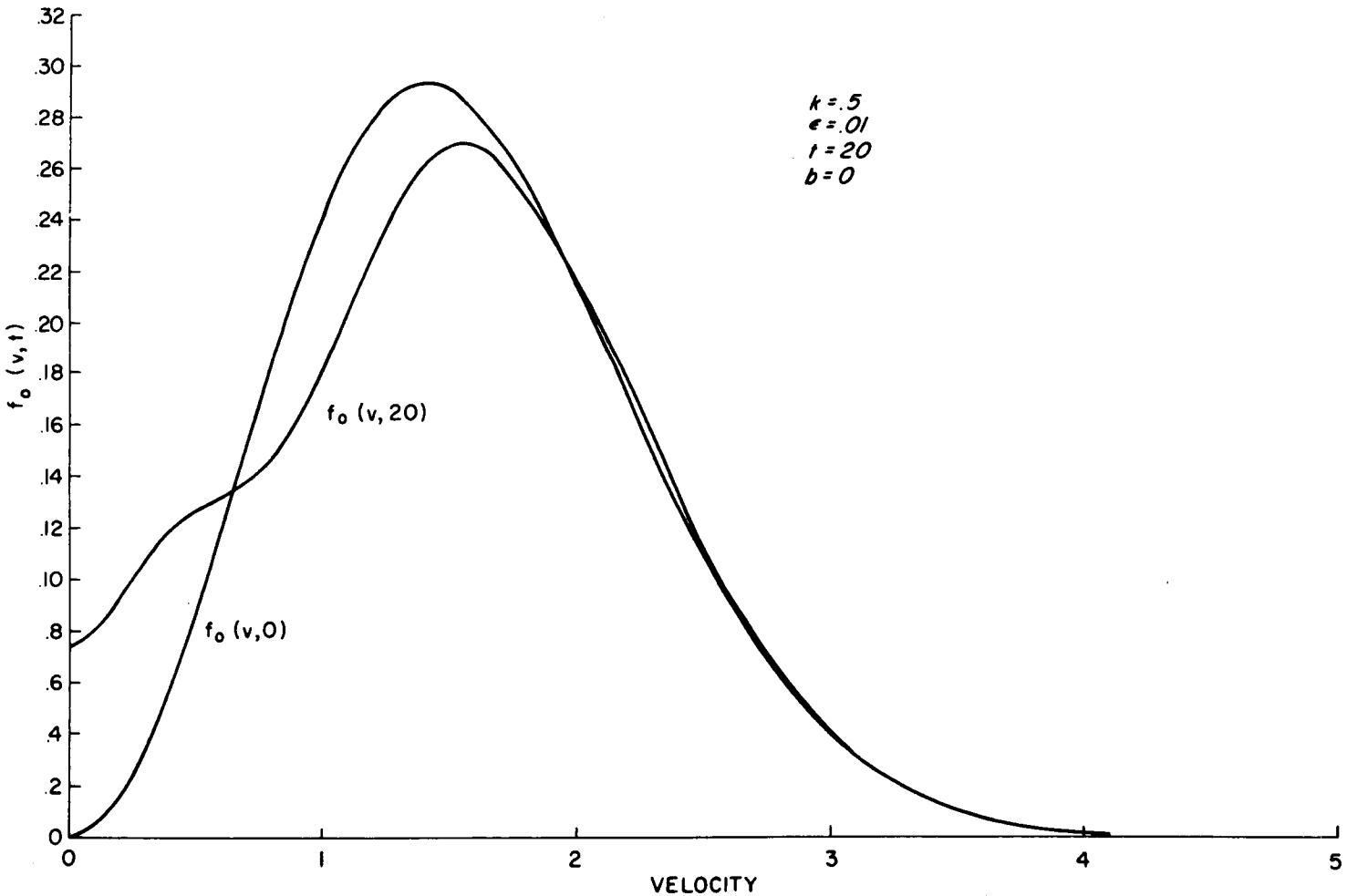
.32
.30
.28
.26
.24
.22
.20
.18
.16
.14
.12
.10
.8
.6
.4
.2
0
$f_o(v,t)$
$f_o(v,20)$
$f_o(v,0)$
k = .5
ε = .01
t = 20
b = 0
0
1
2
3
4
5
VELOCITY

Figure 35b.

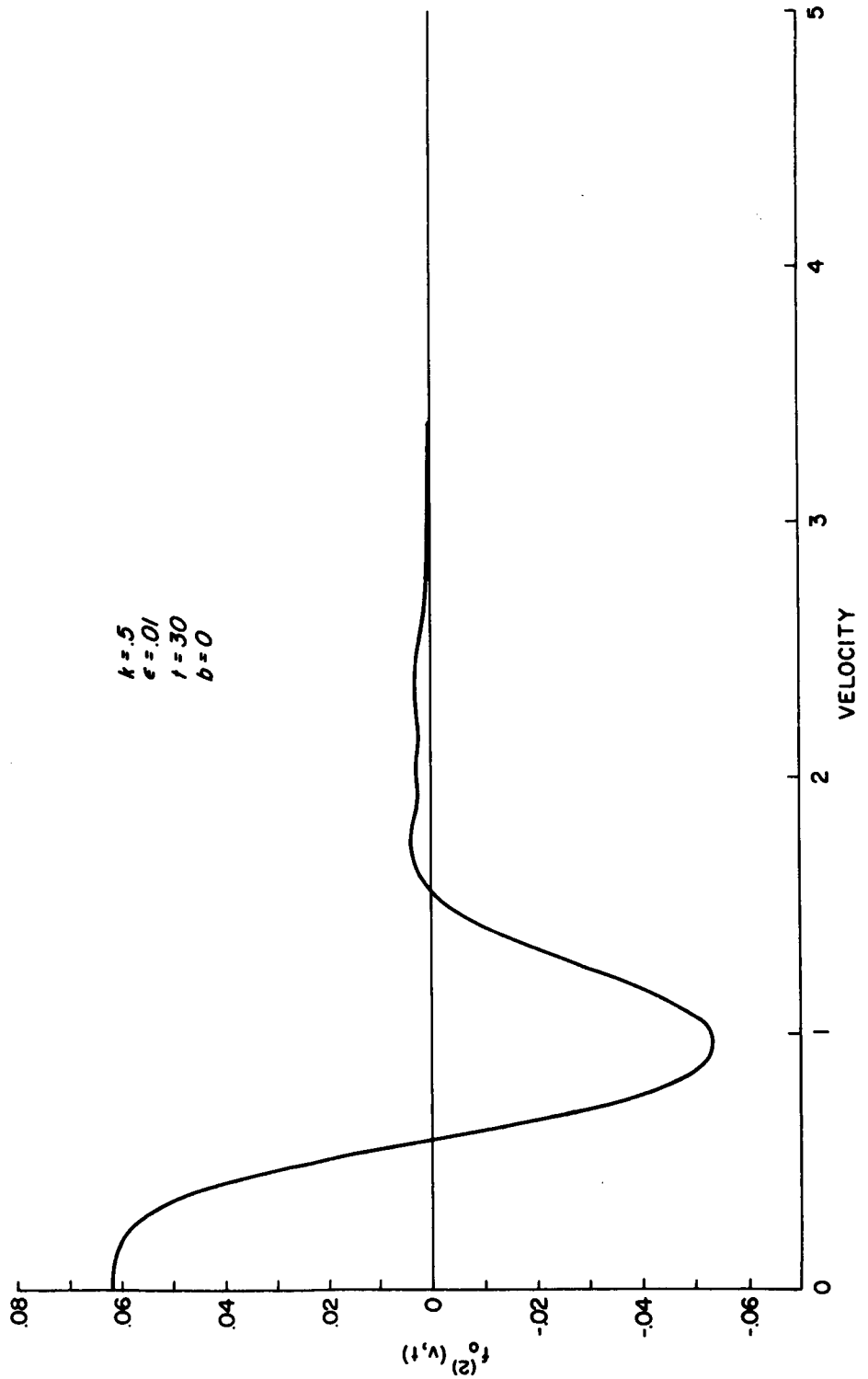

Figure 36a.

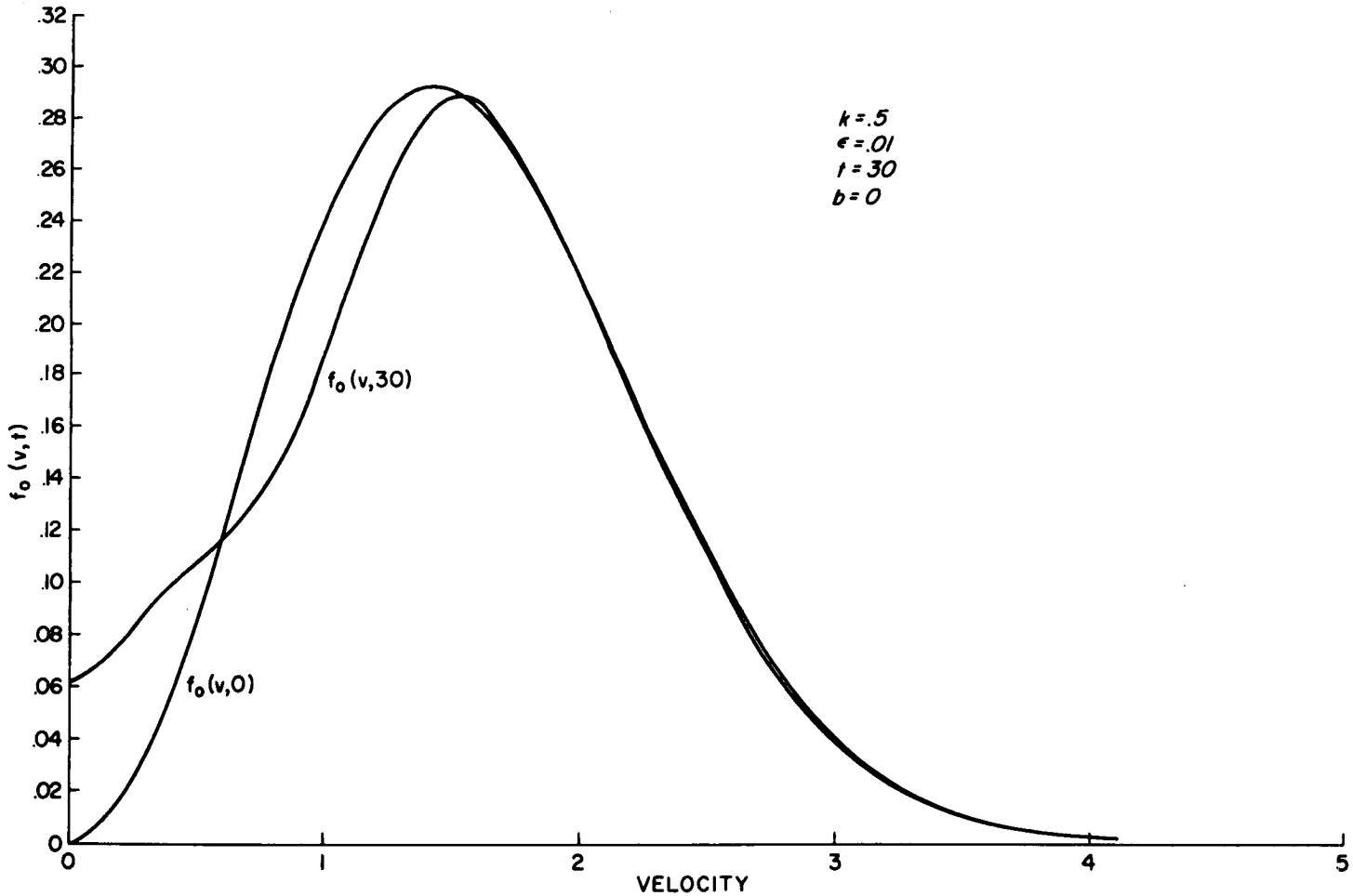
.32
.30
.28
.26
.24
.22
.20
.18
.16
.14
.12
.10
.08
.06
.04
.02
0
$f_0(v,t)$
$f_0(v,30)$
$f_0(v,0)$
k = .5
ϵ = .01
t = 30
b = 0
0
1
2
3
4
5
VELOCITY

Figure 36b.

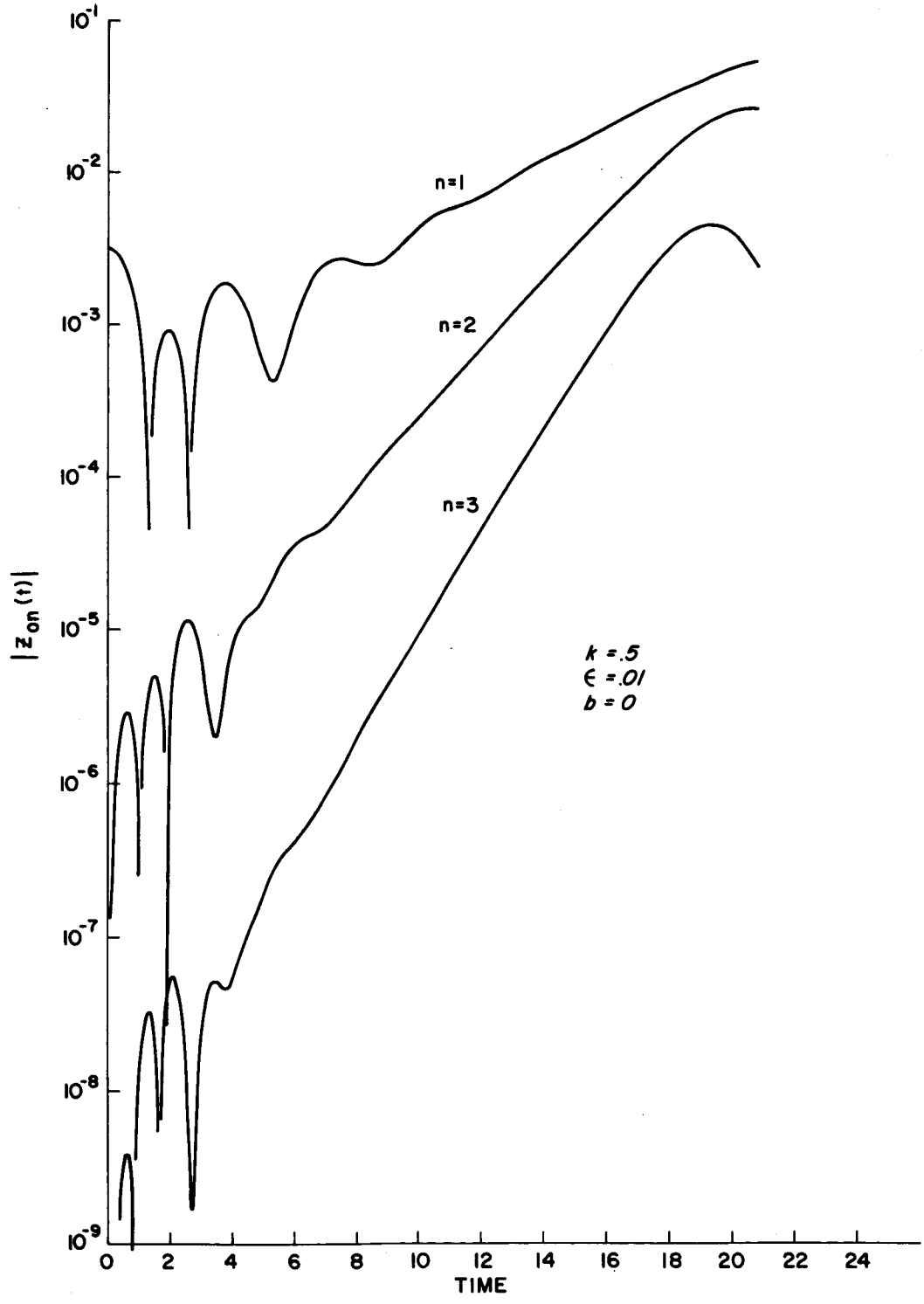
10^{-1}
10^{-2}
10^{-3}
10^{-4}
10^{-5}
10^{-6}
10^{-7}
10^{-8}
10^{-9}
$|z_{on}(t)|$
n=1
n=2
n=3
k = .5
ϵ = .01
b = 0
0
2
4
6
8
10
12
14
16
18
20
22
24
TIME

Figure 37

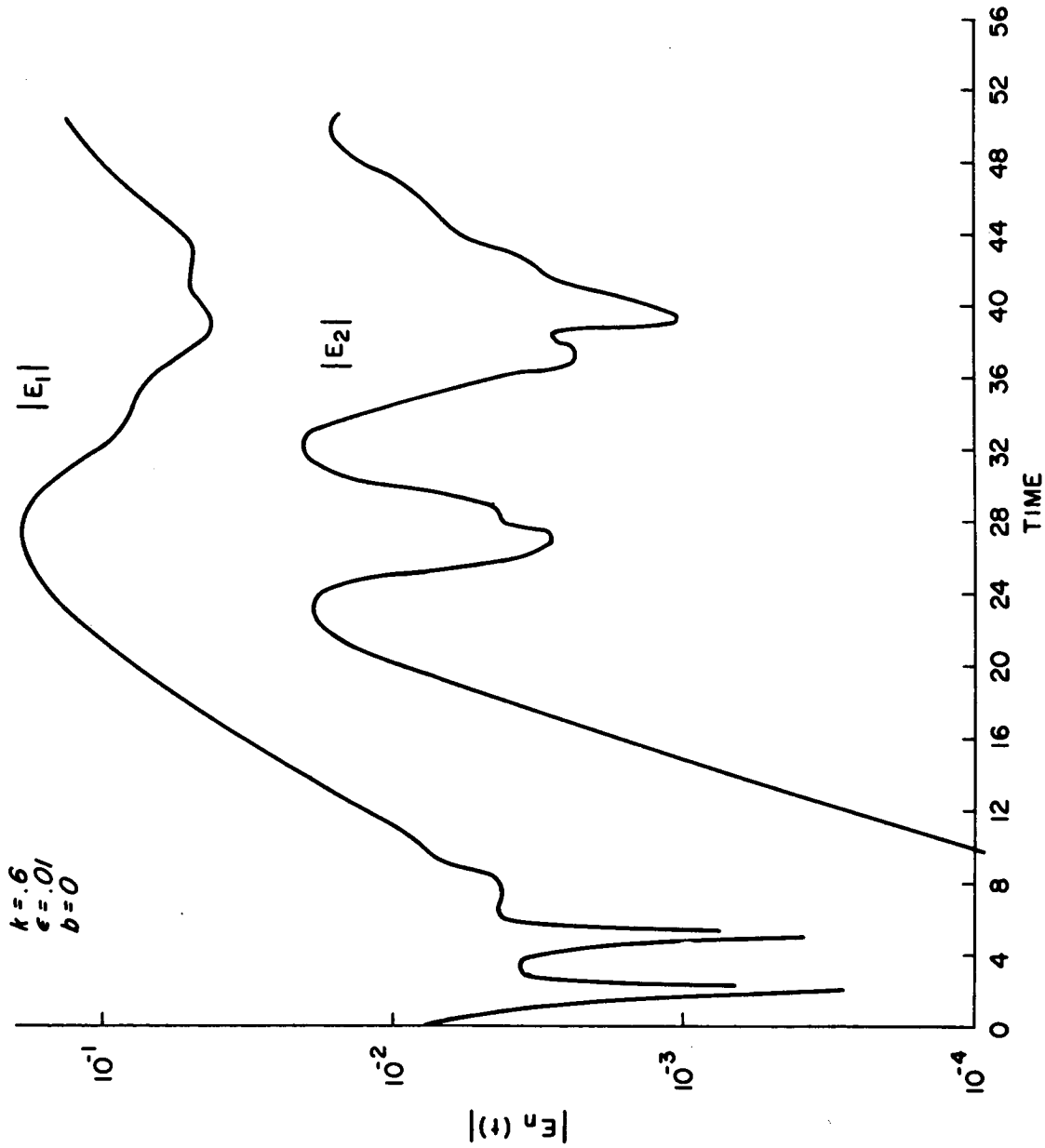
k = .6
ε = .01
b = 0
|E1|
|E2|
10^-1
10^-2
10^-3
10^-4
|En (t)|
0
4
8
12
16
20
24
28
32
36
40
44
48
52
56
TIME

Figure 38

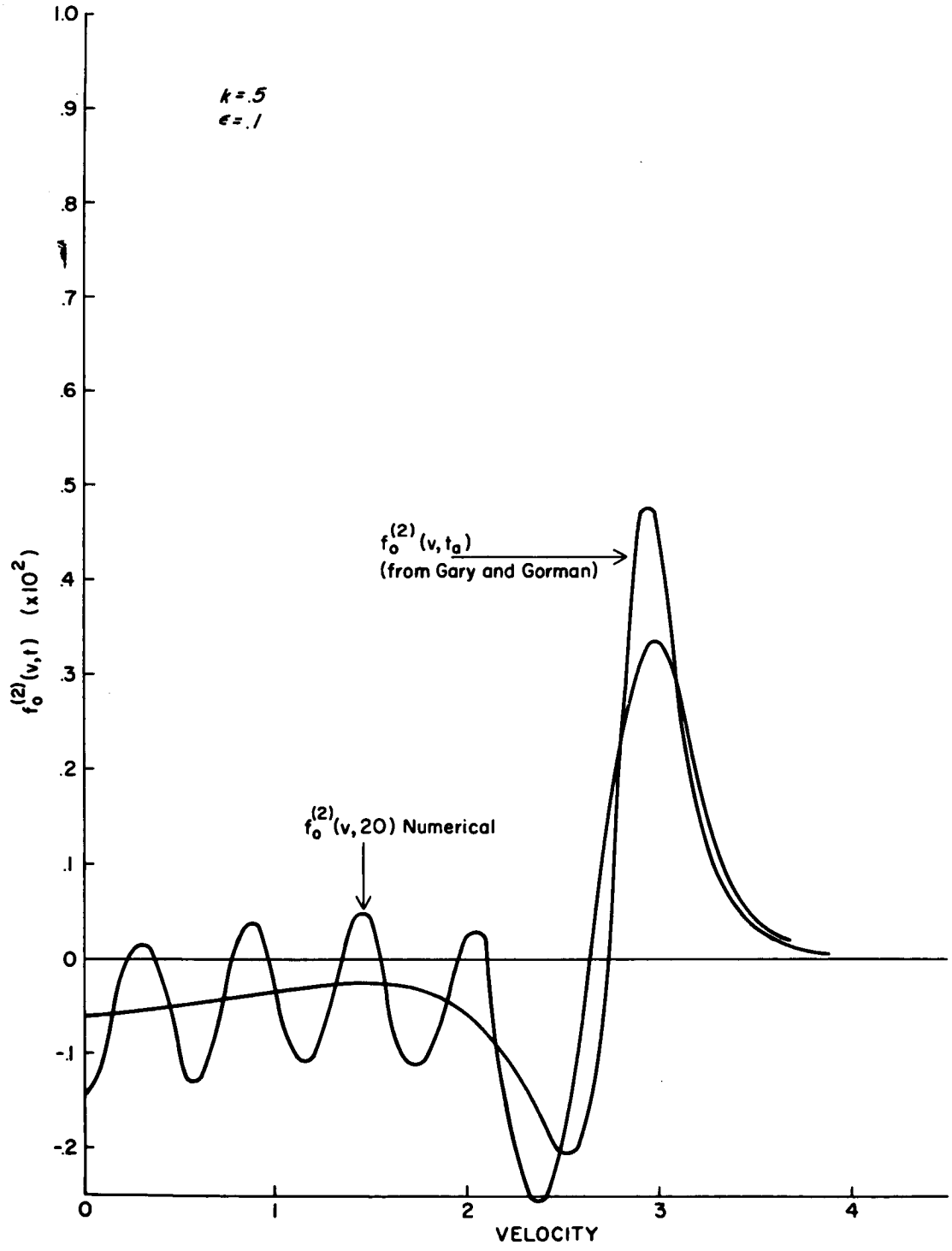
k = .5
ε = .1
1.0
.9
.8
.7
.6
.5
.4
.3
.2
.1
0
-.1
-.2
$f_o^{(2)}(v,t)$ (x10^2)
$f_o^{(2)}(v,t_a)$
(from Gary and Gorman)
$f_o^{(2)}(v,20)$ Numerical
0
1
2
3
4
VELOCITY

Figure 39

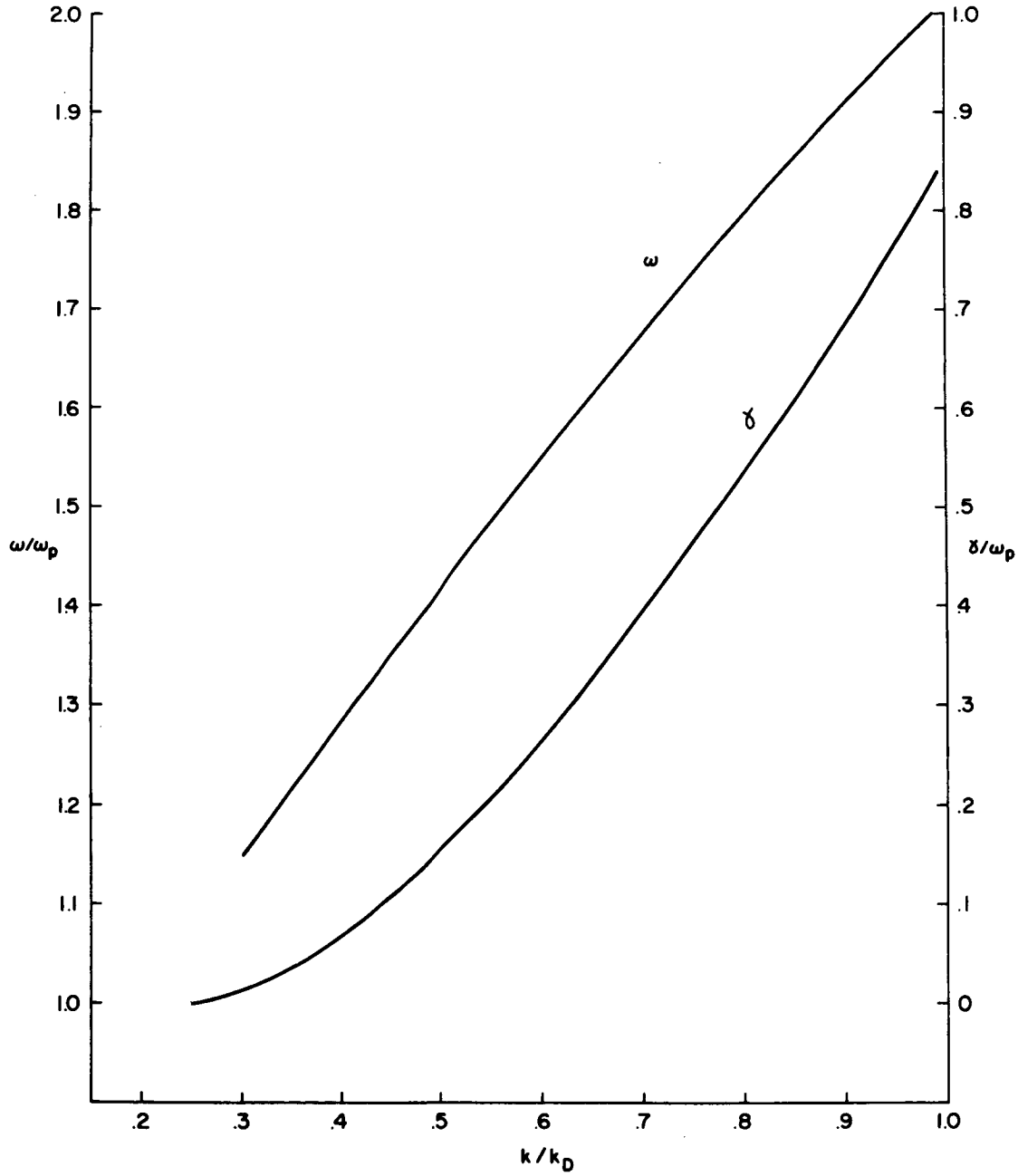
2.0
1.9
1.8
1.7
1.6
1.5
1.4
1.3
1.2
1.1
1.0
ω/ω_p
1.0
.9
.8
.7
.6
.5
.4
.3
.2
.1
0
δ/ω_p
ω
δ
.2
.3
.4
.5
.6
.7
.8
.9
1.0
k/k_D

Figure 40